#416 VTL-PUB-34
AUG. 1976

STREAMER CHAMBER SEARCH FOR NEW STATES OF MATTER WHICH DECAY SEMI-LEPTONICALLY

by

ALAN M. JONCKHEERE

A dissertation submitted in partial fulfillment
of the requirements for the degree of

DOCTOR OF PHILOSOPHY
UNIVERSITY OF WASHINGTON

1976

APPROVED BY H. J. Lubatti
(Chairman of Supervisory Committee)

PROGRAM AUTHORIZED TO OFFER DEGREE Physics

DATE 1976

1976-15
#416

UNIVERSITY OF WASHINGTON

Abstract

STREAMER CHAMBER SEARCH FOR NEW STATES OF MATTER WHICH DECAY SEMI-LEPTONICALLY

by Alan M. Jonckheere

CHAIRMAN OF SUPERVISORY COMMITTEE: Professor H.J. Lubatti
Visual Techniques Laboratory
Department of Physics

A search was made for correlations between muons observed in a downstream spectrometer and neutral strange particles observed to decay inside a one meter streamer chamber. The streamer chamber was triggered on interactions of a 225 GeV/c π^- beam, incident on a Lucite target ($C_5H_8O_2$) mounted inside the chamber, with two muons being detected by a downstream muon spectrometer. Pictures of the interaction were examined for the presence of decays of neutral strange particles, their momentum was measured, and the charged secondaries in the reaction were counted. The momentum of a fraction of the muons was also measured. A control sample of data was taken with the identical trigger, except that muons were not required. By comparing the two samples, we hoped to find an excess in the number of neutral strange decays observed in the dimuon trigger sample. Observation of such a correlation would be strong evidence for the existence of charmed particles being produced in hadron-hadron interactions. No excess was found but a rather low upper limit on the charm signal present was determined.

Also presented is evidence that the dimuon part of the interaction factors from the rest of the interaction, except that the number of charged hadrons produced in association with high mass dimuon pairs appears to be higher than in a normal interaction.

TABLE OF CONTENTS

		PAGE
List of Figures		iii
List of Tables		vi
Acknowledgments		vii
Chapter I.	Introduction	1
Chapter II.	Theory	3
Chapter III.	Searching for Charm	12
Chapter IV.	Streamer Chamber	18
Chapter V.	Experimental Apparatus	30
Chapter VI.	Trigger Electronics and Data Collection	39
Chapter VII.	Measurement and Background	52
Chapter VIII.	Experimental Results	75
Chapter IX.	Model Calculations	126
Chapter X.	Conclusion	134
Appendix A		136
Appendix B		140
References		143

LIST OF FIGURES

FIGURE		PAGE
2-1	Quark-Lepton Correspondence	4
2-2	$K^o \rightarrow W^+W^- \rightarrow \mu^+\mu^-$; Weak Second Order Neutral Current Decay	7
	a) Allowed decay, both SU(3) and SU(4)	
	b) Channel added by SU(4)	
2-3	$K^o \rightarrow Z^o \rightarrow \mu^+\mu^-$; Weak First Order Neutral Current Decay	7
2-4	SU(4) 0^- Mesonic Cuboctahedron; from M. K. Gaillard, B. W. Lee, J. L. Rosner, Rev. Mod. Phy. (April 1975)	8
4-1	Ideal Blumlein Line	21
4-2	Marx High Voltage Generator	23
	a) Marx Generator	
	b) Marx Schematic	
4-3	Streamer Chamber	25
5-1a	Fermilab's M1 Beam Line Schematic, a High Energy-High Intensity Beam Produced at 3.5 mr	31
5-1b	Beam Envelope Obtained in Fermilab's M1 Beam Line	32
5-2	Particle Search Apparatus	35
	a) Plan View of Apparatus	
	b) Muon Telescope Layout	
6-1	Fast Trigger Logic	
	a) Beam/Event Logic	40
	b) Muon Logic	41
	c) Final Trigger/Deadtime Logic	42
	d) Multiple Beam/Interaction Logic	43
6-2	Computer Program Flow Diagrams	
	a) Control Routine Flow Diagram	49
	b) Spill Routine Flow Diagram	50

FIGURE		PAGE
	c) Between Beam Spill Routine Flow Diagram	51
7-1	Examples of Film Taken with the Streamer Chamber	54
	a) 9 prong event with V^o	
	b) 17 prong event with 2 V^o's plus a secondary interaction	
7-2	Primary Interaction Vertex Reconstruction	60
	a) y direction, perpendicular to optic axes	
	b) z direction, parallel to optic axes	
7-3	Neutral Decay Vertex Reconstruction	
	a) Gamma, z coordinate	62
	b) V^o, z coordinate	62
	c) V^o, y coordinate	63
7-4	Intersection Point of Single Muon Tracks with the Plane of the Beam, 2μ·E Trigger; absorber and target originated muons, and 2μ·B used to estimate absorber contribution to the 2μ·E trigger	73
8-1	Average Number of Neutral Strange Decays Observed Versus Number of Charged Tracks	93
	a) No data cuts	
	b) Deleting decays within 10 cm of the Primary Vertex and ±1.5 cm of the High Voltage Wire Plane	
8-2a	2μ·E (SOD) Charged Multiplicity; no cuts	94
8-2b	2μ·E (SOD) Charged Multiplicity with one or more neutral decays; no cuts	95
8-2c	E Trigger Charged Multiplicity with One or More Neutral Decays; no cuts	96
8-3	Decay Distance of Neutrals	97
	a) No cuts on data	

FIGURE		PAGE
	b) Deleting decays within 10 cm of the Primary Vertex and ±1.5 cm of the HV wire plane	
8-4a	Neutral Strange Particle Laboratory Momentum, no cuts	100
8-4b	Neutral Strange Particle Laboratory Momentum, V^o vertex position cuts	101
8-5a	Neutral Strange Particle Transverse Momentum, no data cuts	102
8-5b	Neutral Strange Particle Transverse Momentum, with V^o vertex position cuts	103
8-6a	Longitudinal Center of Mass Momentum (p_L^*) and $x = 2p_L^*/\sqrt{s}$, no data cuts	104
8-6b	Longitudinal Center of Mass Momentum (p_L^*) and $x = 2p_L^*/\sqrt{s}$, with V^o vertex cuts	105
8-7a	$K_s^o \rightarrow \pi^+\pi^-$ Acceptance	107
8-7b	$\Lambda^o \rightarrow p\pi^-$ Acceptance	108
8-8a	Single Muon Acceptance, with the SOD Magnet Energized (50 ± 6 kg-m)	110
8-8b	Single Muon Acceptance with no field in the SOD Magnet	111
8-9	Single Muon Acceptance vs. p_L^* (c.m.) for $d\sigma/dp_T \sim e^{-P_T^2}$, SOD Magnet Energized	112
8-10	Single Muon Longitudinal Laboratory Momentum	114
8-11	Single Muon Transverse Momentum	115
8-12	Single Muon Longitudinal Center of Mass Momentum (p_L^*)	116
8-13	Dimuon Mass Spectrum	117
8-14	Ψ-Charm-Anticharm Associated Production Mechanism	119
8-15	Average Charged Multiplicity vs. Dimuon Mass	121
8-16	Muon Strange Particle Effective Mass	122

LIST OF TABLES

TABLE		PAGE
4-1	Streamer Formation Condition; $E^3\tau_B/p = c$	20
4-2	Streamer Chamber Parameters	
	a) Design Parameters	28
	b) Operating Parameters	29
7-1	Targetting Study - Streamer Chamber Efficiency	56
7-2	Total Targetting Efficiency	58
8-1	Target - Cross Section Parameters	76
8-2	Trigger Cross Sections	77
8-3	Results of Event Selection on Beam Conditions	83
8-4	Results of Selecting Neutral Decays on the Basis of its Vertex Position	84
8-5	Charm Probabilities	88
8-6	Charm Cross Section Upper Limits as a Function of Selection Criteria, Assuming a A Dependence of the Nuclear Cross Section	91
8-7	Upper Limits at 90% Confidence Level of the Cross Section of the Charm Signal Present in the Data	124
9-1a	D^+D^- Acceptance (SOD)	129
9-1b	D^+D^- Acceptance (Non-SOD)	130
9-2	Upper Limit on $\sigma_{D^+D^-}B^2$ for Three Models of $D\bar{D}$ Production	132

ACKNOWLEDGMENTS

I cannot give enough thanks to all of the people who have helped make this dissertation possible. However, I would like to take this opportunity to extend my thanks to some of the most important.

First, I would like to thank my wife, Barbara, who helped me through all of the years of graduate school and who typed the drafts of this dissertation; my advisor, Dr. H. J. Lubatti, who more than anyone else made the experiment possible; and our secretary, Carol Jones, for typing the final copy of this paper and for all the help she has been to me in the past years.

The experiment could not have been performed without the long hours put in by our collaborators, both here at Seattle, at Orsay, and at Davis. These were: V. Cook, S. Csorna, D. Holmgren, H. J. Lubatti, P. Malecki, K. Moriyasu, and B. Robinson at Seattle; D. Fournier, P. Heusse, and J. J. Veillet at Orsay; J. H. Klems, W. Ko, R. L. Lander, and D. E. Pellett at Davis. Of these, I would single out for special thanks; Dr. Moriyasu for the many helpful discussions we have had throughout my graduate career; and Dr. Robinson for helping me assemble and test the apparatus at Fermilab before the other personnel had arrived.

The technical staff at all three institutions also deserve a large vote of thanks. It has been a great pleasure to work with; R. Kenyon, W. Wallick, D. Reid, L. Cameron, K. Osawa, and others on the design and construction of the proportional chambers, their electronics, and the interface to the computer; F. Rohrbach, V. Cook, R. Gregg, D. Forbush, J. Schultz, and F. Toevs on the design and while constructing the streamer chamber. P. Rançon of Orsay must be given special thanks for designing and building the high-speed cameras for the experiment, and the staff at Davis

deserves thanks for their work on the calorimeter and the muon telescope.

I would also like to thank the personnel at Fermilab, especially P. Koehler, and the operations and rigging crews who supplied invaluable assistance.

The analysis of the data was greatly eased by the willing assistance of the scanning staffs at the three institutions. I would especially like to thank B. Edwards and M. Fasy for their help.

The assistance of S. Ellis and R. Cahn is very much appreciated. Many helpful discussions on the theory of charm during the writing of this dissertation and their comments on the written version have proven invaluable to my understanding of the subject. And last but not least, I would like to thank the members of my advisory committee for their help during my years at Seattle, and the entire faculty of the Physics Department for the very excellent education they have provided.

Thank you, one and all.

I. INTRODUCTION

In November of 1974, one of those rare events occurred which make elementary particle physics the exciting field it is. The discovery of a new, unexpected particle was announced simultaneously by two separate groups of experimenters. The Stanford Linear Accelerator Center-Lawrence Berkeley Laboratory (SLAC-LBL) collaboration found the new state in electron-positron collisions in the colliding beams of SPEAR at SLAC.[1] The Brookhaven National Laboratory-Massachusetts Institute of Technology (BNL-MIT) group saw the particle's dimuon decay mode while studying proton-Berylium interactions at BNL.[2]

This new particle, named the Psi (ψ) at SLAC and the J at BNL, was soon joined by another, discovered by the SLAC-LBL group and named the ψ'. The masses of the two particles were quickly determined to be 3095 and 3684 MeV/c^2 respectively. The distinguishing characteristic of these particles is their extremely narrow width, 70 and 225 KeV respectively. This is surprising because such massive states would be expected to decay via the strong interaction with the "normal" hadronic width of $\sim$ 250 MeV if they were hadrons. Since the width of any state is inversely proportional to its lifetime, the small widths of the new particles implies that some mechanism is suppressing their decay by a factor of over 1000. The simplest assumption one can make as to the nature of the suppression mechanism is that some new quantum number has appeared in the ψ. This quantum number must be conserved in strong interactions, and so, perhaps coupled with a dynamical suppression, retards the decay of the ψ. It is the question of the nature of this new quantum number that has stirred up the high energy community. How does it fit into the scheme of things?

This dissertation is a description of a streamer chamber experiment performed at the Fermi National Accelerator Laboratory by groups of physicists from the University of Washington, Seattle, Washington; the University of California at Davis, Davis, California; and the Laboratoire de l'Accélérateur Linéaire, Université de Paris-Sud, Orsay, France. This is the Seattle-Orsay-Davis Collaboration (SOD). The experiment was performed in early 1975 to answer some of the questions raised by the ψ/J.

II. THEORY

A number of possibilities exist as to the nature of the new quantum number indicated by the ψ/J. I shall not attempt to discuss all of the theories embodying the various possibilities. They all have problems. I will, however, sketch the ideas behind one of the most intriguing classes of theories, based on the charm hypothesis. For a detailed discussion of the various possibilities, I refer the reader to several excellent review articles.[3]

As is well known, nature has divided all known particles into two major classes: the leptons and the hadrons, neglecting the field quanta, which are special cases. There are four known leptons (and their anti-particles). These can be grouped into two doublets, the electron and its neutrino, and the muon and its neutrino. Neglecting the ψ's it is possible to generate the quantum numbers of all known hadrons from three constituent quarks, a doublet, the u (up) and d (down) quarks and a singlet, the s (sidewise or strange) quark. As long ago as 1964 Bjorken and Glashow[4] proposed adding a fourth quark which they combined with the s quark to form a second doublet, producing a one to one correspondence between the leptons and the hadrons. This quark was differentiated from the "normal" quarks by a new quantum number which they, "tongue-in-cheek", called charm.

The correspondence between the hadrons (quarks) and leptons is illustrated in Figure 2-1. The correspondence requires the new c quark to have the same charge as the u quark. In terms of these quarks and leptons, the weak and electro-magnetic currents take the same form for both the hadrons and the leptons. In matrix notation the weak current is:

QUARK (HADRON) - LEPTON

$$\begin{pmatrix} u \\ d' \end{pmatrix} \begin{pmatrix} c \\ s' \end{pmatrix} \cdot \begin{pmatrix} \nu_e \\ e^- \end{pmatrix} \begin{pmatrix} \nu_\mu \\ \mu^- \end{pmatrix}$$

$$d' = d\cos\theta_c + s\sin\theta_c$$

$$s' = s\cos\theta_c - d\sin\theta_c$$

FIG. 2-1

Quark-Lepton Correspondence

$$J^{WK}_{H\mu} = \bar{q}\gamma_\mu(1+\gamma_5)C_H q \quad \text{for the hadrons,}$$

$$J^{WK}_{L\mu} = \bar{\ell}\gamma_\mu(1+\gamma_5)C_L \ell \quad \text{for the leptons,}$$

where q and ℓ are the four component column vectors:

$$q = \begin{pmatrix} c \\ u \\ d \\ s \end{pmatrix}; \qquad \ell = \begin{pmatrix} \nu_e \\ \nu_\mu \\ e^- \\ \mu^- \end{pmatrix}$$

C_H and C_L are the 4 x 4 matrices:

$$C_H = \left(\begin{array}{c|c} 0 & U \\ \hline 0 & 0 \end{array}\right); \quad C_L = \left(\begin{array}{c|c} 0 & I \\ \hline 0 & 0 \end{array}\right)$$

$$U = \begin{pmatrix} -\sin\theta_c & \cos\theta_c \\ \cos\theta_c & \sin\theta_c \end{pmatrix}; \quad I = \begin{pmatrix} 1 & 0 \\ 0 & 1 \end{pmatrix}$$

Similar terms can be written for the electro-magnetic current, using the same C_H and C_L.[5,6]

The effect of the unitary 2 x 2 matrix U is very important. It mixes quark states of the same charge, in this case, the d and s quarks. This mixing comes about because the states of well defined mass are not eigenstates of the weak interaction. In fact the u and c quarks could also be mixed but this only adds an unobservable phase to C_H, which can be removed by a suitable definition of the quarks. So by convention we speak only of $d \longleftrightarrow s$ mixing. With this choice of phase, θ_c is the well-known Cabibbo angle.

Expanding the weak hadronic current, we can observe the effect of this mixing. Suppressing the space part of the current, we have:

$$J_H^{WK} = \bar{u}\,(d\cos\theta_c + s\sin\theta_c) + \bar{c}\,(s\cos\theta_c - d\sin\theta_c)$$
$$= \bar{u}\,d' + \bar{c}\,s'$$

The first term is the well established part of the weak current which gives rise to strangeness changing decays. The second term is new. It couples the new charmed quark to both the s and d quarks and implies that when a charmed quark decays, it decays to a strange quark with amplitude proportional to $\cos\theta_c$. Its decay to the non-strange quark is suppressed by the $\sin\theta_c$ factor.

The four-quark scheme lay dormant for several years until Glashow, Iliopoulos and Maiani[5] pointed out that it is just such a scheme that is needed to cancel strangeness-changing neutral currents. In the three-quark scheme, one would expect second-order decays like $K^\circ \to \mu^+\mu^-$ to proceed as shown in Figure 2-2a. Such decays are not seen. The charmed quark provides a very natural suppression of this type of process by providing the alternate path shown in Figure 2-2b. Because of the $-\sin\theta_c$ at the upper vertex in Figure 2-2b these diagrams cancel, neglecting differences in the quark masses. The need for such a cancellation becomes even more pressing when one considers the gauge theories with their neutral currents. Here, one would expect the reaction $K^\circ \to \mu^+\mu^-$ to proceed by the first-order process in Figure 2-3. It is easy to show[5] that in the four-quark scheme the neutral current is diagonal: $Z^\circ \sim u\bar{u} + c\bar{c} - d\bar{d} - s\bar{s}$, where I have suppressed the space part of the current. Thus, the Z° cannot couple two different quarks, but only a quark and its antiquark. The graph in Figure 2-3 is, therefore, forbidden in the four-quark scheme.

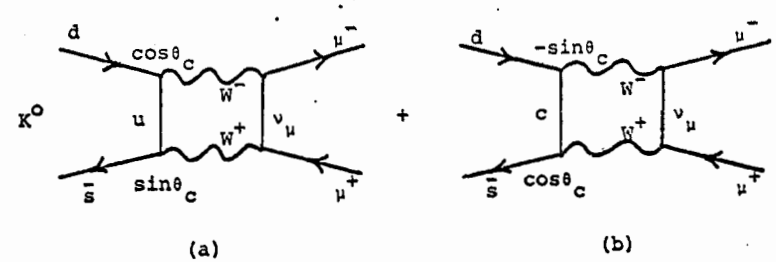

$$\sim (\cos\theta_c \sin\theta_c) \quad + \quad (-\cos\theta_c \sin\theta_c)$$

FIG. 2-2

$K^\circ \to W^+W^- \to \mu^+\mu^-$

Weak Second Order Neutral Current Decay

a) Allowed decay, both SU(3) and SU(4)

b) Channel added by SU(4)

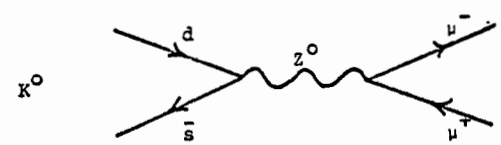

FIG. 2-3

$K^\circ \to Z^\circ \to \mu^+\mu^-$

Weak First Order Neutral Current Decay

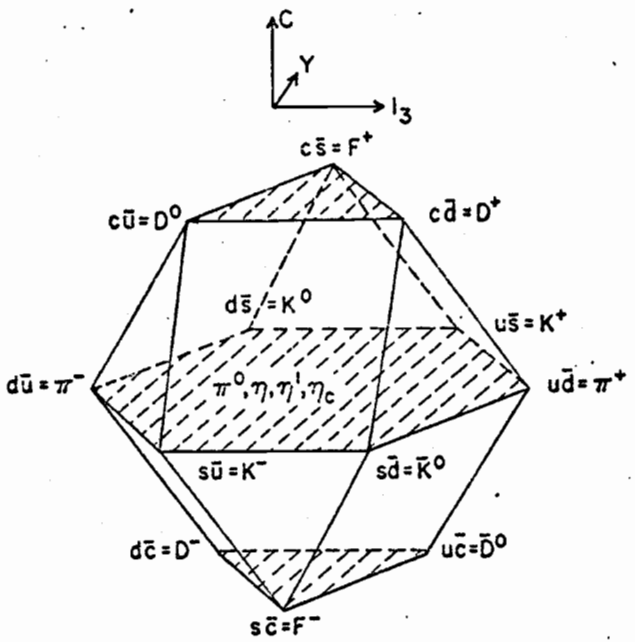

FIGURE 2-4
SU(4) 0^- MESONIC CUBOCTAHEDRON
from M.K. Gaillard, B.W. Lee, and J. L. Rosner,
Rev. Mod. Phys. (April 1975)

The introduction of the charmed quark has profound implications for particle spectroscopy. The most obvious effect is that the spectrum of hadronic matter is enlarged from SU(3) to SU(4). For example, the familiar mesonic 0^- nonet (8+1) of SU(3) is enlarged to a 16-plet (15+1) in SU(4).[7] This enlarged multiplet is shown in Figure 2-4. The seven new states form an SU(3) triplet and an antitriplet with C = +1 and -1 respectively and a singlet with C = 0. These states should not be too much more massive than the non-charmed states in the multiplet. From the known rates for the various neutral current, strangeness-changing processes as well as the known K_L^0 K_S^0 mass difference, an upper limit of a few GeV/c^2 can be put on the charmed quark mass. This in turn leads to estimates of the charmed meson masses that are at most a few GeV/c^2 higher than their non-charmed partners.[7]

The lightest of these new states will have lifetimes characteristic of weak decays. They cannot decay strongly to less massive charmed states. The leading decays will have amplitudes proportional to the weak coupling constant, G, and dimensional considerations lead to decay widths proportional to $G^2(\text{mass})^5$. Inserting reasonable masses for the charmed states and noting the similarities between decays of charmed and strange particles, one guesses that the charmed states should have lifetimes in the neighborhood of 10^{-13} sec.[7] In addition, since $c \to s \cos\theta_c$ they will decay primarily to states containing a strange quark. For example, the D^+ of Figure 2-4 will decay semi-leptonically to a state with the quantum numbers of the $\bar{K}^0$, with a strength proportional to $\cos^2\theta_c$. For more details on the spectroscopy and decay modes of the charmed quark model, including the baryon states, I refer the reader to Gaillard, Lee, and Rosner.[7]

The charm scheme seems to provide a ready-made explanation for the long lifetimes of the ψ and ψ'. In this context the ψ would be a state with "hidden" charm. It might be a bound $c\bar{c}$ state, the partner of the ρ, ϕ, and ω in the 1^- multiplet. The ψ' would then be a radial excitation of this "charmonium" system. This view has been strengthened by the observation of radiative decays of the ψ' to P_c, χ and χ' and of the ψ to the X.[8] Their long lifetimes would then follow if the ψ' were even slightly below threshold for production of charmed pairs. In this case they would have to decay strongly by violating "Zweig's Rule".[9] This rule states that interactions involving non-connected quark lines are suppressed. Thus the decay of the ϕ (an $s\bar{s}$ state) to non-strange states is suppressed relative to decays into two strange particles, even though much more phase space is available for the non-strange decays.

Associating the ψ with the SU(3) singlet sets the mass scale for the rest of the SU(4) charmed states. The lightest of the charmed states, presumably the D meson, should have a mass near 2 GeV/c^2.[7] The lightest baryon would be somewhat more massive, but still under 4 GeV/c^2. With this information and noting the similarities between possible production mechanisms of charmed and strange pairs, it is possible to try to estimate the total production cross section for charmed pairs. Unfortunately, these estimates vary widely depending on the particular mechanism assumed. An estimate by Snow[10] who considers diffractive production of massive states, leads to a cross section which scales as $(\text{mass})^{-2}$ which implies, for a charmed mass of 2-4 GeV/c^2, a production cross section as high as several tens of microbarns.[7] However, estimates of two-body associated production based on Regge pole phenomenology are far smaller.[11]

Another question which is crucial in any search for charmed states is that of their decay ratios. In particular, what is the ratio of leptonic, or semi-leptonic decays to non-leptonic. On the basis of 20 dominance (the SU(4) extension of SU(3) octet dominance or the $\Delta I = \frac{1}{2}$ rule), the weak decays of charmed hadrons should be predominantly non-leptonic, with semi-leptonic decays contributing less than 10% of the total and leptonic decays being even smaller.[6] It has been pointed out [12] that 20 dominance may not be as effective as is octet dominance due to the large mass of the c quark. If 20 dominance does not enhance the non-leptonic decays at all, then simple counting gives semi-leptonic branching ratios of 20% for each species of lepton ($c \to 2$ leptons and 3 quarks equally). Such large branching ratios to leptons seem to be ruled out by the O'Neill experiment at SPEAR,[13] which puts an upper limit on the order of 10% for this ratio. This limit, however, is far from unassailable.

The preceding discussion suggests the types of observations which would establish the existence of charm and the properties of charmed states which may make their observation possible. The most crucial test of the charm hypothesis is the existence of a rich spectrum of new states. At least some of these should decay with very long lifetimes, on the order of 10^{-13} seconds. They should decay principly to states containing a strange particle and may have substantial semi-leptonic decay modes, on the order of 10% branching ratios to muons.

III. SEARCHING FOR CHARM

Since the observation of the ψ there have been many attempts to establish the existence of charm. The first attempts were made at the e^+e^- colliding beams at SLAC shortly after the discovery of the ψ. The SLAC-LBL group noted that the ratio of $\sigma(e^+e^- \to \text{hadrons})/\sigma(e^+e^- \to \mu^+\mu^-) \equiv R$ takes a dramatic jump from ~ 2.5 to ~ 5.5 at a center of mass energy near 4 GeV. If one assumes that the constituents of the hadrons are point, spin ½ particles, this ratio should be just the sum of the squares of the charges of the constituents. Thus, the rise in R at 4 GeV might be associated with a threshold where a new type of constituent is beginning to be produced, probably by associated production of pairs of new states containing the new constituent. They have, therefore, searched in the region above 4 GeV for evidence of narrow peaks in the two and multibody mass spectra, especially in those spectra involving a strange particle. Initially, they observed no clear signal. However, they have now greatly increased their data sample, and very recently have reported the observation of narrow peaks in the $K^{\pm}\pi^{\mp}$ and $K^{\pm}\pi^{\mp}\pi^{\pm}\pi^{\mp}$ channels at an effective mass of 1865 ± 15 MeV/c^2.[14] The properties of this new particle indicate that it is very probably the D meson of Figure 2-4. The observed cross section times branching ratio of the two decay modes are 0.20 ± .05 nb and 0.67 ± 0.11 nb for the $K\pi$ and $K3\pi$ modes, respectively, compared with the average total hadronic production cross section in the energy region searched of 27 ± 3 nb. These numbers indicate that the charmed particles have substantial branching ratios to multiparticle states, as had been suspected previously. It is difficult to determine just what fraction of the total charm production cross section these modes represent since there are indications of something else going on at the same energies. They see a number of events containing a μe pair with missing neutrals.[15] These are

being interpreted as production of a heavy lepton. It is therefore uncertain just how much of the rise in R is due to charm production, and how much is due to the heavy lepton.

There is also some evidence that charm has been seen in neutrino-proton interactions.[16] A few dimuon events have been observed and it is claimed that these are inconsistent with being decays of the intermediate vector boson of the weak interaction, or with a new heavy lepton. Thus, they might be the result of the decay of a new hadron with a new quantum number, which might be charm.

Searches for the new states have been made in bubble chambers in hadron-hadron interactions. These searches have looked for neutral decays of the longest lived charmed states,[17] enhancements in the mass spectra which include a neutral strange particle,[18] and enhanced neutral strange particle production when a muon is also present.[19] All of these searches have had negative results. The negative results are not difficult to explain. A particle with a lifetime of 10^{-13} seconds would be difficult to detect in bubble chambers, even at the highest Fermilab energies. Such a track would be at most a few mm long. The others suffer mostly from lack of statistics; they set limits on the production cross sections in exclusive channels of a few microbarns and in the semi-inclusive μ-V^0 channel of 300-500 microbarns.

Another way to search for new particle production is to look for threshold effects which would be characteristic of the decay of some massive, long-lived object. This has been done by Bintinger et al[20] who looked at single muon production as a function of transverse momentum. They failed to see any effect which could be attributed to either two or three-body decay of such a state with a mass of 2.3 GeV/c^2, setting limits on

the cross section times branching ratio of 400 nb and 2μb for two and three-body decays respectively, assuming a specific production distribution.

The most extensive searches for charm in hadron-hadron interactions have looked for two-body decay modes, especially in the Kπ system.[21] These searches have, in general, been negative although Abolins et al[22] have seen a marginally significant enhancement in the Kπ spectrum at 2.3 GeV/c^2. We will have to wait and see if this enhancement holds up to the test of time and increased statistics. These two-body searches are very difficult. They suffer from the same problems as do the similar searches at SPEAR, namely small branching ratios to an exclusive channel plus many more possible wrong combinations which dilute any signal present.

So the problem still exists - where do we look to find charm in hadron-hadron interactions? One fact is abundantly clear from the above discussion. Charm is extremely elusive. The ideas discussed above, however, give us hints of what types of experiments might successfully see charm. First, the experiment should be "inclusive". That is, it should be sensitive to as many decay modes as possible, especially the high multiplicity modes. It should be sensitive to production of strange particles since most decays of charmed states will contain a strange particle in the final state, either a K or a Λ. And lastly, a trigger should be chosen to enhance the charm signal.

A good candidate for a trigger which would enhance the charm signal is to trigger on produced leptons, either electrons or muons. As mentioned above, the lightest charmed state may have branching ratios to leptons as high as 10%. This is several orders of magnitude larger than such "normal" particles as ρ, φ, ω and η. Thus, the decrease in rate of measured charm production caused by introducing the branching ratio, or

even the square of the branching ratio when triggering on two leptons is more than compensated by the increase of the signal to the background ratio. In this connection, a muon trigger would be easier to use than an electron trigger since background from converting gammas would be absent. Thus an apparatus which is sensitive to strange particles and which can be triggered by muons would have a good chance of establishing that charm exists, merely by finding an enhanced strange particle signal correlated with the muons, if triggers from muons from pion and kaon decay can be suppressed. Performing the experiment at Fermilab helps suppress such decay triggers. The factor of βγ in the lifetime introduced by the boost to the laboratory frame greatly diminishes pion and kaon decays when compared to colliding beam experiments. Such an apparatus would have to be able to accept moderately high beam flux. The μ/π ratio is only 10^{-4} at p_T greater than 1 GeV/c.[23] Thus, the muon trigger rates would not be high. In addition enough additional quantities should be measurable so that if an enhancement were seen, the charm signal could be further isolated. In particular, one should be able to measure the neutral strange particle momentum spectrum and the spectrum of the other hadrons produced with the triggering muons as well as the momentum spectrum of the muons. These measurements could tell one a great deal about the source of the strange particles and the muons, and about the mechanism producing the charmed states, if such were found.

Triggering on muons has an additional advantage - it addresses the open question of anomalous lepton production. In particular, what does the spectrum of hadrons look like when a prompt muon is produced? Anomalous lepton-production has been studied at several laboratories[23] by studying the inclusive lepton spectra, but no one has, as yet, studied in

detail the hadrons produced in association with these leptons.

The University of Washington's one meter streamer chamber is ideally suited for the studies outlined above. It is a superlative, triggerable vertex detector which is capable of accepting beam rates of up to 10^6 particles/sec. It is a visual detector with resolution comparable to a bubble chamber. It has the special advantage of being able to look at processes with very small cross sections if an appropriate trigger can be established. One can easily accumulate 10 events per nanobarn of cross section in a few days of data taking.

An efficient muon trigger is relatively easy to install. Thus, we determined that we could study the hadrons produced in association with triggering muons. In particular, we could study correlations between the muons and neutral strange particles which decay in the chamber. These correlations can be studied with a minimum of experimental bias by always comparing the events collected with the muon trigger to a "control" sample taken under identical conditions but without the muon requirements.

Under these conditions, if charm is being produced at appreciable levels at Fermilab energies, we expected to be able to observe an enhancement in neutral strange particles produced in correlation with triggering muons. The source of the additional strange particles should be reflected in their momentum distributions and perhaps in the spectra of the co-produced hadrons.

The experiment described in this dissertation is the second experiment of this type run. In March of 1975, the Seattle-Orsay-Davis collaboration performed a very similar experiment using much of the same equipment as was used in the present experiment. The earlier run was a quick test to see if such an experiment was feasible. The results of

the earlier run indicated that indeed charm might be observed using this technique. We observed a three-standard deviation enhancement of neutral strange particle production when we compared the samples of data taken with and without a muon requirement. This result was of only marginal statistical significance and there were several background signals which were not well determined. We, therefore, asked for additional running time from Fermilab with which we hoped to collect additional data with an improved system. In particular, we wished to improve both the muon trigger and the system's trigger diagnostics. This dissertation describes the experiment performed with the improved system.

IV. STREAMER CHAMBER

The streamer chamber as a particle detector shares many of the attributes of bubble chambers. It is a visual device with nearly 4π geometry. The ionization trails of charged particles passing through the chamber are made visible and photographed in stereo by high-speed cameras. By measuring the particle tracks on film and using large computer geometry programs, one is able to reconstruct the paths of the particles in space. Since the chamber is housed in a large magnet, this allows the momentum of the particle to be determined. Thus data collection, measurement, and most of the analysis of streamer chamber data are identical to bubble chambers. In addition, the inherent measurement accuracy of the streamer chamber is very nearly the same and may, in fact, be better than in bubble chambers. Although the streamers in a streamer chamber are larger than the bubbles in a bubble chamber, with attendant larger setting errors, the fact that the streamer chamber is gas filled, while bubble chambers are liquid filled means that streamer chambers have much less multiple scattering. The increased setting error and decreased multiple scattering on measuring accuracy nearly cancel over a large momentum range.[24] It is the manner of making the particle tracks visible that makes the streamer chamber different and in some ways more powerful than the bubble chamber.

The natural phenomena used by a streamer chamber to make particle tracks visible is that sparks can form in a gas which contains a high electric field. The trick is to control the formation of these sparks.

The usual mechanism for forming the initial conducting path for a spark is to accelerate a free electron in the gas, such as are present along the ionization trail left by a high energy particle, forming a Townsend avalanche. The avalanche will, in general, not be visible. However, if the field is high enough, it is possible for the electron

density at the head of the avalanche to reach a point where the electric field from the free electrons cancels the externally applied field between the "head" and the "tail" of the avalanche. At this point, spark formation shifts to the "streamer" mode. In this mode spark propagation is via photoionization of the surrounding gas. Photoions formed just outside the "head" and the "tail" of the original streamer are in regions where the electric field is nearly twice as high as the applied field. These, therefore quickly avalanche and combine with the original avalanche causing the streamer to grow very rapidly in both directions along the applied field lines. These streamers are easily bright enough to photograph. I refer the reader to references 25 and 26 for more complete descriptions of streamer propagation. The trick is to shut off the electric field while spark formation is in the streamer mode but before the spark has spanned the gap. At typical electric fields, streamers grow at approximately 10^8 cm/sec. This implies that a high-voltage pulse of the order of 10 nsec wide would give streamers one cm long.

To produce good streamers at atmospheric pressure, the pulse on the chamber must have a height and width which satisfy: $E^3\tau_B/p^2=C$,[27-28] where E is in kV/cm, τ_B is the pulse width in nsec at 10% above the base, p is the pressure in atmospheres and C is an empirical constant which depends on the gas used.[28] Table 4-1 lists experimental values of the constant C for a few gases. For a Ne-He (90-10) gas mix at atmospheric pressure, an electric field of approximately 25kV/cm is needed for a 10 nsec pulse. For our chamber with two 15 cm gaps, this implies a high voltage pulse of approximately 375 kV.

Producing such narrow high voltage pulses requires special techniques. The device used in most streamer chamber systems to perform the necessary

GAS	$E^3 \tau_B/P$ #
He-Ne (10-90)	$1.6 \pm 0.2 \times 10^5$
He-Ne (25-75)	$1.7 \pm 0.2 \times 10^5$
He	$4.8 \pm 0.5 \times 10^5$
H_2	$29 \pm 4 \times 10^5$
H_2 + 50 ppmSF_6	$22 \pm 4 \times 10^5$
H_2 = 0.5% CH_4	$23 \pm 3 \times 10^5$
CH_4	$80 \pm 8 \times 10^5$

E = Electric field in Kv/cm.

τ_B = Pulse width at 10% field in nsec.

P = Pressure in atmospheres.

TABLE 4-1
STREAMER FORMATION CONDITION
$E^3 \tau_B/p = C$

pulse shaping is the Blumlein line. An ideal Blumlein network is shown in Figure 4-1. Conceptually its operation is very simple. One charges the intermediate conductor B to some voltage, V_o. When switch A is closed, the discharge pulse travels down channels 1 and 2. At point C these pulses "see" three channels, two with impedance Z_o and one with impedance $2Z_o$. One-half of each pulse is transmitted down channel 3, one-quarter of each is reflected down each of channels 1 and 2. A voltage $-V_o$ is therefore developed on the transmission line 3. The pulse in channel 1, upon reaching B sees an open circuit and is again reflected, with no phase change. The pulse in channel 2, upon reaching point A, sees a closed circuit and is reflected with a 180° phase change. Upon reaching point C, the second time

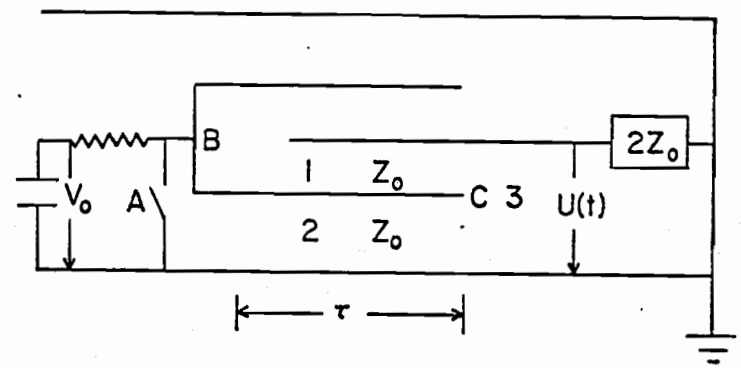

FIGURE 4-1
IDEAL BLUMLEIN LINE

these pulses are equal in magnitude but of opposite polarity. Thus they cancel, shutting off the pulse in channel 3, voltage U(t). If τ is the transmission time for a pulse from A to C and from B to C then the width of the pulse U(t) is just 2τ. If the transmission line is terminated with a resistive load of $2Z_o$ the energy of the pulse is transferred to the load and no further reflections occur. The streamer chamber itself is part of the transmission line.

This discussion was for an ideal Blumlein line. A real system is much more complicated and I refer the reader to the literature, especially to F. Rohrbach et al[28] who give a good discussion of the technical problems of streamer chamber construction.

In our system as well as most other streamer chamber systems, the applied voltage V_o is not a DC voltage. It is a pulse supplied by a Marx high voltage generator. The marx is shown schematically in Figure 4-2. It is essentially ten banks of capacitors which are charged in parallel through charging resistors and discharged in series through the spark gaps in the Marx tube. The system is charged by two high voltage power supplies to a maximum voltage of ± 25 KV. This gives the capability of voltages on the streamer chamber of up to 500 KV (10 stages x 2 polarities x 25 KV). The maximum repetition rate of the system is limited by the Marx charging time (∿ 100 msec) plus the time it takes the sparks in the Marx tube to quench (150-200 msec). Both of these times could be shortened but for the experiments we have considered this is unnecessary.

The Marx pulse, when applied to the intermediate conductor of the Blumlein line causes a spark gap to fire. There are three gaps which can be operated simultaneously, normally, however, only one was in use at any one time. This gap acts as the switch (A in Figure 4-1) which triggers the

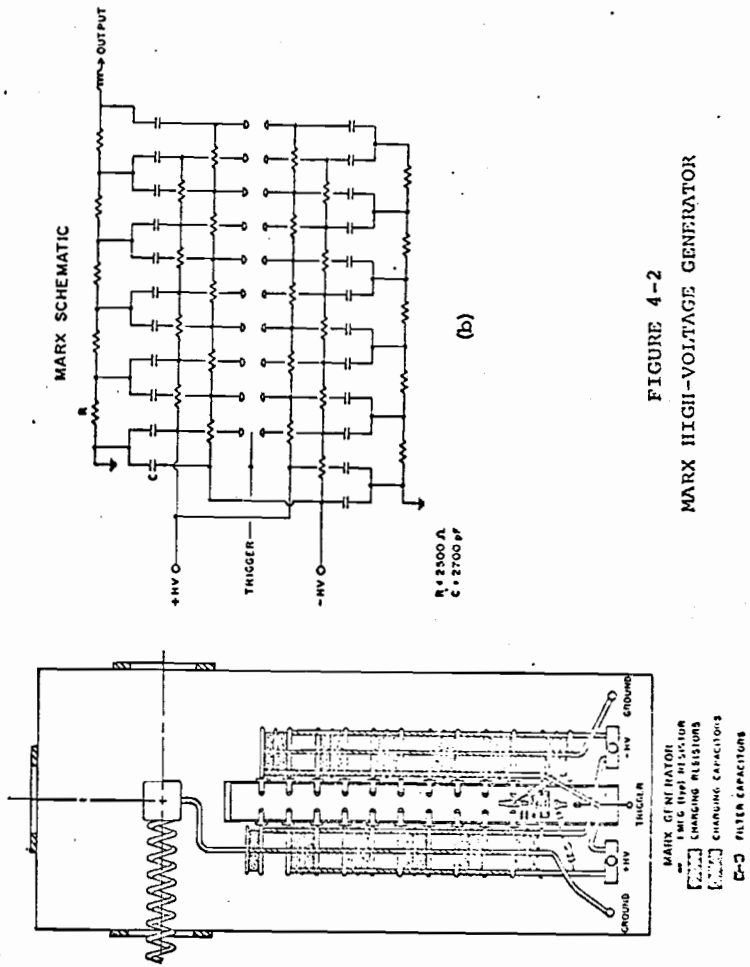

FIGURE 4-2
MARX HIGH-VOLTAGE GENERATOR

streamer chamber pulse. This pulse is transmitted into the streamer chamber by an oil-filled coaxial transmission line and an SF_6 filled transition section which makes the transition from the coaxial geometry of the Blumlein line to the strip geometry of the streamer chamber. These sections of the system, along with the streamer chamber itself, are shown in Figure 4-3.

Because this system was designed to be used with downstream spectrometer systems, great care was taken to minimize the amount of material inside and downstream of the chamber itself. This means that the high voltage pulse must enter the chamber from the upstream end. This in turn implies that a beam pipe capable of being evacuated must be incorporated into the coaxial and transition sections of the high voltage transmission line to minimize upstream interactions of the beam. Because of limited space, this beam pipe was only 3.2 cm inside diameter. The beam pipe extends approximately 2.5 cm into the visible volume of the streamer chamber. Normally, this pipe is sealed by a 13 μm thick mylar gas seal. But for the particle search, since we do not have a hydrogen target for this chamber, a Lucite target was mounted in the end of the beam pipe.

To veto residual upstream interactions, a large veto counter was incorporated into the design of the streamer chamber (W in Figure 4-3). This counter covered the full aperature of the streamer chamber and was mounted flush against the upstream end of the streamer chamber gas cell. It fit tightly to the outside of the beam pipe leaving a 3.8 cm diameter hole. This counter vetoed any particles entering the chamber except those inside of the beam pipe.

To minimize secondary interactions inside the chamber, stretched wire planes were used for the high voltage planes instead of the more

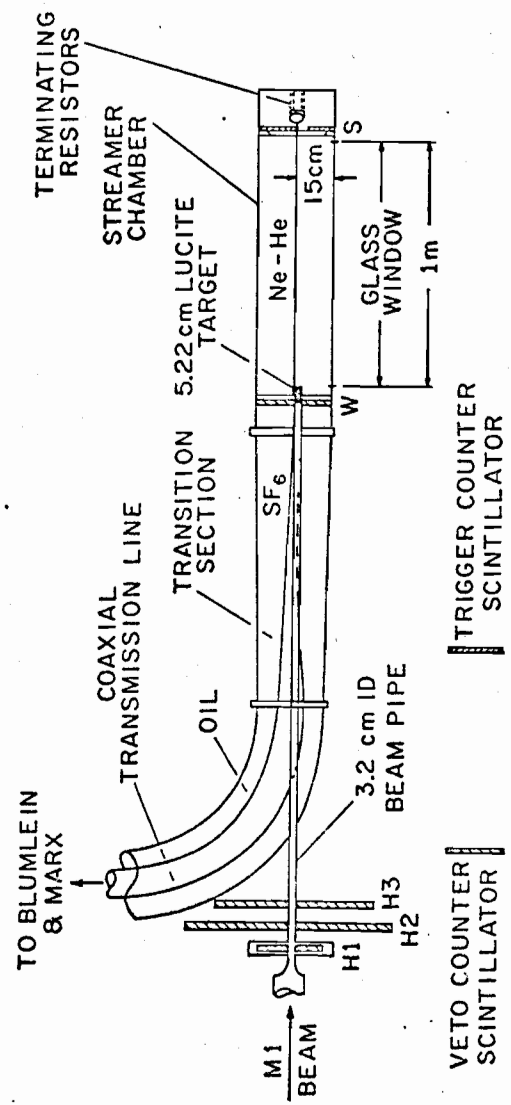

FIGURE 4-3
STREAMER CHAMBER

conventional wire mesh. This has the added advantage of minimizing diffraction of the light from the streamers. To minimize secondary interactions downstream of the chamber the amount of material at the chamber exit was kept to a minimum. In addition, a large trigger counter was built into the chamber just outside the gas cell (S in Figure 4-3). This counter was mounted against the downstream end of the gas cell and contained a 4.45 cm diameter hole to allow non-interacting beam particles to pass. A count from this counter, together with the absence of counts from the upstream veto counters, thus ensured that there had been an interaction inside the chamber. More detailed discussions of the design of the University of Washington's streamer chamber system have been given elsewhere.[29]

The delay between the Marx receiving a trigger pulse and the high voltage pulse being applied to the streamer chamber was found to be less than 500 nsec. Thus, even with extensive fast trigger logic, somewhat less than two microseconds was required from the time an interaction occurred inside the streamer chamber until the chamber actually fired. However, the lifetime of ions in pure Ne-He gas can be several hundred microseconds. Such a long "memory" time would severly limit the beam rates the chamber could accept. A method must therefore be found to decrease and control the lifetime of ions in the chamber. We found that introducing a few parts in 10^7 Sulfur Hexafloride (SF_6) to the Ne-He gas fill was adequate to reduce the chamber memory time to approximately 2 μsec. Since it is necessary to flow gas through the chamber at all times to continually purge oxygen from the system, SF_6 must be continually added to the pure gas. We found that the simplest and a completely adequate way to control the necessary concentration of SF_6 was to manually

control the two separate flow rates into a mixing chamber and thence into the streamer chamber. We purchased a single bottle of premixed Helium-SF_6 with 13 parts per million SF_6. We normally flow the Ne-He gas at 0.25-0.50 lit/min and the He-SF_6 mix at 5-10 cm^3/min. These flow rates are easily controlled using sensitive but commercially available flow meters. At these flow rates, a single bottle of the He-SF_6 mix has been used for several months of continuous flow. Using the very simple gas control system described above, we were able to reduce the memory time of the chamber to 2 μsec, allowing the chamber to accept up to 10^6 beam particles per second with an average of two beam tracks per picture.

The design parameters of the entire system are summarized in Table 4-2a and the chamber operating characteristics are listed in Table 4-2b.

The University of Washington's streamer chamber system described above is a very precise triggerable vertex detector with nearly 4π geometry. It can accept moderately high beam rates of 10^6 particles/sec. and has the capability of accepting four triggers/sec.

HIGH VOLTAGE SOURCE:	2-voltronics high voltage power supplies (type BPO 50-60, 50 KV-70 mA)
MARX:	Dual polarity
	10 stage
	27 nF capacitance/stage-0.27 μF total
SPARK GAPS:	Stainless steel-fixed separation ∿ 25 mm
MARX TUBE:	10 cm dia. Lucite, will withstand up to 5 Atm pressure
BLUMLEIN LINE:	Stainless steel & Lucite
	Coaxial 25Ω line, oil filled
	Conical in region of spark gaps, gas filled
SPARK GAPS:	Stainless steel-variable
	0-25 mm, will withstand ∿ 15 Atm gas pressure
STREAMER CHAMBER:	Dual 15 cm gaps
VISIBLE VOLUME:	30 x 50 x 100 cm^3
MAIN BODY:	1.2 cm Aluminum plate
WINDOW:	6 mm plate glass
HV WIRE PLANES:	.25 mm stainless steel wire, window plane
	.5 mm stainless steel wire, central plane
	2.5 mm separation
GAS CELL:	2.5 cm Lucite, upstream and sides 0.25 cm downstream
TERMINATION:	6-8 carbon resistors (25Ω total)
BEAM PIPE:	3.2 cm ID, 0.3 cm wall Lucite and Stainless steel
W-VETO COUNTERS:	6 mm Scintillator 50 x 30 cm^2 3.8 cm hole
S-TRIGGER COUNTERS:	6 mm Scintillator 50 x 30 cm^2 4.45 cm hole

TABLE 4-2a

STREAMER CHAMBER DESIGN PARAMETERS

MARX:	
High Voltage:	± 20 KV
Spark Gap Pressure:	3 Atm N_2
BLUMLEIN LINE:	
Spark Gap Separation:	16 mm
Spark Gap Pressure:	13.5 Atm
STREAMER CHAMBER:	
Gas:	Ne-He (90-10) + 2×10^{-7} SF_6 (0.25 lit/min flow) at 1 Atm
HV:	375 KV = 25 KV/cm
Beam Pipe:	Air at 1 Atm

TABLE 4-2b

STREAMER CHAMBER OPERATING PARAMETERS

(ALL VALUES ARE TYPICAL)

V. EXPERIMENTAL APPARATUS

At the time that the ψ was discovered, we were assembling and testing our streamer chamber system in the Fermilab's M1 beam line[30] in the Meson Detector Building. We were thus in a position to install the particle search experiment very quickly.

The apparatus used for this search consisted of a beam defining section where great care was taken to get a good, very compact beam onto the experimental target and to veto wide angle beam associated backgrounds. The primary detector was a one meter streamer chamber housed in a large momentum analyzing magnet with its data recorded on high-speed film. The trigger was supplied by the counters built into the streamer chamber which guaranteed that an interaction occurred in the chamber and by eight muon telescopes which were downstream of 5 meters of iron and lead, part of which could be magnetized. The apparatus also included a small calorimeter to measure hadronic punch through in the muon trigger, and six planes of wire spark chambers which allowed us to collect data on the muons which supplied the trigger.

The M1 beam is a high energy, high resolution beam which collects secondary particles produced in a production target at angles near 3.5 mr and is capable of moderate secondary beam fluxes greater than 10^6 particles/sec. The beam line is shown schematically in Figure 5-1a.[30] The beam envelope obtained with our beam tune is shown in Figure 5-1b.[31] The beam is initially gathered and steered away from the forward direction by a series of three Half-Quadrupole magnets and three Septum-Dipole magnets. Half-Quad magnets are Quadrapole magnets which have been split longitudinally. Two of the magnetic poles are replaced by an iron plate. These half magnets are necessary because six beam lines use the meson production target. All collect particles produced within a few milliradians of the forward direction

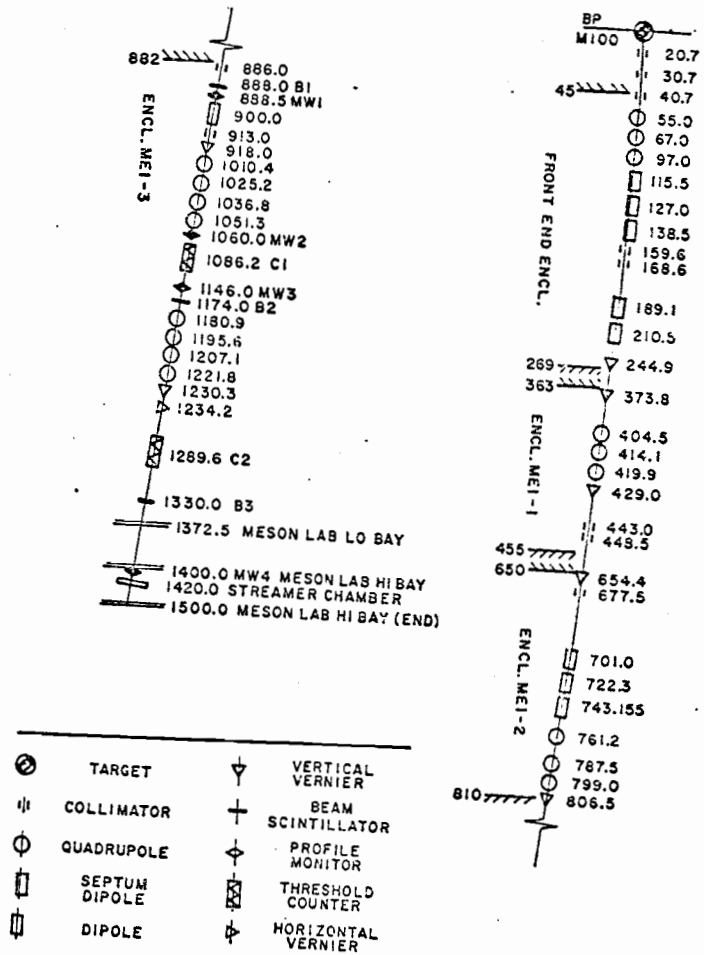

FIGURE 5-1a

FERMILAB'S M1 BEAM LINE SCHEMATIC,
A HIGH ENERGY - HIGH INTENSITY BEAM PRODUCED AT 3.5 mr

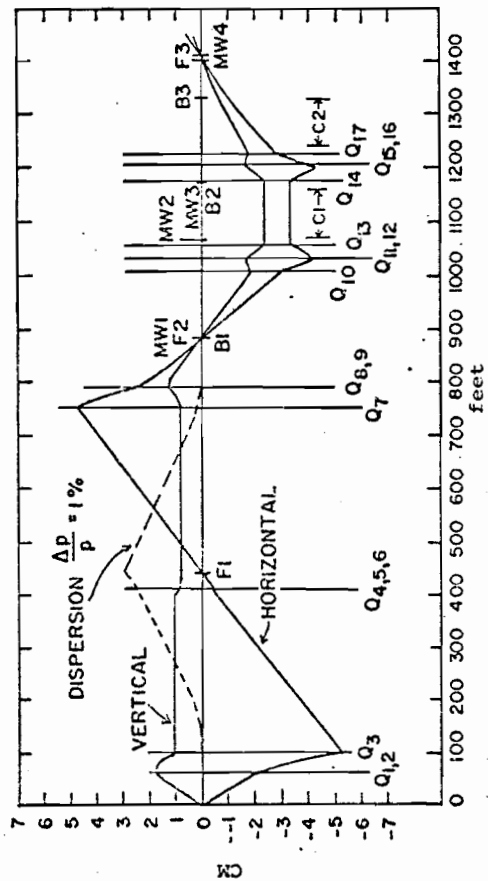

FIGURE 5-1b

BEAM ENVELOPE OBTAINED IN FERMILAB'S M1 BEAM LINE

so the area just in front of the production target is very congested.

These magnets and two following dipole magnets momentum disperse the beam. The momentum dispersed beam is focused in the horizontal plane onto the momentum slit at F1 in Figure 5-1b. This slit picks out the momentum and the momentum "bite" ($\Delta p/p$) desired. The section of the beam line between F1 and F2 recombine the beam and focus it in both planes at F2. It is then taken to a parallel focus in the region between 1050 and 1175 feet. This section contains the first of two threshold Cherenkov counters (C1). In our experiment, the last group of quadrupoles were set to focus the beam at F3, inside the streamer chamber. The second of the Cherenkov counters (C2) is located in this last section of the beam line.

We ran the experiment with a 225 GeV/c negative beam. The species of beam particle was determined by the two upstream threshold Cherenkov counters. Both counters were operated just above the pion threshold. By requiring both counters to have fired, we obtain a very pure pion beam. However, inefficiencies in the counters and our very conservative threshold setting did not allow us to obtain a pure kaon beam. The counters both registered pions for only 85% of the beam. An earlier experiment[32] performed a careful study of the particle species fractions in this beam. Extrapolating their curve for 300 GeV/c incident protons to 225 GeV/c secondaries and correcting for decays in flight, we expect that only 1.5% of the beam is K^-.

The beam was defined by three upstream scintillation counters. The position of these are shown on the beam line schematic, Figure 5-1a, and in Figure 5-1b. They are labeled B1, B2, and B3 respectively. Pulse height analysis was performed on the last beam scintillation counter signal (B3) to discriminate against multiparticle RF "buckets", upstream

interactions and interactions in this scintillator. Beam halo was vetoed by a series of hole anticounters which covered the entire aperature of the detection system. These are labeled H1, H2, and H3 and W in Figure 5-2 which also shows the rest of the apparatus. The W counter was located inside the body of the streamer chamber and was discussed in the previous chapter. H2 and H3 were large counters surrounding the beam pipe just upstream of the point where the beam pipe entered the high voltage transmission line. H1 was a small counter built into the beam pipe, extending through the pipe's walls. It had a hole 2.5 cm in diameter and thus formed the final aperature for the beam into the system.

Because the beam entered the streamer chamber through the 3.2 cm inside diameter beam pipe, it was necessary to hold a very good beam "tune". Therefore, we made continuous use of Fermilab's beam monitoring multiwire proportional chambers (MWPC), the so-called "Type A" chambers. These are small chambers with 2 mm wire spacing. Signals from each wire are individually scaled during a beam spill, thus integrating over the spill. These scalars could be read and displayed using the Meson Lab's beam control computer. We had four pairs of wire chambers placed at the points marked MW1, MW2, MW3, MW4 in Figure 5-1a and b. In addition, we placed another pair of small MWPC's at MW4. These chambers had 1 mm wire spacing and could be read into this experiment's data collection system. Using these beam monitoring chambers, we were able to attain and maintain a beam at the streamer chamber which was only 7 mm in diameter, full width at half maximum, a size which could easily pass through the beam pipe with only a small probability of interacting in the walls of the beam pipe.

The streamer chamber was mounted inside of a large momentum analyzing magnet. This magnet was run with approximately an eight kilogauss magnetic

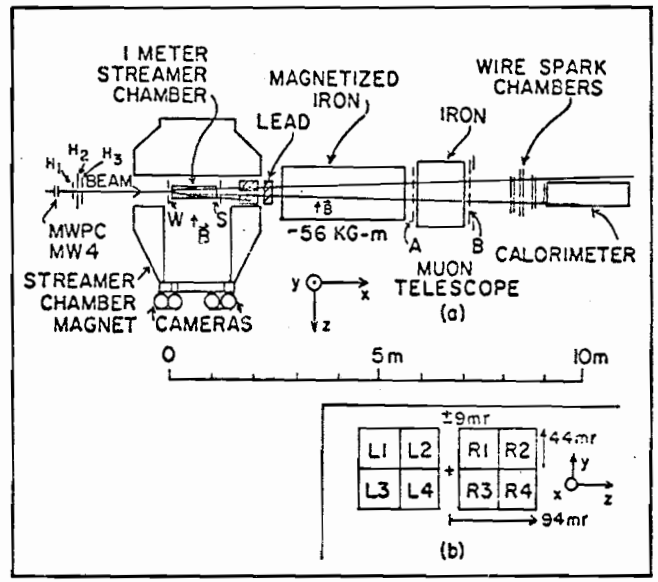

FIGURE 5-2

PARTICLE SEARCH APPARATUS
a) Plan View of Apparatus
b) Muon Telescope Layout

field for this experiment. The cameras for recording data from the streamer chamber were mounted on the magnet approximately 2.5 meters from the chamber's center line. The three cameras viewed the chamber through one of the magnet coils with a maximum stereo angle of approximately 15°.

Downstream of the streamer chamber was the muon spectrometer. This was composed of 5 meters (29 absorbtion lengths) of lead and iron absorber and eight muon telescopes. There were two telescopes in each quadrant around the beam, covering laboratory angles from 9 to 94 milliradians horizontally and from 2 to 44 milliradians vertically. 91 milliradians in the lab corresponds to 90° in the center of mass at this beam energy. The telescope layout is shown in the insert of Figure 5-2. The absorber was placed as close to the target as possible, the first 40 cm of lead was inside the streamer chamber magnet, starting 150 cm from the target. This lead block had a 10 cm square hole through it, centered on the beam. This was necessary to reduce triggers from backscatters to an acceptable level.

Outside of the magnet was a solid 31 cm thick block of lead. Downstream of this block there was a 3 meter section of magnetized iron (the SOD magnet). This magnet was capable of 50 ± 10 Kg-m of bending power, which served to bend low momentum hadrons from the hadronic shower, and muons from pion and kaon decay out of our acceptance. Both the streamer chamber magnet and the SOD magnet bend in the vertical plane. Data samples were collected both with and without the iron magnetized.

The SOD magnet was followed by the eight muon telescopes. The telescopes were composed of scintillation counters in two planes separated by 1.2 meters of iron. Corresponding scintillators in the two planes subtended nearly the same solid angle at the target. By placing corresponding counters in the two planes in coincidence, we required the triggering particle to have

come from the approximate direction of the target. A 10 cm vertical gap was left to eliminate beam muons and very low mass dimuons produced in the forward direction from the trigger. Since both of the magnets bend in the vertical plane, these muons passed, unseen, through the vertical gap.

Downstream of the telescopes we placed three 1 x 1 m^2 spark chambers each having two wire planes. These were intended mostly to monitor background triggers. When the iron was magnetized, we were able to determine the muon momentum by assuming they originated in the target and determining from the spark chambers the track's curvature through the iron. We could also determine approximately where the tracks originated by extrapolating the tracks back toward the target in the non-bending plane. These points will be discussed in more detail in a later chapter.

Behind the wire chambers was placed a calorimeter to measure hadronic punch-through in the trigger. The calorimeter covered the central area around the beam. It was 46 x 46 cm^2, of which only the central 30 x 30 cm^2 was used, and was composed of 24 stages with 3.8 cm of iron alternating with 5 cm of scintillator. We found,[33] even with the magnetized iron off that hadronic punch-through was negligible.

Parts of this apparatus were supplied by each of the collaborators and by Fermilab. The streamer chamber and its electronics and the wire chambers were supplied by Seattle. The high-speed cameras and the large momentum-analyzing magnet were supplied by Orsay. The calorimeter and the muon telescope scintillators came from Davis. The iron and lead for the absorber, including the iron for the SOD magnet, were supplied by Fermilab. The SOD magnet was built in a period of 10 days at Fermilab. The iron was machined by Fermilab, wound by the experimenters in one, all-night effort, and assembled by the experimenters with the able assistance

of the Meson Section personnel. All of this took place after the start of the experiment when political pressures kept us from magnetizing an available section of magnetizable iron.

In addition to the apparatus discussed above, the electronics, discussed in the next chapter, also came from several sources. Most of the fast electronics came from Fermilab's PREP stocks. The on-line computer for data collection was supplied by Seattle, although Fermilab kindly loaned us several modules which greatly increased the capabilities of the bare computer. Parts of the wire chamber and calorimeter read-out electronics were supplied by Seattle, Davis, and Fermilab. This experiment was truly a joint effort.

VI. TRIGGER ELECTRONICS AND DATA COLLECTION

The electronic signals from the various detectors discussed in the previous chapter were transmitted to a central counting room for processing. This area was less than 30 meters from the major pieces of apparatus, minimizing signal transmission delays. It was here that the signals were processed by fast NIM standard logic units and the decision to trigger the streamer chamber was made.

The basic trigger logic is sketched in Figures 6-1a-d. Figure 6-1a shows the Beam (B) and Event (E) definition logic. All scintillator signals, with the exception of the calorimeter signals, were first passed through threshold discriminators to suppress signals due to phototube noise and to shape the signals to NIM standard (0 to -0.7 volts). The beam definition was performed by first putting the beam telescope counters (B1, B2, and B3 in Figures 5-1) into coincidence, forming the Beam Telescope (BT) signal. An "OR" of the anti-counter signals (BA) was then put into anti-coincidence with BT forming the beam definition (B). This "OR" was formed in steps so that the partial "OR's" could be used for beam diagnostics. One scintillator, B3, was used as both a positive counter and an anti-counter. This counter was the last of the three beam telescope counters. Two signals were taken from B3. One signal, B3L, was put through a discriminator which was set to accept a signal corresponding to one or more minimum-ionizing particles. This was the positive signal, input to BT. The second signal, B3H, was passed through a discriminator which was set to accept only signals corresponding to two or more particles. The output of this discriminator was used to veto multi-particle RF "buckets", upstream inelastic interactions, and interactions in B3 itself.

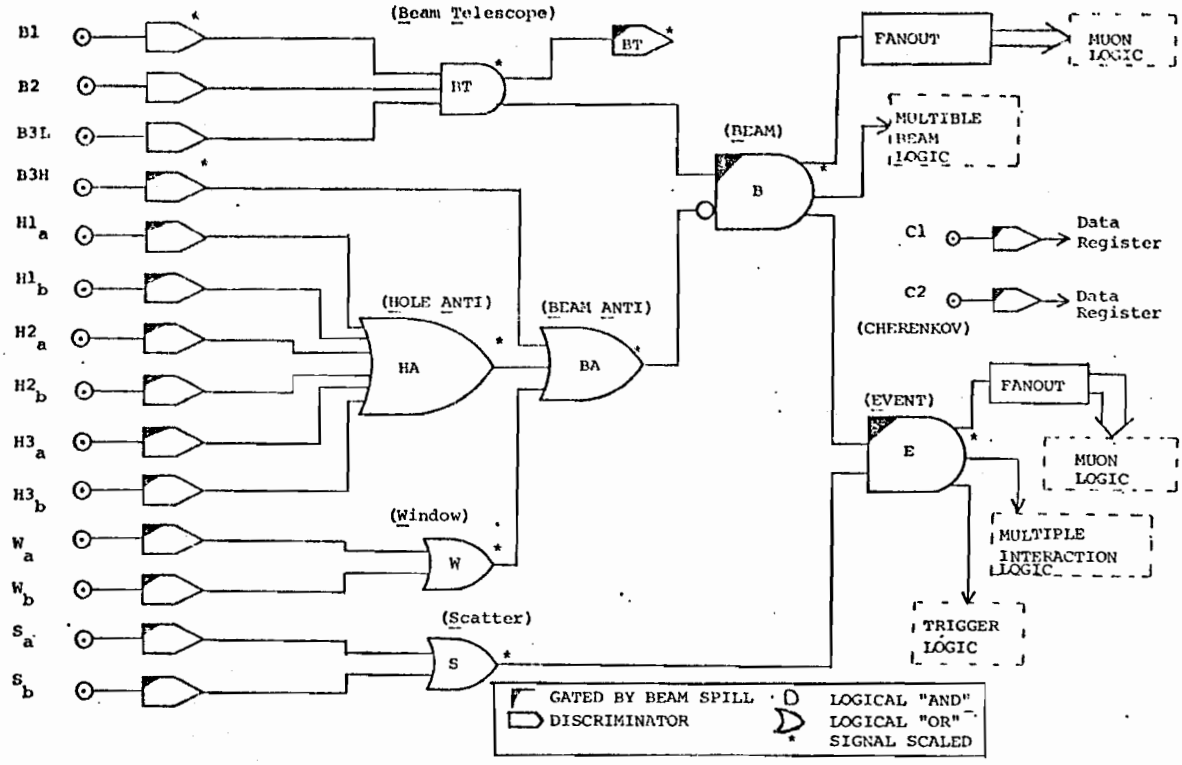

FIGURE 6-1a
BEAM/EVENT LOGIC

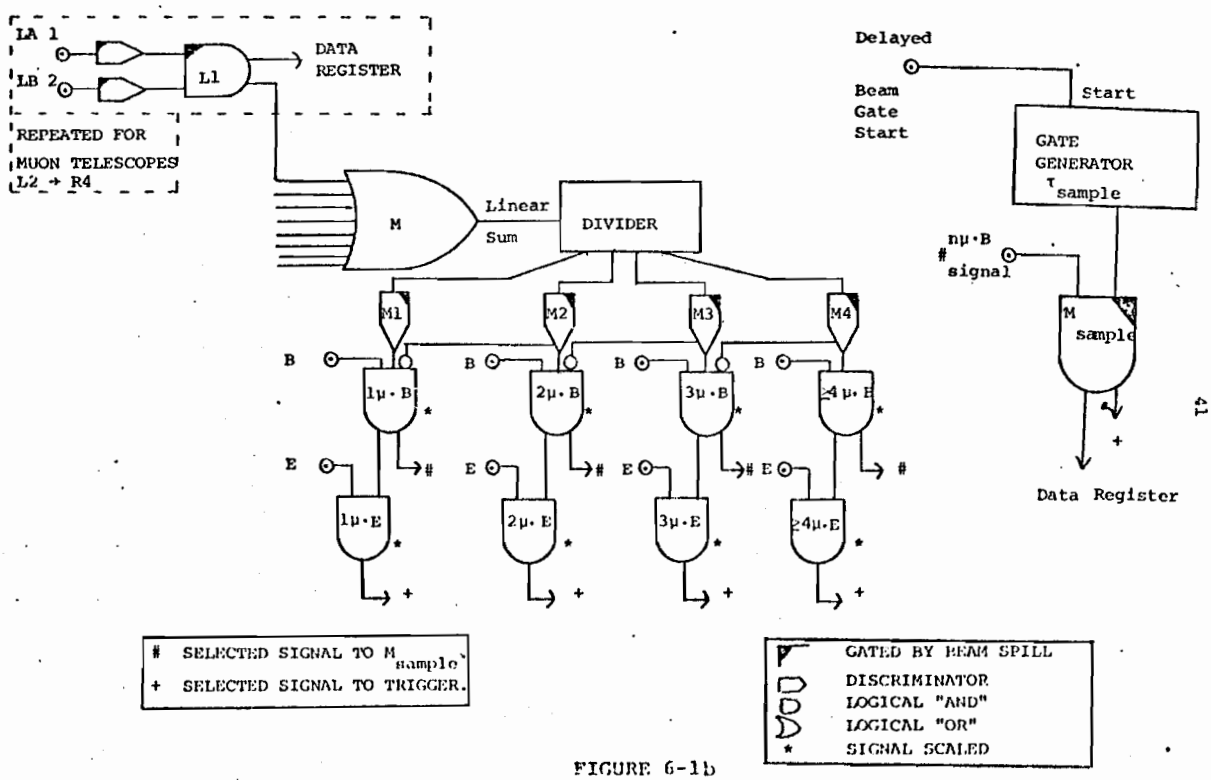

FIGURE 6-1b
MUON LOGIC

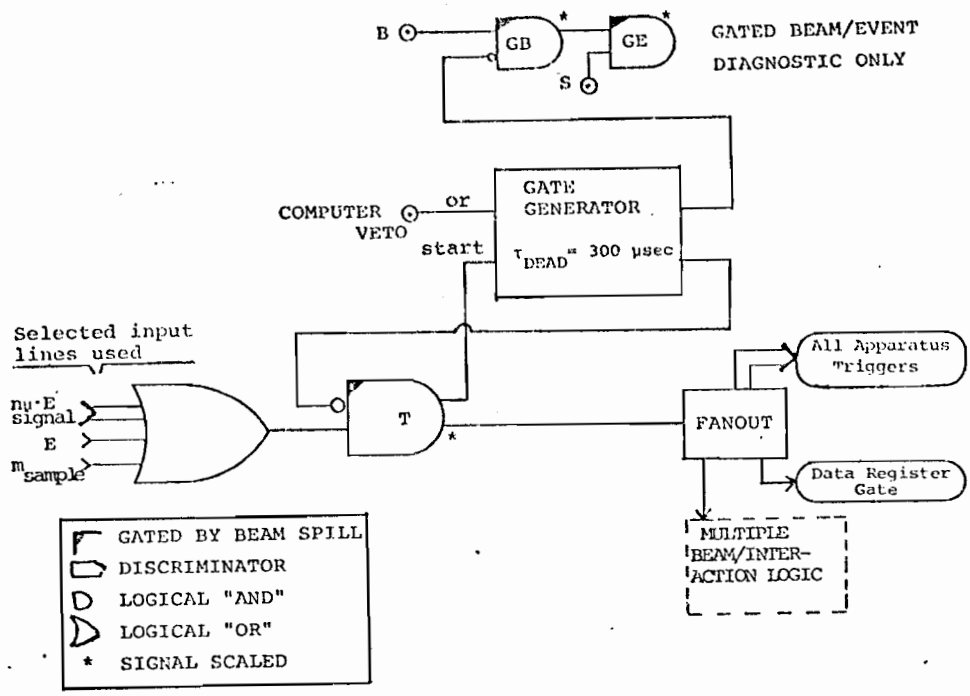

FIGURE 6-1c

FINAL TRIGGER/DEADTIME LOGIC

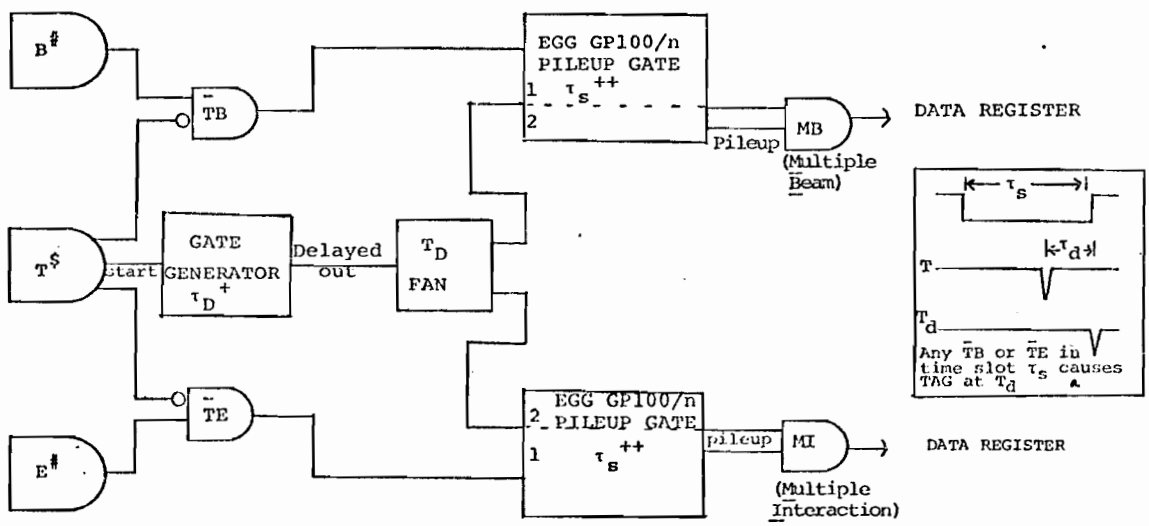

+ τ_D =	Time delay between trigger signal leaving counting room and high voltage being applied to the streamer chamber (≲ 500 ns).
++ τ_s =	Steamer chamber sensitive time (∼ 2μsec).
#	See Figure 6-1a.
$	See Figure 6-1c.

FIGURE 6-1d

MULTIPLE BEAM/INTERACTION LOGIC

The beam definition was then: $B \equiv B1 \cdot B2 \cdot B3L \cdot \overline{(B3H+H1+H2+H3+W)}$ (refer to Figures 4-3, 5-1, and 5-2 for counter positions), where the bar implies the logical "NOT". This definition guaranteed that a beam particle entered the region of the target with at most a small angle elastic scatter upstream. The Cherenkov counters were not included in the beam definition. We felt that there might be something to be learned by comparing events from the pure pion beam with those from the enriched kaon beam. The Cherenkov counter signals were, therefore, input to a data register, gated by the final trigger, for storage.

By adding the requirement that the downstream "scatter" counter (S in Figures 4-3 and 5-2) had fired in coincidence with a beam particle, we guaranteed that an interaction or "event" had occurred inside of the streamer chamber. The event trigger was then: $E \equiv B \cdot S$. These events supplied the primary trigger for the system. Samples of these triggers were taken at intervals throughout the run to act as a control sample for the muon triggers.

Because we ran with up to 8×10^5 beam particles per 800 msec beam spill, with a streamer chamber memory time of nearly 2 μsec, we often had two or more beam tracks visible in the streamer chamber in one picture. Thus, when a interaction occurred with two incident beam particles, the extra track sometimes could not be separated from the secondary tracks from the interaction. Recall that the beam was only 7 mm full width, half height. The same is true when two interactions occurred during the memory time of the streamer chamber. It is not possible to veto an event when such extra beams or interactions occurred during the nearly 500 nsec between the time that the trigger signal left the counting room and the high-voltage pulse was applied to the streamer

chamber. We, therefore, decided to accept all such second beam and second interaction events. But they were tagged so that if necessary, we could delete them from the data samples at a later time. Figure 6-1d shows the circuits used to determine and tag these occurrences.

To the beam and basic event information discussed above must be added the information from the downstream muon spectrometer. The logic for gathering this information is shown in Figure 6-1b. Each of the signals from the sixteen muon counters was passed through the usual pulse height discriminator and then the signals from corresponding counters in the two counter planes were put into coincidence. A muon was defined as a particle which gave a count in both scintillators of one of the eight telescopes. The geometry of the system was such that these particles must originate in the general direction of the target, and thus had to pass through all 5 meters of absorber.

The number of muon telescopes which fired was determined by linearly adding the NIM standard outputs of each of the eight telescope coincidence units and pulse height analyzing the result. The pulse height analysis was done by simply fanning the summed signal out to four threshold disciminators whose thresholds were set to accept one, two, three, and four times the NIM standard pulse height. These signals were put into coincidence with the beam signal (B), and with the event signal (E). Each of the higher level discriminator units was used to veto the next lower level coincidence unit. The outputs of these coincidence units then corresponded to one, two, three, and four or more muons in coincidence with a beam particle or with an event in the streamer chamber.

Any one, or any combination, of the muon requirements discussed above could be used for the streamer chamber trigger. When two or more

muons were required, the data rates were so low that we were able to simultaneously use the "nμ·B" triggers. These were identical to the nμ·E triggers except that the S counter requirement was absent. The primary interactions from these "nμ·B" triggers were mostly in the muon shield, but from the fraction of those which did interact in the target we gain information on the true trigger cross section without the added complication of the hole in the "scatter" counter. In addition, the spark chamber and calorimeter data from these triggers has proven invaluable in determining the source of the muons in the normal "nμ·E" triggers. Because "nμ·B" triggers were much more frequent than the equivalent "nμ·E" triggers, due to the target thickness, the "nμ·B" trigger was gated on for only a fraction of the beam spill, using the Muon Sample circuit in Figure 6-1b. This kept the system deadtime from accepting these triggers at an acceptable level. The outputs of each of the muon telescopes, as well as the muon sample output were input to the data register. Thus, for each trigger we had available, complete information on which counter, or counters had participated, and whether it was a beam (B) or an event (E) type trigger.

Depending on the particular trigger, or triggers we were currently accepting, various of these "nμ·E" or sampled "nμ·B" triggers were input to the final trigger and gating logic pictured in Figure 6-1c. The various timing gates necessary for our system added a slight complication to the trigger electronics. All of the counters in the trigger (except for the beam telescope counters mentioned earlier) were first gated by the beam spill. In order to avoid problems associated with structure in the beam spill, we gated off the first and last 100 msec of the spill where the instantaneous beam rates were sometimes very high. This left

800 msec of the 1 sec spill available for data taking. In addition, the trigger had to be gated off to allow time for the Marx to recharge, the cameras to advance, and the computer to process the data. The Marx deadtime was supplied by a fixed length, 300 msec, pulse generator. The camera and computer deadtimes were supplied by the computer which checked the status of the cameras and only turned off its trigger veto when the cameras were ready and it was ready to receive more data. The camera and computer deadtimes were much shorter than the Marx deadtime (150-200 msec for the cameras and computer versus 300 msec for the Marx). It was necessary to know what effect these deadtimes had on the rates. We, therefore, set up parallel circuits for some of the trigger electronics, giving rate information both with and without these long deadtimes.

In order to continuously monitor the system performance, various scintillator signals and combinations of signals (those marked by * in Figures 6-1) were scaled by CAMAC-compatible, 50 MHz blind scalars. These were displayed using an LRS Type 72 display system. We thus had available continuously updated information on counter performance, beam transmission fractions, beam rates, and event rates.

The pulses from the calorimeter scintillators were fed directly into 12 bit Analog-to-Digital Convertors (ADC). These were CAMAC compatible ADC units which were gated by the streamer chamber trigger pulse. The spark chambers' magnetostrictive delay line signals were input to a Science Accessary Corporation, CAMAC-compatible scalar system which performed the necessary Time-to-Digital conversion (TDC). The ADC and TDC data for each event as well as the MWPC registers and the data registers were read by an on-line Digital Equipment Corporation PDP 11/20 computer. The computer was programmed to histogram the various pieces of

could be displayed at will on a Tektronix type 611 storage oscilloscope. A running summary of the experiment was thus available. The computer also output the data register information as well as data run, film roll, and picture frame numbers to a binary data box attached to the streamer chamber. This data was imprinted on the film before the computer ordered the cameras to advance the film in preparation for the next event. The computer also wrote all of the data collected for each event onto magnetic tape. Once each spill it also read in and wrote out the current scalar readings. Flow diagrams of the computer program are shown in Figures 6-2a-c.

The electronics described in this chapter gave us very tight control and extensive diagnostics of every portion of the experimental apparatus. The diagnostics, as well as the spark chamber and the calorimeter data, were continuously available during the run and all electronic information has been permanently stored on magnetic tape so that it can be correlated with the data stored on the film.

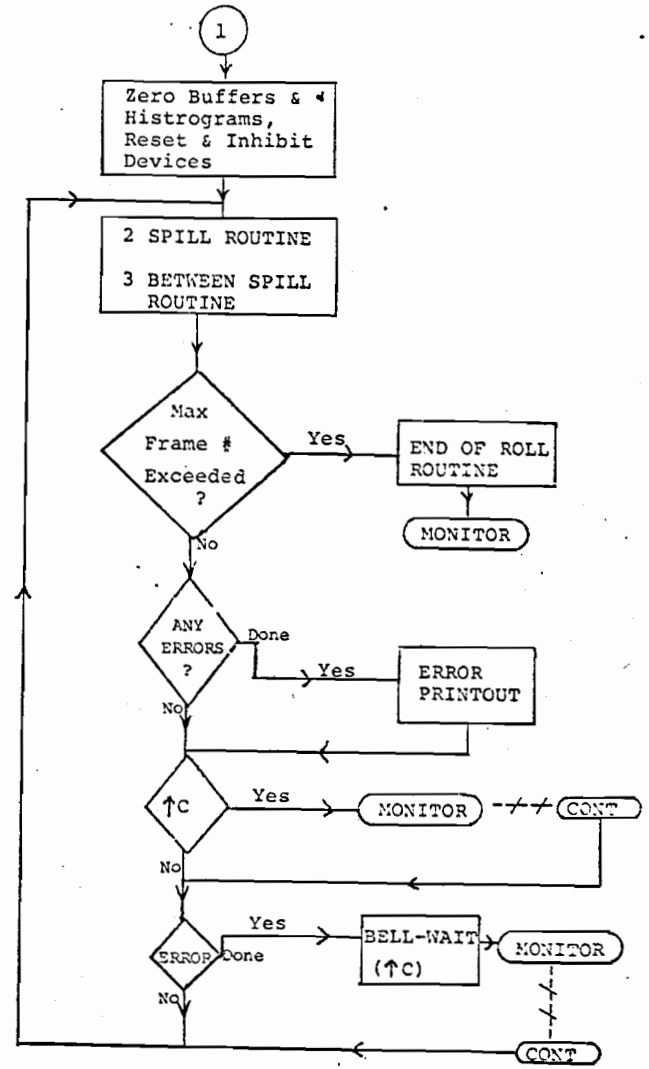

FIGURE 6-2a

CONTROL ROUTINE FLOW DIAGRAM

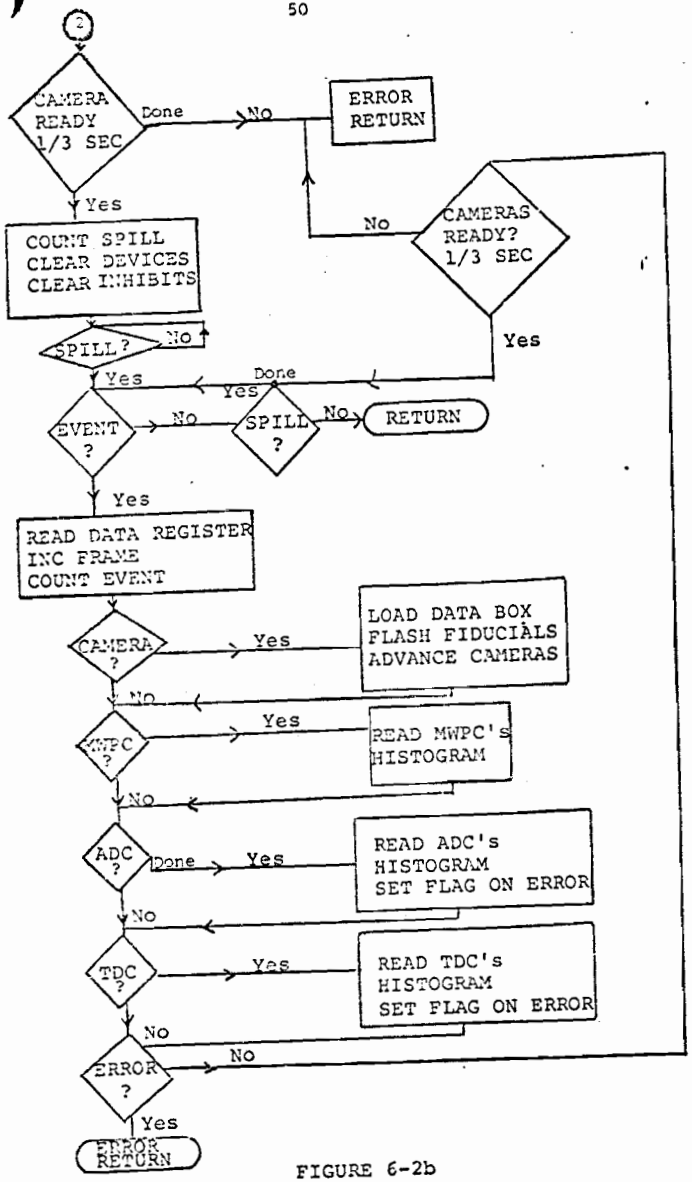

FIGURE 6-2b

SPILL ROUTINE FLOW DIAGRAM

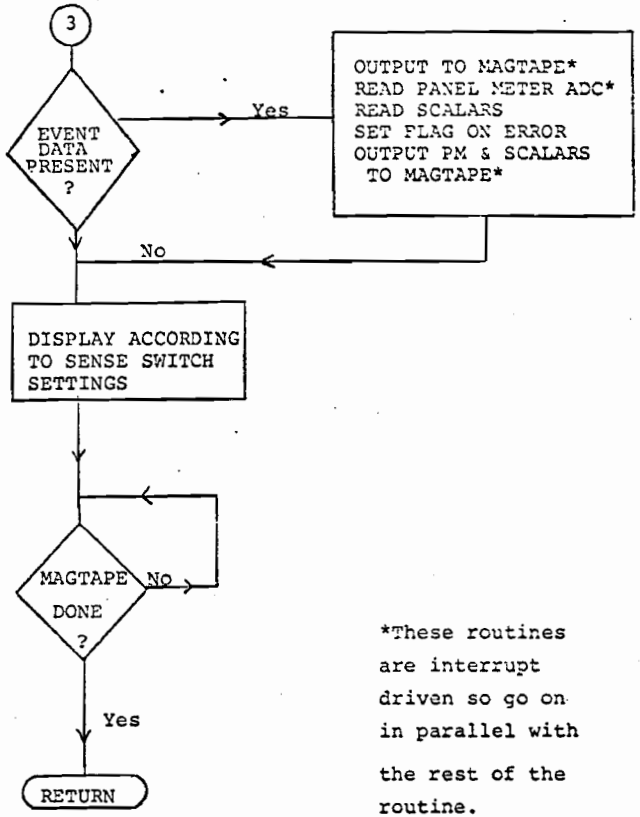

*These routines are interrupt driven so go on in parallel with the rest of the routine.

FIGURE 6-2c

BETWEEN BEAM SPILL ROUTINE FLOW DIAGRAM

VII. MEASUREMENTS AND BACKGROUND

The apparatus and the trigger electronics discussed in the previous chapters were very good at picking out the type of event in which we were interested, that is, an event in the target, with or without muons. But as is always the case, they were not perfect. There are many background signals present which they could not filter out.

Before I consider the question of background signals, it is necessary to discuss briefly just what measurements were made and how they were made. As was discussed in the previous chapter, the occurrence of any of the possible trigger conditions was scaled and recorded on magnetic tape. We, therefore, have a record of the number of beam particles (B) entering the target region, the number of interactions in the chamber (E), and the number of n muon events in coincidence with either a beam or an event ($n\mu \cdot B$ and $n\mu \cdot E$) as a function of operating conditions. In addition, we have the spark chamber data which can provide information on the sign and momentum of some of the muons; the calorimeter data which can, for a small fraction of triggers tell us that we did, in fact, have a muon trigger; and most importantly, we have the streamer chamber data on film. We took some pictures with each of the triggers mentioned above (except for the $1\mu \cdot B$). We therefore have full data from each of them.

Since the film contains the largest store of information from the experiment, it has been scanned with considerable care. All of the film taken after we were sure of our triggers has been scanned twice by the scanning staffs at the three collaborating institutions. A portion of the film (with the SOD magnet on) has been independently scanned at all three institutions. The scanners were instructed to carefully search each picture for neutral decays, either gammas or neutral strange particles (V°'s). These were recorded as such. When any doubt existed as to

whether a pair of tracks was, in fact, a V° or gamma, it was recorded as a doubtful. These are not included in the final data sample but were useful in keeping the search effort high. For the purpose of the scan, a gamma was defined as a neutral V with minimum-ionizing tracks where one or both had curvatures greater than that of a 250 MeV particle. Positive, heavily ionizing tracks with momentum greater than 500 MeV/c were noted. These are good candidates for Lambda's. Data pertinent to the primary interaction were also recorded. These data included the number of fast tracks from the primary; the presence of any fast, dark tracks which are probably nuclear fragments; and the presence of any electrons or positrons coming from the primary vertex. Nuclear fragments and electrons or positrons were not counted in the charge multiplicity. In addition, if a given frame was not scanned, the scanners recorded the reason. After the completion of the two complete scans, the scans were compared and any disagreement was resolved by a physicist. It is the data of this resolved, double scan which is the basis of all of our results.

Figure 7-1 shows two frames of our streamer chamber film. These are fairly typical of the film scanned. You will note from these one of the biggest problems our scanners had. Because of the very large number of tracks present and the relatively small (8 KG) field, the density of tracks in the forward direction is very high. Often the scanners could not tell precisely how many fast tracks there were in a given event. When the differences between the two scans were resolved, a one-track disagreement was allowed. In this case, the track count was arbitrarily taken from the second of the two scans. A larger discrepancy than this was resolved by a physicist.

Before we continue, I would like to make one very important point. Since ultimately we will be calculating the cross section for charm

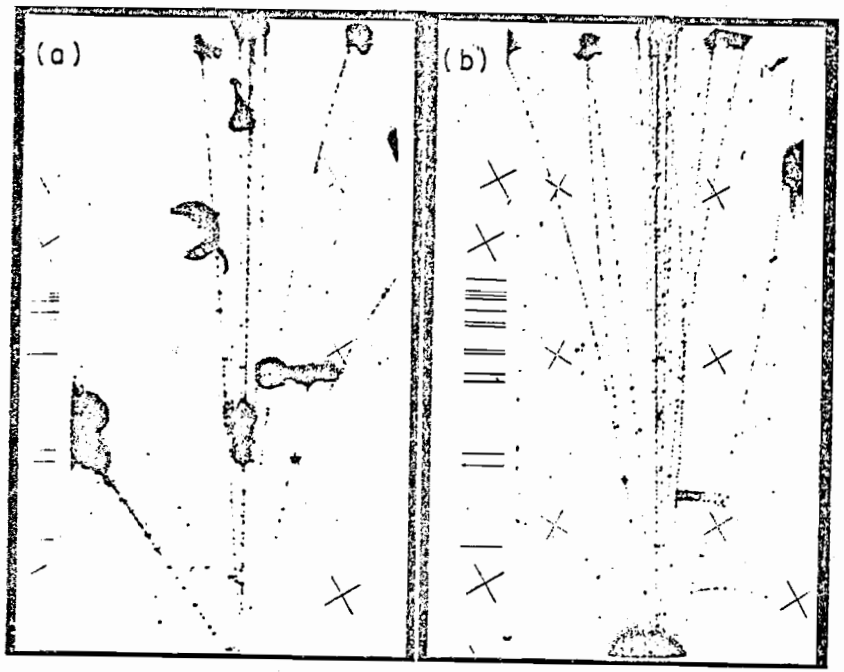

FIGURE 7-1

EXAMPLE OF FILM TAKEN WITH THE STREAMER CHAMBER

a) 9-prong event with V°

b) 17-prong event with 2 V°'s plus a secondary interaction

production by comparing the dimuon (2μ·E) triggers with the E trigger, the errors which are quoted for the quantities measured during the film scans are the statistical errors only. The major strength of this experiment is that we can use such a direct comparison and are, therefore, insensitive to systematic effects. Although there are doubtlessly large systematic effects in the number of neutral decays found, the number of charged tracks counted, as was mentioned above, and even in which pictures were kept, or rejected, it was fairly easy to make certain that whatever biases were present were the same for the different data samples, independent of the trigger. Since the triggers were mixed on the same rolls of film, both to reduce differences due to operating conditions and to improve data taking efficiency by taking multiple triggers simultaneously, the scanners did not know which trigger resulted in a given picture. Thus, no psychological biases could enter the scan. It will also be shown that picture quality, as measured by rejected frames, did not vary a great deal between the triggers, except for the 2μ·B trigger. Because this trigger produced pictures which primarily contained only beam tracks, it was a special problem.

From the double, resolved scan we obtain the efficiency for obtaining pictures of events which occurred in the target. This data is summarized in Table 7-1. The reject types listed in this table are broken down by trigger or roll subgroups only if they vary significantly with one of these. You will notice that the streamer chamber was very efficient. The fraction of blank or very faint frames was 11% early in the run but decreased to only 3% at the end. The "beam only" triggers listed in Table 7-1 were caused by the beam interacting in the material downstream of the chamber with a "backscattered" secondary entering the S

REJECTED PICTURE TYPE	FRACTION OF TOTAL	TRIGGER	ROLLS
Old Tracks†	.139 ± .004	All	All
Upstream††	.060 ± .002	All	All
Close Second*	.011 ± .001	All	All
Downstream**	.004 ± .001	All	All
Beam only⊖	.106 ± .004	All (except 2μ·B)	All
Beam only⊖	.111 ± .006	E	All
Beam only⊖	.104 ± .015	2μ·E (non-SOD)	All
Beam only⊖	.157 ± .012	2μ·E (SOD)	All
Beam only⊖	.176 ± .033	3μ·E	All
Beam only⊖	.093 ± .016	1μ·E (SOD)	All
Blank‡	.114 ± .007	All	Non-SOD
Blank‡	.098 ± .008	All	SOD (early)
Blank‡	.047 ± .004	All	SOD (middle)
Blank‡	.031 ± .004	All	SOD (late)

† Many tracks with large gaps indicating they are old, may or may not also contain a "good" interaction.

†† Primary interaction was upstream of the target.

* Two interactions in or near the target.

** Primary interaction downstream of the target.

⊖ Only beam tracks visible, no interaction.

‡ Blank or faint pictures.

TABLE 7-1

TARGETTING STUDY - STREAMER CHAMBER EFFICIENCY

counter. These show a variation with the trigger. The trigger with the highest probability of being due to pion decay (1μ·E) has fewer of these than does the E trigger while those with extremely small cross sections (2μ·E and 3μ·E) have more. From these numbers, we see that the overall system efficiency was rather high. The fraction of all pictures which were bright enough to scan, were not obscurred by old tracks, and had a single interaction in the target was near 60% throughout the run, varying only slightly by trigger.

By removing from this data sample those pictures where the scanners could not be sure whether or not an event had occurred in the target, we can determine how efficient the trigger apparatus was at choosing interactions in the target. This result is listed in Table 7-2 along with the raw trigger rates and the corrected "in target" trigger rates. You will note that these trigger efficiencies range from 70% for the 2μ·E (SOD) trigger to 85% for the 1μ·E (SOD), (neglecting the 3μ·E and 2μ·B triggers). This variation is caused mostly by variation in the number of "beam only" pictures. You will also notice that the dimuon trigger rates were very low. With the SOD magnet on, for example, we took one good 2μ·E picture each 15 beam spills (at 5×10^5 particles/spill), or on the average, one-half good picture per minute (8 spills/min).

Once a complete list of events was available, with the trigger responsible, and whether or not a V° was present, we went back to the film to garner more information about the events of interest. In particular, we wanted to know the position and momentum spectra of the V°'s found. The tracks of each of the V°'s and gammas found in the resolved double scan were manually digitized on an Image Plane Digitizer (IPD) with a setting error of approximately 10 μm on film which translates to 280 μm in space

TRIGGER	EFFICIENCY†,††	INTERACTION RATES #TRIG/B(RAW)††	#TRIG/B(CORRECTED)††
E	.79 ± .02	.0459	.036 ± .001
Non-SOD			
1μ·E	No pictures Assume .80	1.4×10^{-4}	1.13×10^{-4}
2μ·E	.80 ± .07	$9.0 \pm .3 \times 10^{-7}$	$7.2 \pm .7 \times 10^{-7}$
3μ·E	.83 ± .13	$2.0 \pm .4 \times 10^{-8}$	$1.7 \pm .4 \times 10^{-8}$
1μ·B	No pictures	$1.174 \pm .001 \times 10^{-3}$	-
2μ·B	No pictures	$17.5 \pm 1 \times 10^{-6}$	-
SOD			
1μ·E	.85 ± .07	3.51×10^{-5}	$3.0 \pm .2 \times 10^{-5}$
2μ·E	.70 ± .03	$1.87 \pm .05 \times 10^{-7}$	$1.31 \pm .07 \times 10^{-7}$
3μ·E	.51 ± .10	$1.50 \pm .3 \times 10^{-8}$	$7.6 \pm 2.1 \times 10^{-9}$
1μ·B	No pictures	0.420×10^{-3}	-
2μ·B	.112 ± .009	$8.08 \pm .003 \times 10^{-6}$	$9.0 \pm .7 \times 10^{-7}$
2μ·E corrected for muon origin			$0.72 \pm .08 \times 10^{-7}$

† Efficiency = (Good + Close Second Interaction)/(Total - Old - Beam Only)

†† Errors quoted are statistical only. If no error is quoted, the error is less than the last significant digit.

TABLE 7-2

TOTAL TARGETTING EFFICIENCY

for our cameras. Special care was taken to assure that the point measured at the V° or gamma vertex was the same point on all three views when the vertex was clear enough to allow this. These points were then reconstructed in space. This being the first time this optical system had been used and in the interest of getting a result quickly, we did not do a full-scale optical determination. Pin-hole optics was assumed. This is a reasonably good approximately for this system. These cameras were designed to minimize the distortion introduced by the camera lenses. This was done by tilting the film planes and optic axes of the lenses so that the axes of the cameras intersect approximately in the center of the streamer chamber, thereby making greater use of the center of the lenses than in an untilted system.

A feeling for the accuracy of the reconstruction may be gained by studying Figure 7-2. Figure 7-2a shows the reconstructed primary vertex position in the direction perpendicular to the beam and to the average optic axis (the y direction, the coordinant system used is shown in Figure 5-2). Figure 7-2b shows the same thing for the direction parallel to the average optic axis (the z direction). The peak in 7-2a has a half width of approximately 7 mm which reflects the width of the beam. The width in the z direction is nearly 20 mm. Two effects account for this broadening in addition to pin-hole optics assumption. The first is that since the primary vertex is inside the Lucite target, it is never visible. Thus, the measured vertex position on each view is an estimate by the scanners of where it actually is. Any errors in this estimation are seen primarily in the z direction due to the small stereo angle. The second contributing factor to the broadening in the z direction is the length of the streamers. We ran the streamer chamber with higher than normal voltage.

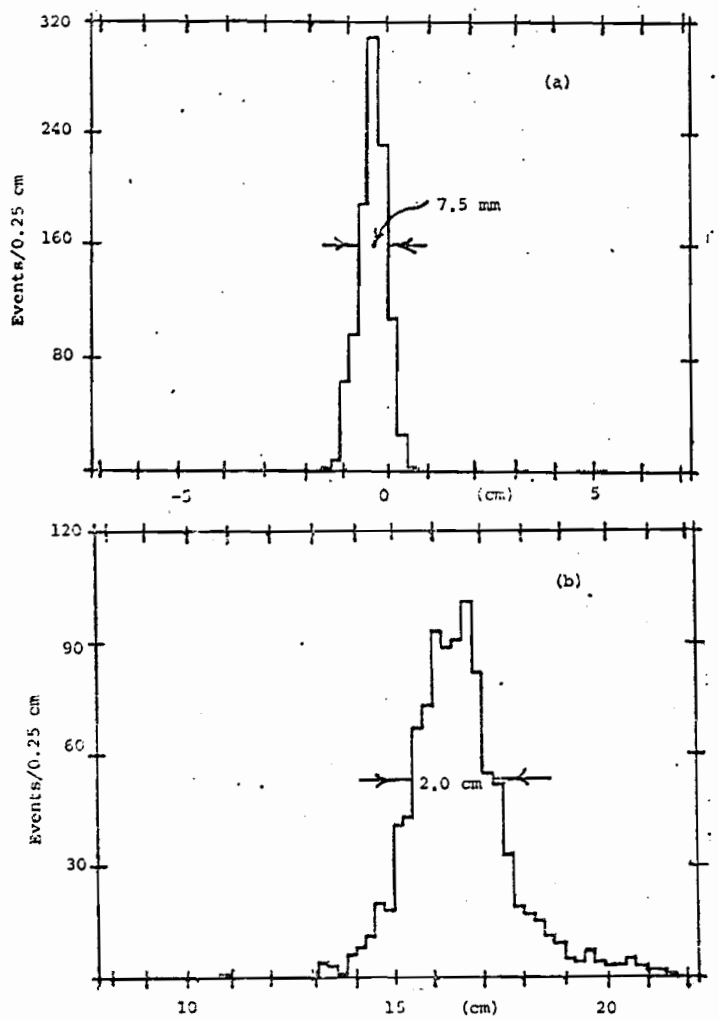

FIGURE 7-2

PRIMARY INTERACTION VERTEX RECONSTRUCTION

a) y direction, perpendicular to optic axes
b) z direction, parallel to optic axes

This gave us very bright streamers which made identification of V°'s easier at the expense of forming rather long streamers (2-3 cm), which since the electric field was in the z direction, adds a rather large uncertainty to the track position, in the z direction only.

Another way to study the precision of the reconstruction is to study the reconstructed position of identified gammas. Since the streamer chamber is gas filled, the probability of a gamma converting in the gas is virtually zero. However, the high-voltage wire plane in the center of the chamber provides sufficient mass to convert significant numbers of gammas. The gammas identified by the criteria given earlier should, therefore, be reconstructed on a plane at the z position of the central wire plane. This distribution for identified gammas is shown in Figure 7-3a and should be compared to 7-3b which is the same plot for the V° sample. The main peak in this distribution has a full width which is consistent with that found from the primary vertex. However, this distribution shows an appreciable tail. Comparing the position of this tail with the beam position, one sees that this tail is somehow connected with the beam, or the forward secondaries from the primary interactions.

In order to determine the origin of this tail, we once again turned to the film and carefully studied each of the 73 gammas in question. They had several origins;

i) Gammas with flares at the vertex. These flares were very bright areas caused by delta rays knocked out of the wires by the e^+e^- pair. This made it impossible to pick a corresponding point at the vertex. In such a case, the scanner was instructed to choose a point which could be identified in all three views and was as close as possible to the vertex. This point was most likely to be a point on one of the fast secondary

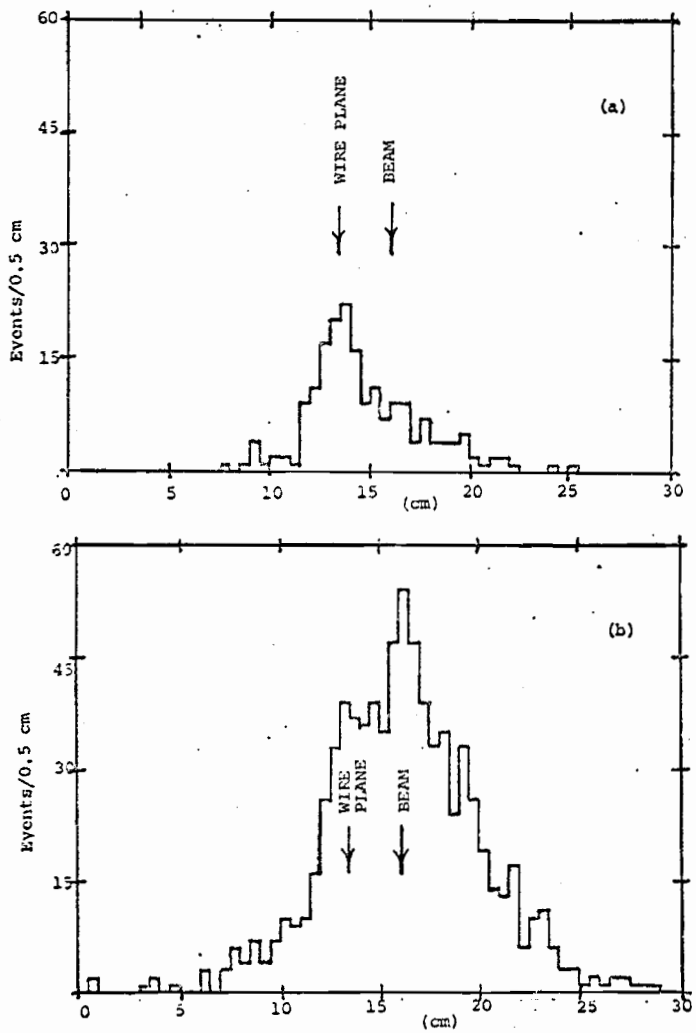

FIGURE 7-3

NEUTRAL DECAY VERTEX RECONSTRUCTION
a) Gammas, z coordinant
b) V°, z coordinant

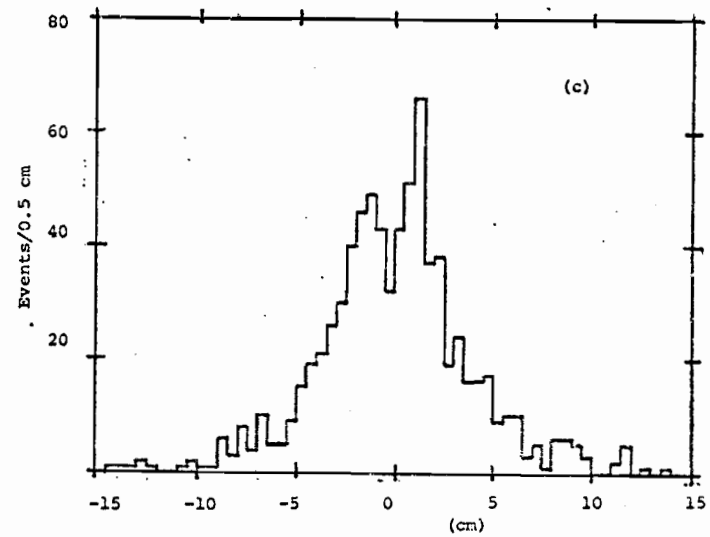

FIGURE 7-3c

NEUTRAL DECAY VERTEX RECONSTRUCTION
c) V°, y coordinant

tracks which would likely be near the beam position.

ii) Fast delta rays incorrectly matched with a positive track.

iii) e^+e^- pairs originating near the downstream end of the target on frames that were light enough that it was not clear whether they converted inside or outside of the target.

iv) Slow K°'s which were mistaken for gammas. This can happen if a track is very close to the limit of the curvature for defining gammas and has an appreciable momentum component parallel to the magnetic field.

The problems mentioned above are all peculiar to identification and measurement of slow gammas; the first because only gammas convert on the wire plane and if enough energy was lost to start a flare, the e^+ or e^- will in general be identified; the second and third because a scanner seeing either a slow electron or positron will try very hard to match it with a second track. A small fraction of these will be incorrectly matched. The tail will, therefore, not be present in the fast gamma sample which is identified as V°'s.

The discussion above indicates that we must make a fairly generous cut to delete most of the gammas, significantly reducing the number of V°'s accepted. That such a separation is necessary is evident by studying Figures 7-3b and c. These are the reconstructed z and y vertex positions of the V°'s. The z position peak is not only significantly wider, but it is not symmetric about the beam position. From the asymmetry, we estimate that approximately 10% of the identified V°'s are in fact fast gammas. This could significantly alter our results if the number of gammas were somehow dependent on the trigger. The results of making the cut on the central wire plane will be discussed in the next chapter along with other cuts we have made. The y position plot demonstrates the overall scanning

efficiency for V°'s. The dip in the center of this peak is due to V°'s which were lost in the very forward direction. We estimate that the scanners did not see approximately 10% of the V°'s because they were obscurred by the forward "jet" of fast particles. However, the loss of neutral strange particle decays in the forward direction, as well as the loss by deleting those found to be near the central wire plane does not bias the data samples. The losses are the same for both triggers. Their overall effect is to reduce the effective fiducial volume of the chamber, and thus reduce the phase space open to observed decays. Since the reduction is the same for both samples, it does not introduce a bias.

Now that we know the efficiency of our basic trigger and of the streamer chamber and we have a feeling for the measurements made in the streamer chamber, we must determine how efficient the various muon triggers were. In particular, we must determine what background signals were present in the muon definition and at what level.

As mentioned earlier, the calorimeter data indicate that the hadronic component in the muon triggers was negligible. No hadronic signal was seen in 448 events where a particle entered the calorimeter. This is only a small fraction of all triggers taken since the calorimeter covered only the central area (30 x 30 cm^2) of the apparatus.

The largest background present in any of the triggers was due to pion decay in flight. When these triggers were originally installed, it was our hope that we could use the single muon trigger (1μ-E) to collect the primary muon data sample. This has the obvious advantage that we would be measuring a quantity proportional to the branching ratio to muons of the charmed state. A dimuon requirement demands that both members of the $c\bar{c}$

(Charmed-Anti-charmed) pair decay to muons, introducing the branching ratio squared. Unfortunately, we quickly found that the one-muon trigger was dominated by pion decay. The measured rates of 3×10^{-3} of all interactions without the SOD magnet and 0.8×10^{-3} with the SOD magnet are very close to that expected from pion decay. The question of pion decay background is extremely important for this experiment. Because of the very nature of the experiment, we could not place the absorber closer to the target than 152 cm. The streamer chamber extends to that point. Adding one mean absorbtion path in lead (18 cm) to this gives a minimum decay path of 170 cm. In order to determine just how much background we do have, we must therefore resort to Monte Carlo techniques.

The method used in this study[34] was to start with real data, the reconstructed track data from a 205 GeV/c $\pi^- p$ exposure in the 30" bubble chamber at Fermilab.[35] The tracks from this exposure were propagated through the streamer chamber magnet's magnetic field and were allowed to decay with the probability determined by their momentum and track length, assuming all particles were pions. Those that did not decay were allowed to interact one collision length into the absorber. It was assumed that the number of secondaries produced in this collision followed a Poisson distribution, and that the energy was shared evenly between each of the secondaries. Each of these was allowed to decay or reinteract, etc. until the energy available to a possible decay muon was too little for the muon to be able to traverse the remaining absorber. Any muons produced in the sequence described above were propagated through the remaining absorber, taking energy loss and multiple scattering into

account. The number of such decay muons which would have fired one of the eight muon telescopes was tabulated as a function of the number of charged tracks from the primary interaction. To increase statistics, this entire sequence was repeated several times with a randomly chosen azimuthal angle for each event. The probability of each topology producing one or more muons in our trigger has been folded into our observed multiplicity distribution to determine the fraction of decay trigger events we would expect. This study has only one weakness. The bubble chamber statistics are very poor at higher multiplicities where we still have substantial signal. Recall that there was a large (4.45 cm) hole in the main trigger counter, the scatter (S) counter, and a thick (5.22 cm) solid Lucite target was used. Taken together, these raise the observed average multiplicity substantially. It was, therefore, necessary to extrapolate to the higher multiplicities. This extrapolation is somewhat uncertain. Even so, several interesting results emerged from this study. The first is that fewer than 20% of decay muons result from tertiary particles produced in the absorber. Thus, this study was fairly insensitive to the assumed momentum distribution of the tertiary particles. Secondly, the predicted single muon trigger rates are consistent with the rates actually observed. Thirdly, the dimuon trigger rate predicted from pion decay was only 2% of the observed rate with the SOD magnet. Because of these results, we concluded that the dimuon trigger must be used for our primary muon sample. Pion decay is a negligible contribution to this trigger, at least with the SOD magnet energized.

A second way to estimate the background from pion decay in the dimuon trigger and to check the Monte Carlo results is to assume that all of the

single muon triggers were due to pion or kaon decay. Then the dimuon trigger rate from decays is less than 3/8 of the square of the one-muon rate $[(2\mu\cdot E/E)_D \lesssim 3/8\ (1\mu\cdot E/E)^2]$. The 3/8 results from a factor of 1/2 to correct for double counting and 3/4 from our acceptance. This limit is derived in detail in Appendix A. From the measured rates, tabulated in Table 7-2, we find upper limits of the contribution of pion or kaon decay to the dimuon triggers ot 7.2% and 18% with and without the SOD magnet energized, respectively.

A similar calculation can be used to check the assumptions made in the Monte Carlo program. In particular, we can check that the contribution to the pion and kaon decay trigger rate from decays in the absorber is indeed small compared to decays before the absorber. This is done by noting that the cascade from a beam particle is nearly the same whether or not it first interacts in the target, or in the absorber. This follows from the experimental observation that most of the energy of an interaction is carried by those particles produced in the very forward direction. With this in mind, we substitute the $1\mu\cdot B/B$ rate for the $1\mu\cdot E/E$ rate in the above calculation. The $1\mu\cdot B$ rate was principally due to beam particles which interacted first in the absorber, as was discussed in the preceding chapter. This gives 0.8% and 3.0% for the SOD and non-SOD cases, respectively. These numbers are 11% and 17%, respectively, of the corresponding numbers requiring an interaction in the target. This is in good agreement with the Monte Carlo calculation.

We, therefore, conclude that when the SOD magnet was energized the contribution to the dimuon trigger from pion and kaon decays was negligible. Even with the magnet off, the dimuon trigger rate from these decays was less than 18% of the total.

In the case of pion decay, this is all that needs to be said. They merely produced a small number of extra dimuon triggers which could not contribute to any excess of observed neutral strange particles. However, since strange particles are produced in pairs, this is not true of the triggers from kaon decay. This question is discussed in detail in Appendix B, where I show that one would expect to observe a neutral strange particle decaying in the streamer chamber in approximately 4% of those triggers produced by pion and kaon decay. Thus, even for the data with the SOD magnet off we would expect to see less than a 1% increase in neutral strange particle production attributed to this source. We conclude, therefore, that decays in flight of pions and kaons were not a problem.

A source of muons which is harder to measure is due to muons directly produced in the absorber by the interaction secondaries. Muons produced upstream are vetoed by the halo counters or pass through the various holes in the counters and cannot produce triggers. This is not true of muons produced in the absorber. In order to estimate the fraction of our dimuon triggers which came from this source, we use the data from the six spark chamber wire planes.

Recall that the three spark chambers were located downstream of the last of the absorber and muon telescopes. The chambers were placed starting 1.0 meters downstream of the last telescope scintillator plane (8.1 m from the target), and were spaced at intervals of approximately 0.4 meters. The central chamber was rotated by 45° with respect to the outside pair of chambers in order to minimize the number of ambiguous tracks. Magnetostrictive readout was used which gave position resolution of approximately 1/3 mm. With the 40 cm separation between chambers,

this implies an angular resolution of better than 1 mrad. A muon with the beam momentum will be displaced, on the average, by 1.1 mrad and 3 mm in angle and position, respectively, by multiple scattering through the absorber. The system's resolution was therefore dominated by multiple scattering in the absorber. This produces an approximately constant 15% uncertainty in the muon momentum.

Because of the large amount of multiple scattering and the large number of secondary hadrons, it is very difficult to match the tracks measured in the spark chambers with tracks measured in the streamer chamber. Thus, only the final angles and positions of the muons are measured. However, by assuming a production point, the track's momentum can be calculated from the angle and position in the bend plane. Recall that both the streamer chamber and the SOD magnets bend in the verticle plane. With the momentum known, one can predict the amount of multiple scattering present in the non-bend plane and can then attempt to separate those produced in the target from those produced in the absorber. Unfortunately, this separation is not clean. A "typical" muon might be displaced 10 cm from the beam at the first spark chamber. This is 8 meters from the target and approximately 6 meters from a point one interaction length into the absorber for a beam particle which passes through the hole in the first lead block. The difference in the production angle from these two possibilities is only 4 milliradians, an angular difference which is easily within the error from multiple scattering for a particle with momentum less than 70 GeV/c. A clean track by track separation of the muon origin is therefore not possible.

We were able to reconstruct two tracks in only a small fraction of the dimuon triggers. The spark chambers did not cover the full aperture of the apparatus. In addition, they were inefficient, especially for multiple tracks. These chambers were designed several years ago for an elastic scattering experiment. They have foil rather than wire high-voltage planes. Thus, "spark robbing" was a severe problem. This occurs when one spark dominates the spark formation process, "robbing" most of the energy from other sparks. Because the chambers were old, they had deteriorated to the point where there were often spurious sparks in the chambers. In addition, the magnetostrictive "wands" showed very severe attenuation of the spark signals.

However, the eight muon telescopes which provided the muon trigger gave an extra constraint on the tracks in the spark chambers. By constraining possible tracks to extrapolate back through one of the triggering telescopes, we could use four point tracks and still unambiguously choose the correct combinations of sparks to form two tracks in most cases. The target origin constraint in the non-bend plane also helps in this regard. Taken together we[36] were able to reconstruct single muon tracks in approximately 50% of the dimuon triggers and two tracks in 10% of the triggers.

Using the reconstructed muon tracks, we were able to study the question of the origin of the muon. Did they originate in the target or in the absorber? We studied this point using both the $2\mu\cdot E$ and the $2\mu\cdot B$ triggers. The $2\mu\cdot B$ triggers provide a substantial sample of events with the production point inside the absorber with which we can compare the $2\mu\cdot E$ distributions. Extrapolating single tracks back toward the target in the non-bend plane and plotting the intersection point with the plane of

the beam, one has a plot of the track's apparent origin. The intersection point for the 2μ·E events with interactions in the target and for the 2μ·B events with their primary interactions in the absorber, and the difference in these distributions is plotted in Figure 7-4. The 2μ·E and 2μ·B curves have been normalized to have the same area in the region between 260 cm and 510 cm from the target. This region is well inside the absorber where differences in the cascade absorbtion of the hadrons from the two triggers should be small. The differences in the two curves is then a measure of the target associated dimuon production. With this method, we find that 55 ± 4% of the 2μ·E trigger dimuons were target associated.

Another method of determining the origin of the dimuons is to examine the intersection point when two tracks are reconstructed. This should in principle be a better determination of the dimuon origin since the angle between the two tracks is, on the average, twice the production angle of one track. We found that the origin of 5 of the 42 2μ·B reconstructed dimuons was upstream of the target, while 19 of 57 2μ·E events had apparent origins there. By assuming that half of the target associated dimuons will reconstruct upstream and half downstream of the target, we find that 56 ± 22% of the dimuons are target associated.

A third, but not independent, method of determining the dimuon origin is to calculate a Chisquare for both tracks from the positions and angles found in the spark chambers, assuming a target origin and an absorber origin.[37] The lower χ^2 should then identify the true origin of the event. This has been done for all 2μ·E and 2μ·B triggers without regard to the location of the primary interaction. It was found that 49 of 90 reconstructed dimuon events from the 2μ·E (SOD) trigger fit the target origin assumption, while 15 of 83 events from the 2μ·B trigger fit. Correcting

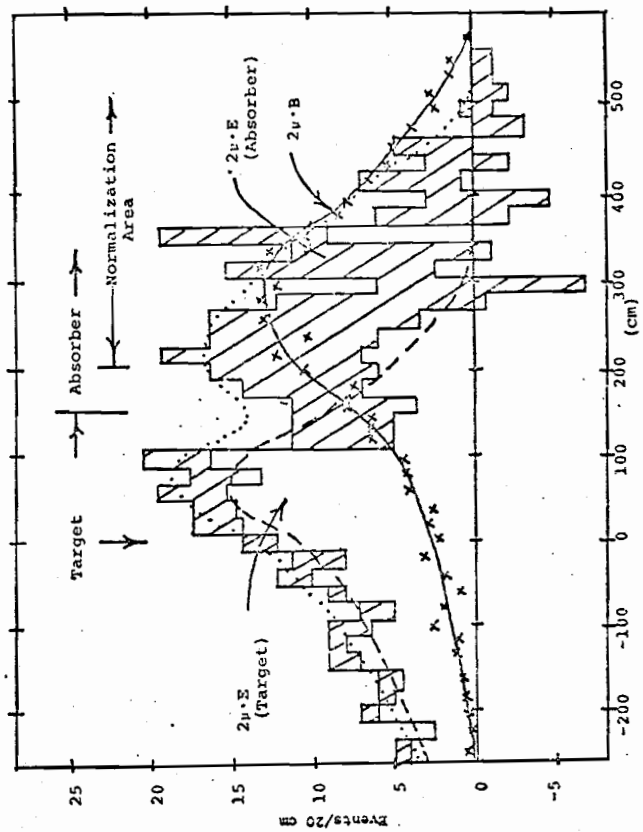

FIGURE 7-4

INTERSECTION POINT OF SINGLE MUON TRACKS WITH THE PLANE OF THE BEAM: 2μ·E TRIGGER; ABSORBER AND TARGET OPTIMIZED MUONS; 2μ·B USED TO ESTIMATE THE ABSORBER CONTRIBUTION TO THE 2μ·E TRIGGER. THE CURVES ARE A GUIDE TO THE EYES ONLY.

these numbers for event origin leads to an estimate of 57 ± 8% target associated dimuons with an interaction in the target.

Since those results are self-consistent, we take the weighted average as our best estimate and find that 55 ± 3% of the 2μ·E triggers were caused by target associated dimuons.

The fraction of dimuon triggers which do not originate in the target does not directly effect the results of the experiment. There is no reason for believing that the primary interaction for those events where a muon or muons are produced by a secondary should be any different than those events seen with the E trigger. In particular, the number of and momentum distributions of the neutral strange particles should be the same. Thus, the only effect of these non-target origin triggers is to supply a factor of two larger background signal than one might hope to have, and thus lower our sensitivity. Thus, I conclude that most of our muon triggers were due to prompt muons, and that over half of these originated in the streamer chamber target.

VIII. EXPERIMENTAL RESULTS

Now that we have an understanding of the apparatus, its capabilities, the types of accuracy of the measurements made, and of the background signals present in the triggers, we are in a position to look in detail at the data collected.

Before we can make any statements about what we see, or do not see in the data, we need to convert the trigger rates listed in Table 7-2 into cross sections. This table lists the fraction of beam tracks which interacted in the target and satisfied the other trigger requirements. These can be converted to cross sections by using the standard transmission formula: $I = I_o \exp(-\ell\eta\sigma_M)$ where, I is the number of transmitted beam particles for I_o incident particles; ℓ is the target length; η is the molecular number density; and σ_M is the molecular cross section. Then the cross section per nucleon is:

$$\sigma_N = \frac{\sigma_M}{C_n} = \frac{1}{C_n \eta \ell}\,[-\ln(1-\varepsilon)]$$

where ε is the fraction of interacting beam particles ($\varepsilon = (I-I_o)/I_o$) and: $C_n \equiv \sum_i A_i^n = 5(12)^n + 8(1)^n + 2(16)^n$ for Lucite ($C_5H_8O_2$),

$$C_n = 46.91 \quad n = 0.67$$
$$= 56.24 \quad = 0.75$$
$$= 100.00 \quad = 1.0$$

where A is the atomic number of the nucleous in question. These choices for the A dependence of the nuclear cross section are representative values only. The value n = 0.67 is predicted from simple geometric arguments. The value n = 1 is predicted for "valence" quark interactions where the nucleous is expected to be transparent to the incoming beam, and has been observed for production of dimuons with mass greater than 1 GeV/c^2.[38]

The n = 0.75 dependence is an experimental value determined for the total $\pi^- A$ cross section at 100 and 175 GeV/c.[39] Using the target parameters listed in Table 8-1 and the formula given above, it is a simple matter to calculate the cross sections corresponding to the rates listed in Table 7-2. These cross sections are tabulated in Table 8-2 for the three assumed atomic number dependences. The dimuon cross sections are listed twice. The first is the trigger cross section, which includes muons produced in the absorber. The second has had these removed, assuming that the fraction of absorber to target originated dimuons is the same without the SOD magnet as it was measured to be with the SOD magnet (.55 ± .03 target associated/total).

ρ = density = 1.26 ± .03 gm/cm^3

ℓ = thickness = 2.055 ± .055" = 5.2197 ± .0013 cm

A = molar wt = 100.11831 gm/mole
Lucite ($C_5H_8O_2$)

N_A = Avogadro's # = 6.022045×10^{23}/mole

η = # density = $\rho N_A/A = 7.58 \times 10^{21}$/cm^3

$\frac{1}{\eta\ell}$ = 2.528×10^{-23} = 25.28 barn

TABLE 8-1
TARGET CROSS SECTION PARAMETERS

Having only one target, we cannot make a direct determination of the atomic number dependence of the nuclear cross sections, although we can make some estimates. The $A^{0.67}$ dependence is very probably too slow a dependence, at least for the E trigger. From Table 8-2 we see that this dependence

σ_n TRIG	NON-SOD (581-601) n^* = 0.67	0.75	1.0	SOD (672-793) 0.67	0.75	1.0
E(mb)	19.8	16.5	9.3	19.8	16.5	9.3
1μ·E† (μb)	60.9	50.8	28.6	16.2	13.5	7.6
2μ·E(nb)	388	324	182	70.6	58.9	33.1
3μ·E (nb)	9.2	7.6	4.3	4.1	3.4	1.9
2μ·E(nb) corrected for muon origin	213	178	100	38.8	32.4	18.2

† The 1μ·E trigger rates are consistent with being due to pion decay.

* Nuclear cross section varies as A^n.

TABLE 8-2
TRIGGER CROSS SECTIONS

gives a trigger cross section of 20 mb. But because of the 4.45 cm diameter hole, we did not trigger on the elastic or the majority of the low-mass diffractive cross sections. At 175 GeV/c, the $\pi^- p$ cross section of 24 mb,[41] we would expect the E trigger cross section to be less than 18 mb and probably closer to the 16.5 mb found assuming the $A^{0.75}$ dependence. The atomic number dependence of the 2μ·E trigger is even more difficult to determine. However, we would not expect the dimuon cross section to vary slower than the E trigger cross section. We expect, therefore, that the 2μ·E trigger cross section was in the 30-60 nb range. We now see that our experimental sensitivity was fairly good. We collected 719 2μ·E (SOD)

events (395 with target-associated muons) in four days of running which means that we have 22 events per nanobarn of dimuon cross section, assuming the A dependence.

Now that we know the sensitivity of the experiment, we must look in detail at the quantity we were attempting to measure and how it is extracted from the data. We wished to measure the cross section for production of a state which carries the charm quantum number. However, we actually counted the number of pictures containing one or more neutral decays, and the total number of neutral decays seen, with and without a dimuon requirement. These numbers divided by the number of events observed are the best estimators of the probabilities for observing an event with one or more neutral decays, and for observing any neutral decay.

We have, therefore, directly measured:

i) α_E = the probability of observing one or more neutral decays in an event with the E trigger;

ii) $\langle V^\circ \rangle_E$ = the probability of observing any neutral strange decay with the E trigger;

iii) $\alpha_{2\mu}$ = the probability of observing one or more neutral decays with the dimuon trigger; and

iv) $\langle V^\circ \rangle_{2\mu}$ = the probability of observing any neutral strange decay with the dimuon trigger.

The neutral strange particles with either trigger can have two sources. The first is from "normal" associated production of strange particles. The second is from decays of charmed states, which should decay preferentially to states containing a strange hadron. These sources should be independent and if we also assume that they are nonexclusive,

then we may use standard combinatorial probability analysis to write the probability of observing one or more strange particles from the two sources as:

$$\alpha = \alpha_s + \alpha_c - \alpha_s \cdot \alpha_c \qquad (8\text{-}1)$$

where α_s and α_c are the probabilities of observing one or more strange particles produced by the normal mechanism and via charm production, respectively. Likewise, the probability of observing any strange decay is the sum of the contributions from the two sources:

$$\langle V^\circ \rangle = \langle V^\circ \rangle_s + \langle V^\circ \rangle_c . \qquad (8\text{-}2)$$

Since charm is a quantum number for which one must search, it is a safe assumption that the contribution to strange particle production from charm decays is negligible in the E trigger data sample. For the E trigger, Equations 8-1 and 8-2 become:

$$\alpha_E = \alpha_s$$

$$\langle V^\circ \rangle_E = \langle V^\circ \rangle_s .$$

Substituting these into 8-1 and 8-2, we have for the dimuon trigger:

$$\alpha_{2\mu} = \alpha_E + \alpha_c - \alpha_E \cdot \alpha_c$$

$$\langle V^\circ \rangle_{2\mu} = \langle V^\circ \rangle_E + \langle V^\circ \rangle_c .$$

Solving for the charm contributions, we find:

$$\alpha_c = (\alpha_{2\mu} - \alpha_E)/(1 - \alpha_E) \qquad (3\text{-}3)$$

$$\langle V^\circ \rangle_c = \langle V^\circ \rangle_{2\mu} - \langle V^\circ \rangle_E . \qquad (3\text{-}4)$$

These equations depend only on the assumptions that:

i) the contribution to strange particle production from the decay of the charmed states is negligible compared to the normal mechanism in the total cross section, and, therefore, in the E trigger data sample;

ii) charm production and normal strange particle production are independent and nonexclusive; and

iii) normal strange particle production is independent of dimuon production.

The first assumption is a very safe assumption as I believe everyone will agree. The second is reasonable. The only part of this assumption that one might argue with is that they are nonexclusive. This assumption would tend to overestimate the charm contribution, if it were invalid. If the two were exclusive, for example, the factor $(1 - \alpha_E)^{-1}$ in Equation 8-3 would become unity. I will show later that, in fact, this is the conservative approach. The third assumption is tantamount to defining charm production as being any mechanism that produces neutral strange particles correlated with muons. This assumption also tends to overestimate the charm cross section.

Equations 8-3 and 8-4 demonstrate the method used to extract the probabilities of observing neutral strange particle decays which are correlated with two muons. These probabilities can be converted to cross sections by multiplying by the trigger cross section for the data sample from which they come, the $2\mu \cdot E$ cross sections calculated earlier. The resulting cross sections will then involve not only the production cross section of the charmed state, but also branching ratios to neutral strange particles, branching ratios to muons and the probabilities that the final state neutrals and muons were detected. The form that these expressions

take will be discussed in the next chapter where I discuss several Monte Carlo calculations which were performed to determine the detection efficiencies of the apparatus.

Before we can attempt to extract the charm production cross section from α_c and $< V^\circ >_c$, we must determine how sensitive these numbers are to various event and neutral decay selection criteria. We will first examine the individual data samples to determine how sensitive each sample is to the selection criteria. Then we will examine α_c and $< V^\circ >_c$ as a function of the same criteria.

The numbers which have the most significance when comparing data samples and selection criteria are:

i) the total number of events in a given trigger sample;

ii) the average charged multiplicity ($< n_{CH} >$) of the sample;

iii) the dispersion of the multiplicity distribution $\left(D = \sqrt{< n_{CH} >^2 - < n_{CH}^2 >}\right)$, this is a measure of the width of the distribution;

iv) the number of events containing one or more neutral decays;

v) the fraction of events this represents (α);

vi) the average charged multiplicity of the events with neutral decays ($< n_{CH} >_V$);

vii) the dispersion (D_V) of these events;

viii) the total number of neutral decays; and

ix) the average number of neutral decays per event ($< V^\circ >$).

These are listed for each of the three primary triggers, the E (total cross section), the 2μ·E (SOD), and the 2μ·E (non-SOD) triggers in the data tables, Tables 8-3 and 8-4. The fraction of events containing at least one neutral decay and the average number of neutral decays were chosen for obvious reasons. The average charged multiplicities and dispersions are given because the production of massive states could exhibit its presence in these quantities. In addition, they summarize the effect of the various selection requirements on the hadronic spectra, as do the neutral decay quantities.

All of these data are from the Seattle scan only. These are the only samples which I can study in detail. Later, I will add in the data scanned at the other labs.

We first investigate the effect of selecting events on the basis of the beam conditions of the experiment as determined by the electronic logic discussed in Chapter VI. There are three circumstances that could affect the results:

i) the presence of extra interactions in an event, not seen by the scanners;

ii) the presence of extra beam tracks not seen by the scanners;

iii) and, the kaon contamination in the beam

The first two conditions could affect the results, if the beam conditions were different for the two triggers. This should not be a large affect, since the triggers were interspersed at regular and frequent intervals. Any affect of the kaon contamination should also be small, since we know that the number of kaons in the beam was small. Indeed, we see from Table 8-3 that choosing those events where none of these occurred has little, if any, affect.

EVENTS	$\langle n_{ch} \rangle$	D	EVENTS W/V°	α	$\langle n_{ch} \rangle_V$	D_V	# of V°	$\langle V° \rangle'$	CUTS
E TRIGGER									
1908	12.4 ± .3	6.1 ± .3	270	.1415 ± .0080	13.4 ± .9	6.6 ± .7	308	.1614 ± .0096	NONE
1890	12.4 ± .3	6.1 ± .3	268	.1418 ± .0080	13.4 ± .9	6.6 ± .7	306	.1619 ± .0097	I *
848	12.1 ± .5	6.2 ± .4	120	.1415 ± .0120	12.8 ±1.3	6.8 ±1.0	135	.1592 ± .0142	I + B**
1597	12.4 ± .3	6.2 ± .3	227	.1421 ± .0087	13.5 ±1.0	6.8 ± .8	258	.1616 ± .0104	I + π***
2μ·E (SOD) TRIGGER									
719	12.7 ± .5	6.5 ± .4	103	.1433 ± .0131	13.8 ±1.5	6.7 ±1.2	109	.1516 ± .0142	NONE
678	12.5 ± .5	6.3 ± .84	95	.1401 ± .0133	13.4 ±1.5	6.5 ±1.2	101	.1490 ± .0146	I *
284	11.9 ± .8	5.9 ± .6	42	.1478 ± .0211	12.6 ±2.2	6.3 ±1.7	43	.1514 ± .0219	I + B**
541	12.4 ± .6	6.2 ± .5	74	.1368 ± .0148	13.2 ±1.7	6.2 ±1.4	78	.1442 ± .0160	I + π***
2μ·E (NON-SOD) TRIGGER									
325	13.3 ± .8	5.5 ± .8	54	.1662 ± .0206	13.8 ±2.0	6.1 ±1.9	60	.1846 ± .0240	NONE
309	13.1 ± .8	5.5 ± .8	51	.1650 ± .0211	13.6 ±2.1	6.2 ±1.9	56	.1812 ± .0242	I *
112	13.0 ±1.4	6.4 ±1.1	21	.1875 ± .0369	14.1 ±3.6	8.2 ±2.4	24	.2143 ± .0446	I + B**
309	13.1 ± .8	5.5 ± .8	51	.1650 ± .0211	13.6 ±2.1	6.2 ±1.9	56	.1812 ± .0242	I + π***

* Events with second interactions determined by the electronic logic are deleted.
** Events with second interactions and extra beam tracks are deleted.
*** Events with second interactions are deleted and an incident pion is required.

TABLE 8-3

RESULTS OF EVENT SELECTION ON BEAM CONDITIONS

EVENTS	$\langle n_{ch} \rangle$	D	EVENTS W/V°	α	$\langle n_{ch} \rangle_V$	D_V	# of V°	$\langle V° \rangle$	CUTS (cm) WIRE+	CUTS (cm) VERTEX++
E TRIGGER										
1908	12.4 ± .3	6.1 ± .3	269	.1410 ± .0080	13.0 ± .9	6.1 ± .7	300	.1572 ± .0093	-	-
			193	.1011 ± .0069	12.6 ±1.0	6.0 ± .8	211	.1106 ± .0070	±1.5	-
			161	.0843 ± .0064	13.0 ±1.1	6.2 ± .9	172	.0901 ± .0070	±1.5	10.
			171	.0896 ± .0065	13.0 ±1.1	6.1 ± .8	183	.0959 ± .0072	±1.25	10.
			149	.0781 ± .0061	12.9 ±1.2	6.1 ± .9	160	.0839 ± .0068	±1.75	10.
2μ·E (SOD)										
719	12.7 ± .5	6.5 ± .4	98	.1363 ± .01280	13.6 ±1.5	6.9 ±1.1	103	.1433 ± .0138	-	-
			77	.1071 ± .0115	13.2 ±1.7	6.9 ±1.2	81	.1127 ± .0124	±1.5	-
			62	.0862 ± .0105	13.7 ±2.0	7.2 ±1.3	65	.0904 ± .0112	±1.5	10.
			66	.0918 ± .0108	14.0 ±1.9	7.2 ±1.4	69	.0960 ± .0115	±1.25	10.
			59	.0821 ± .0102	13.9 ±2.1	7.3 ±1.4	62	.0862 ± .0110	±1.75	10.
2μ·E (non-SOD)										
325	13.3 ± .8	5.5 ± .8	49	.1508 ± .0198	12.6 ±2.0	6.2 ±1.8	57	.1754 ± .0244	-	-
			39	.1200 ± .0180	13.2 ±2.4	6.7 ±2.0	43	.1323 ± .0207	±1.5	-
			31	.0954 ± .0163	13.6 ±2.8	7.0 ±2.2	34	.1046 ± .0186	±1.5	10.
			31	.0954 ± .0163	13.6 ±2.8	7.0 ±2.2	34	.1046 ± .0186	±1.25	10.
			29	.0892 ± .0158	13.6 ±2.9	7.2 ±2.2	32	.0985 ± .0181	±1.75	10.

+Neutral decays within this distance to the central wire plane are deleted.
++Neutral decays within this distance to the primary interaction are deleted.

TABLE 8-4

RESULTS OF SELECTING NEUTRAL DECAYS ON THE BASIS OF ITS VERTEX POSITION

In addition to examining the effect of making these selections on the overall average numbers, we have examined their effect on the various distributions, including the various charged multiplicities, the decay vertex position distributions, and the strange particle momentum distributions. None of them change significantly. Since these cuts make no significant difference in the experimental results and there is no a priori reason to favor making any of them, we have decided to use the full data sample, without making these "cuts" on the data for the rest of this investigation.

The next question to investigate is the question of gamma contamination in the data sample. Since most of the gammas seen will have come from π° decay, the number present in the strange particle sample could be sensitive to fairly small variations in the physics of the interaction. As was discussed in the previous chapter, any gammas which convert in the streamer chamber must do so in the wires of the central high-voltage plane. Thus deleting those V°'s which have their vertex near the central wire plane will delete most of the gamma contamination from the sample. Because the vertex reconstruction is not as precise as one would like, we have tried several different widths for the wire cut; ± 1.25 cm, ± 1.50 cm, and ± 1.75 cm. The ± 1.25 cm width corresponds to cutting at the full width, half maximum of the gamma distribution of Figure 7-3a, ± 1.75 cm corresponds to approximately the full width at the base of this distribution, and ± 1.50 cm is an intermediate value. We have also investigated the effect of deleting those V°'s which decayed close to the primary vertex, and, therefore close to the target. These are suspect because it is often difficult to determine if such a pair of tracks is actually a neutral decay. We have, therefore, deleted V°'s which decayed closer than 10 cm to the primary vertex. The results of making these selections are tabulated in

Table 8-4 for the three triggers. The total number of events, their charged multiplicities and multiplicity dispersions are taken from Table 8-3 and are listed here only for reference. The V°'s in the full doubly scanned and resolved sample which could not be measured have been deleted from the samples, even though they were clearly V°'s. We lost 8, 6, and 3 V°'s from the E, 2μ·E (SOD) and 2μ·E (non-SOD) samples, respectively, as unmeasurable. Obviously, the number of V°'s varies with the cut, but their distributions do not vary significantly as measured by the average charged multiplicities and dispersions of the sample.

We can now examine the effect of making these data selections on the charm probabilities. Table 8-5 lists α_c and $< V^\circ >_c$ calculated using the E and 2μ·E values in Tables 8-3 and 8-4, and the Equations 8-3 and 8-4. Also listed are the results of the non-SOD data scanned at Orsay and Davis and the weighted average of those results for the three labs. We use the weighted average because scanning rules and procedures used at the three labs were slightly different. The Orsay group, for example, were much more conservative in their definition of an acceptable neutral decay. They, therefore, found approximately 10% fewer decays than did we at Seattle. However, except for the number of V°'s found, the three scans of the SOD data agree in all other respects. Most importantly, the difference in the E and the 2μ·E samples was found to be zero at all three labs. All of the SOD data were scanned at all three labs. The non-SOD data, on the other hand, did not show such a uniformity. Nonoverlapping portions of this data were scanned at the three labs. Both the Orsay and Seattle labs found a one-standard deviation excess of V°'s in the 2μ·E (non-SOD) data. The Davis sample shows a two-standard deviation excess in the E trigger. This is the only difference found between the samples and is reflected in the

weighted averages listed in Table 8-5. These differences in scanning rules are a further test of the sensitivity of the result to data selection. We conclude that we see no evidence of the production of neutral strange decays which are correlated with the triggering dimuons.

Since we see no charm signal, we are forced to calculate an upper limit on the amount of charm which could be present in our sample without being seen. Before we can do this, however, we need to say a few words on how the errors on the listed probabilities were calculated, since an upper limit depends crucially on the errors assigned. As was mentioned earlier, the errors quoted are statistical only. Systematic errors should cancel by taking the differences between the E and 2μ·E samples scanned at each lab. Then, the standard deviation of the mean is:
$\delta = [\sum_i^n (x_i - \mu)^2/n(n-1)]^{\frac{1}{2}}$, where μ is the mean, n is the number of events and x_i is the measured value. In the case of α, x_i is zero or one; an event either contains one or more decays or it does not. In this case, this reduces to: $\delta = [\alpha(\alpha-1)/(n-1)]^{\frac{1}{2}}$. For the average number of decays, x_i is the number observed in a given picture, and: $\delta = [(<(V^\circ)^2> - <V^\circ>^2)/(n-1)]^{\frac{1}{2}}$. The standard deviations listed in Tables 8-3 and 8-4 were calculated using these formulae.

The parent distributions from which these means are drawn should be binomial in the case of α and multinomial in the case of $< V^\circ >$. However, since the number of trials (pictures) is reasonably large, both of these distributions are very nearly normal (gaussian). We therefore calculated the standard deviation of $< V^\circ >_c$ by adding the standard deviations of $< V^\circ >_E$ and $< V^\circ >_{2\mu}$ in quadrature: $\delta_c^{V^\circ} = \left[(\delta_{2\mu}^{V^\circ})^2 + (\delta_E^{V^\circ})\right]^{\frac{1}{2}}$. The calculation for δ_c^{α} has the usual modification to account for the standard deviation of the denominator.

SOD		NON-SOD		DATA	
α_c	$\langle V^\circ \rangle_c$	α_c	$\langle V^\circ \rangle_c$	Event Selection	
.0021 ± .0179	-.0098 ± .0171	.0288 ± .0257	.0232 ± .0258	-	
-.0020 ± .0181	-.0129 ± .0175	.0270 ± .0263	.0193 ± .0261	I *	
.0075 ± .0283	-.0078 ± .0261	.0536 ± .0452	.0051 ± .0468	I + B**	
-.0062 ± .0200	-.0174 ± .0191	.0267 ± .0266	.0196 ± .0263	I + π***	
				Neutral Selection	
				Wire+ (cm)	Vortex#
-.0055 ± .0176	-.0139 ± .0166	.0114 ± .0249	.0182 ± .0261	-	-
.0067 ± .0149	.0021 ± .0147	.0210 ± .0214	.0217 ± .0222	±1.5	-
.0021 ± .0134	.0003 ± .0132	.0121 ± .0191	.0145 ± .0199	±1.5	10.
.0024 ± .0136	.0001 ± .0136	.0064 ± .0193	.0087 ± .0199	±1.25	10.
.0043 ± .0129	.0023 ± .0129	.0120 ± .0184	.0146 ± .0193	±1.75	10.
SEATTLE		.0288 ± .0257	.0232 ± .0258	NONE	
ORSAY		.0141 ± .0204	-------	NONE	
DAVIS		-.0364 ± .0165	-.0338 ± .0167	NONE	
Weighted Average of Seattle-Orsay-Davis Scan		-.0044 ± .0265	-.0170 ± .0260	NONE	

* Events with a second interaction not seen by the scanners are deleted.
** Events with a second interaction or extra beam track are deleted.
***Events with a second interaction are deleted and an incident pion is required.
\+ Decays closer to the central wire plan than this distance are deleted.
\# Decays closer than this distance to the primary interaction are deleted.

FIGURE 8-5

CHARM PROBABILITIES

We then define the upper limit as: $\Sigma_\alpha = (1.28\ \delta_c^\alpha + \alpha_c)\alpha_{2\mu}$, and; $E_{\langle V^\circ \rangle} = (1.28\ \delta_c^{V^\circ} + \langle V^\circ \rangle_c)\alpha_{2\mu}$. The factor of 1.28 in the equations above are found by solving the integral equation for x:

$$0.9 = \int_x^\infty \frac{1}{\sqrt{2\pi}}\, e^{-t^2/2} dt.$$

We are only concerned with the probability that the effect observed could be larger, thus the $+\infty$ integration limit. The cross section in the limits ($\sigma_{2\mu}$) converts from probabilities to observed cross sections as mentioned earlier. This is the total dimuon trigger cross section, uncorrected for muon origin, since we cannot make an event by event separation on the basis of muon origin.

Table 8-6 lists the results of this calculation for each of the probabilities listed in Table 8-5, assuming the A atomic number dependence of the cross sections listed in Table 8-2. There are several things evident from this table and the preceding tables. The first is that the upper limits do not strongly depend on the selection criteria. There is only one criteria which leads to a limit which is much higher than the others. This is when we select those events with neither an extra interaction (loss: ∿ 1% of all events) nor an extra beam (loss: ∿ 55% of all events) within the memory time of the streamer chamber. This increase in the limit is due to loss of statistical significance caused by this selection. It also demonstrates the vulnerability of 90% upper limits. There are several small limits listed, and the negative limits implied by the Davis non-SOD data. We have checked the Davis data and can find no systemmatic reason for their having observed fewer neutral decays in their 2μ·E samples, or Seattle and Orsay observing more in their samples. The effect of this difference in the data samples

is to increase the standard deviation, and, therefore, the upper limits of the non-SOD data.

It is clear from Table 8-6 that it does not matter a great deal, in terms of the upper limit, which selection criteria we use. Except that to be conservative, we will not choose the extremes.

We can now check some of the assumptions made earlier in deriving the expressions for the charmed probabilities. I stated that the assumption of the nonexclusivity of charm and normal strange particle production was the conservative approach, since it overestimates the charm contribution. We see now that this is the case. Anything that overestimates an upper limit is conservative.

Another assumption we made was that strange particle production is independent of dimuon production. If this, in fact, is true, and it seems to be, it would be one of the most surprising and important results of the experiment. To demonstrate this result, we will examine each of the distributions accessible to us. In particular, we will demonstrate that none of these variables show a difference, within statistics, that might be a manifestation of charm production. I will not attempt to show all of the distributions that we have studied. As a representative sample, I will concentrate on the $2\mu \cdot E$ (SOD) data, comparing it with the E trigger data and bubble chamber data where applicable.

We first examine the distribution of neutral decays among the event topologies. These are shown in Figures 8-1a and b. Figure 8-1a shows the full $2\mu \cdot E$ (SOD) and E trigger data samples, while Figure 8-1b shows the effect of deleting those decays within 10 cm of the primary vertex and

SOD		NON-SOD			
$\Sigma\alpha_c$	$\Sigma\langle V^\circ\rangle_c$	$\Sigma\alpha_c$	$\Sigma\langle V^\circ\rangle_c$	DATA CUT	
ALL VALUES ARE NANOBARN/NUCLEON				Event Selection	
0.8	0.4	11	10	-	
0.7	0.3	11	9.6	I	
1.5	0.8	20	21	I + B	
0.6	0.2	11	9.6	I + π	
				Neutral Selection	
				Wire	Vertex
0.6	0.1	7.9	9.6	-	-
0.8	0.7	9.0	9.0	±1.5	-
0.6	0.6	6.7	7.3	±1.5	10.
0.6	0.5	5.6	6.2	±1.25	10.
0.7	0.6	5.6	7.3	±1.75	10.
SEATTLE		11	10	None	
ORSAY		7.3	--	NONE	
DAVIS		- 2.8	- 2.3	NONE	
Weighted Average of Seattle-Orsay-Davis		5.3	3.0	NONE	

TABLE 8-6

CHARM CROSS SECTION UPPER LIMITS AS A FUNCTION OF SELECTION CRITERIA, ASSUMING AN A DEPENDENCE OF THE NUCLEAR CROSS SECTION

± 1.5 cm of the central, high-voltage wire plane. We can detect no significant difference between the two samples and deleting the gammas reveals nothing new. Also shown for comparison are the average number of K_s^o's seen in a 200 GeV/c $\pi^- d$ exposure in the 30" bubble chamber at Fermilab (DKSW).[42] We are in reasonable agreement with this, considering that our neutral decays are unfitted.

The same near identity of distributions is evident when one plots the charged multiplicity of the samples, even when one requires a neutral decay. These are shown in Figure 8-2, where for comparison, I have overplotted the curve from the measured E trigger distribution (the dotted curve).

The only quantity left to examine is the neutral strange particle momentum spectrum. This has been done in two ways for the data sample scanned in Seattle only. The first is independent of the momentum fits and is nearly independent of vertex measurement accuracy. We plot the distance from the primary vertex to the decay vertex. Figures 8-3a and b show these plots for the decays observed in the E and the 2μ;E (SOD) data samples plotted on a semi-logarithmic scale. Figure 8-3a has had no neutral selection criteria applied and shows several effects. The loss in scanning efficiency for decays very near the target is evident. It is also clear from the non-exponential shape of this distribution, that it contains a significant non-strange particle component. It is not a simple matter of subtracting a constant background from gammas as one might expect. Gammas do not have a uniform probability of converting everywhere along the length of the chamber. The high-voltage wire plane is offset from the beam by 2.5 cm. Thus, only very wide angle gammas will strike the wires near the target and if a gamma does strike a wire there, it will have a shorter path inside the wire than one that strikes a wire at a smaller angle.

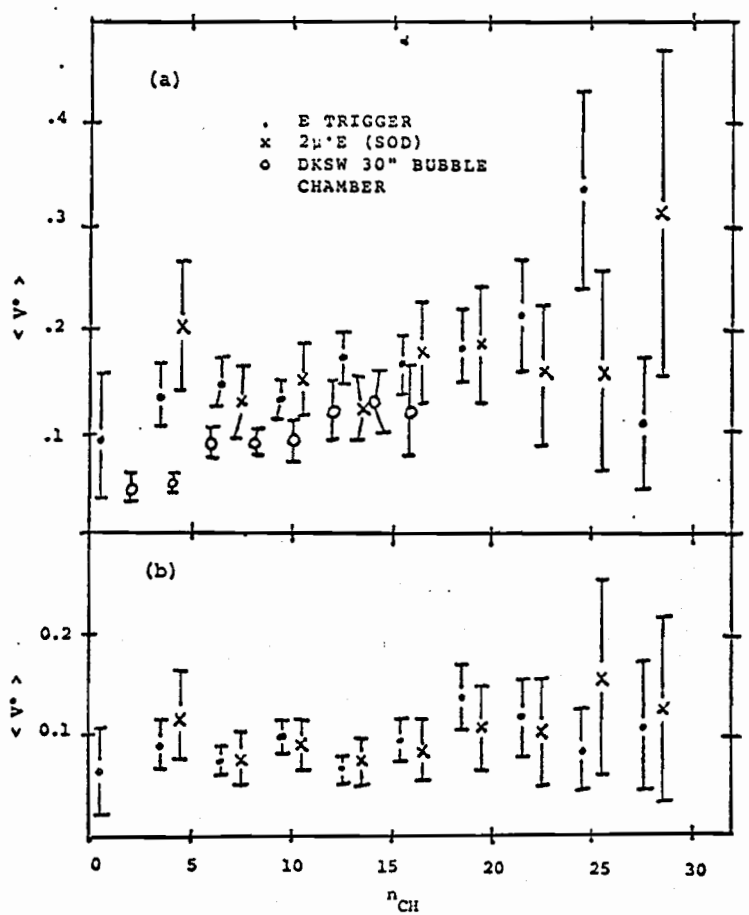

FIGURE 8-1
AVERAGE NUMBER OF NEUTRAL STRANGE DECAYS OBSERVED VERSUS NUMBER OF CHARGED TRACKS

a) No data cuts
b) Deleting decays within 10 cm of the primary vertex and ± 1.5 cm of the high-voltage wire plane

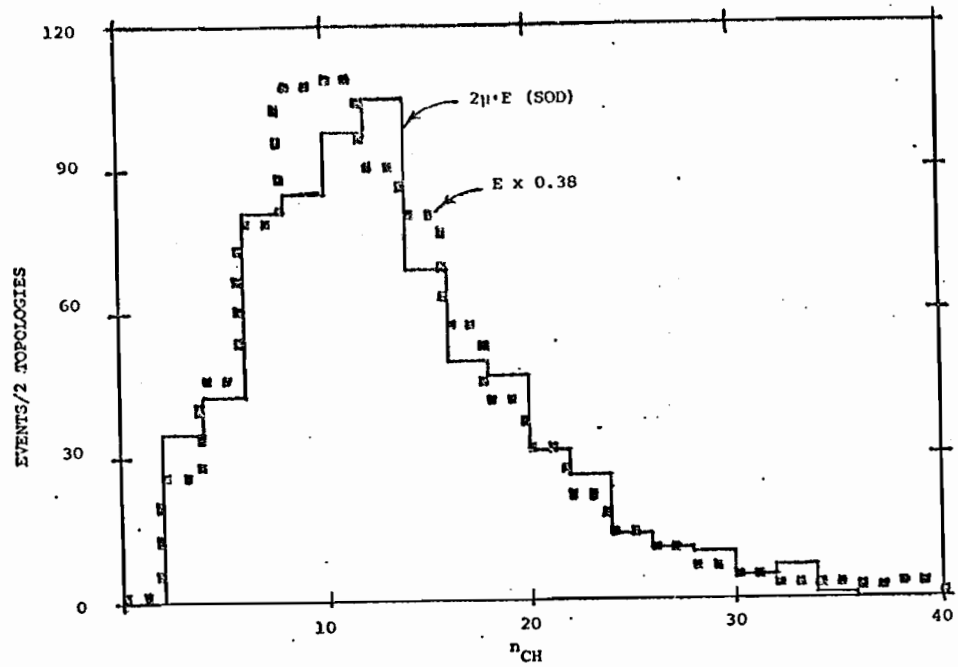

FIGURE 8-2a

2μ·E (SOD) CHARGED MULTIPLICITY
NO CUTS

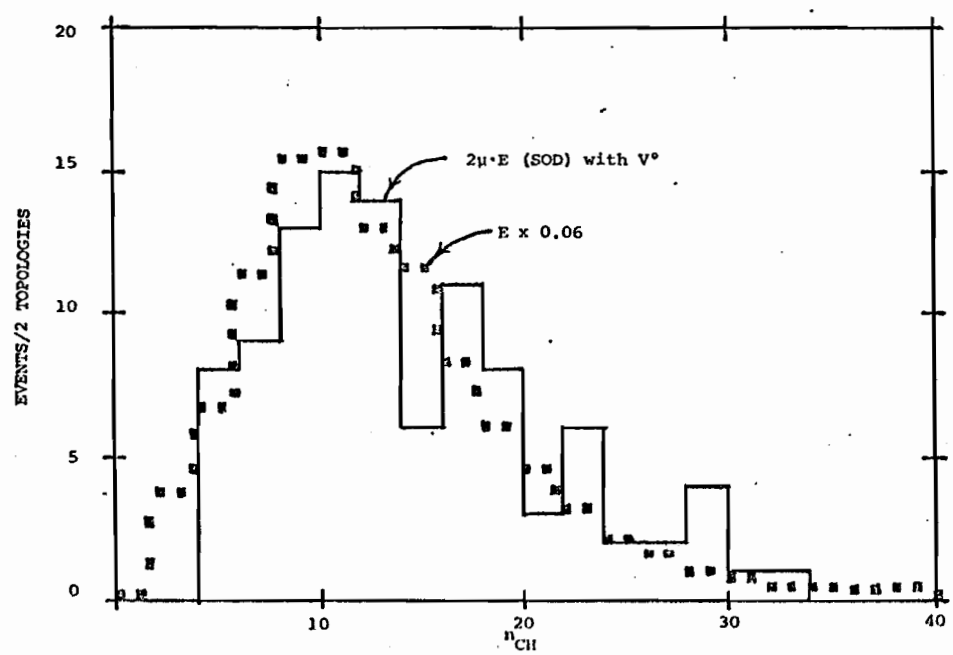

FIGURE 8-2b

2μ·E (SOD) CHARGED MULTIPLICITY WITH ONE OR MORE NEUTRAL DECAYS
NO CUTS

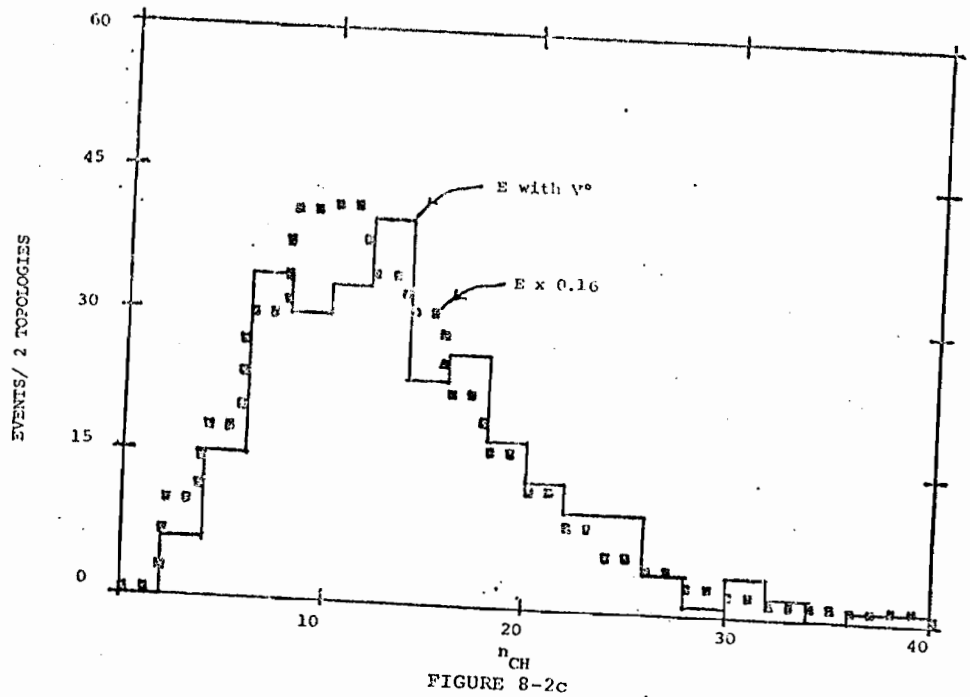

FIGURE 8-2c

E TRIGGER CHARGED MULTIPLICITY WITH ONE OR MORE NEUTRAL DECAYS
NO CUTS

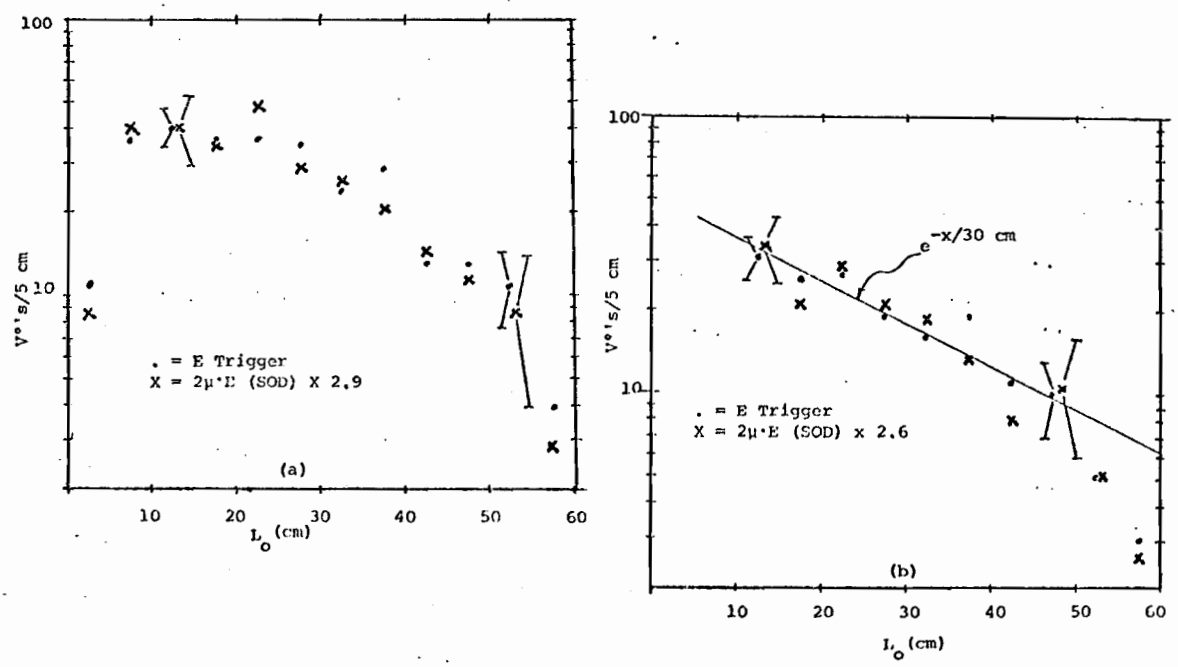

FIGURE 8-3

DECAY DISTANCE OF NEUTRALS
a) No cuts on data
b) Deleting decays within 10 cm of the primary vertex and ± 1.5 cm of the HV wire plane

Furthermore, for smaller angles, such that a gamma could strike a wire far from the target, the angular region occupied by the wires decreases. Thus, the gammas tend to convert in the central region of the chamber producing the curved shape observed. Figure 8-3b has had the 10 cm vertex and ± 1.5 cm high-voltage wire cuts applied. This plot shows a smooth exponential fall with a characteristic length of approximately 30 cm. The line in this plot is an "eyeball" fit to the data. This length corresponds to K_s^o's with average momentum of 5.5 GeV/c. This plot also shows the fall in scanning efficiency in the downstream half of the chamber. Neutral decays which convert near the downstream end of the chamber are much more likely to be fast with small opening angles. Thus, they are more likely to be obscurred by the other fast tracks, and the small opening angle makes them difficult to identify.

The second method used to study the momentum distributions of the neutral strange particles was to measure both tracks of the V° and thereby reconstruct their momenta. Normally, one would input these measurements into a large three-view geometry program for full spatial reconstruction. However, since we at present have only pin-hole optics for this system, such a reconstruction would be questionable at best. We decided, therefore, to determine the momentum of the tracks from the curvature in one view, choosing the view which had the best measurement. The assumption we make is that the magnetic field is perpendicular to the plane of the film in the view we chose. This is not a bad approximation; it is wrong by at most 15° which decreased the measured momenta by approximately 5%. We, therefore, measure the momenta of the tracks in a plane nearly perpendicular to the magnetic field. The sum of these is the momentum of the neutral in that plane. Since we know the neutral's direction in space from the vertex

reconstruction, it is a simple matter to calculate its momentum component parallel to the field. We, of course, cannot determine the individual tracks' momentum parallel to the field, so we cannot determine the mass of the neutral. This is the reason that our data are not subdivided into its K_s^o and $\Lambda°$ components. However, we do have measurements of the neutral strange particle momenta.

The measured total momentum in the lab of the V°'s is shown in Figure 8-4 and the transverse momentum (p_T) is shown in Figure 8-5, for the E and 2μ·E (SOD) triggers, with and without the V° vertex cuts. For completeness, in Figure 8-6, I have plotted the data as a function of the longitudinal momentum in the reaction center of momentum frame (p_L^*), and of $x = 2p_L^*/\sqrt{s}$, where $\sqrt{s}$ is the total energy available to the reaction in the center of momentum frame. I have also included, for comparison, data taken from the DKSW 200 GeV/c $\pi^- d$ bubble chamber exposure,[42] weighted by the acceptance of this experiment. The total number of V°'s plotted here is somewhat fewer than in the previous figures because some events were lost due to cuts on the quality of the measurement. For example, we have demanded that the tracks' fitted curvature be of opposite sign. We have lost 7 V°'s due to this cut and a total of 12 V°'s from all of the measurement quality cuts on the 2μ·E (SOD) sample. One can see, once again, that within statistics, the E and the 2μ·E triggers give identical results. Comparing the figures with and without the V° vertex cut, one sees little if any change caused by the cut except in the p_T distribution. Here we are deleting a fair number of real V°'s along with the gammas and the cut is an off-center fiducial volume cut. It discriminates most heavily against the high p_T V°'s. This makes the agreement with the bubble chamber data somewhat worse but does not significantly change the agreement between the two

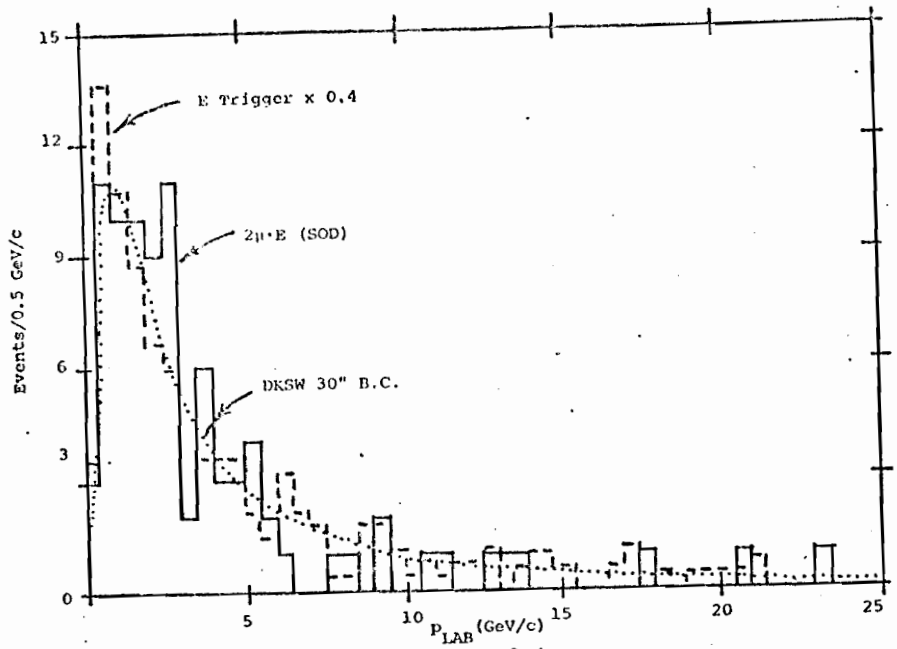

FIGURE 8-4a

NEUTRAL STRANGE PARTICLE LABORATORY MOMENTUM, NO DATA CUTS

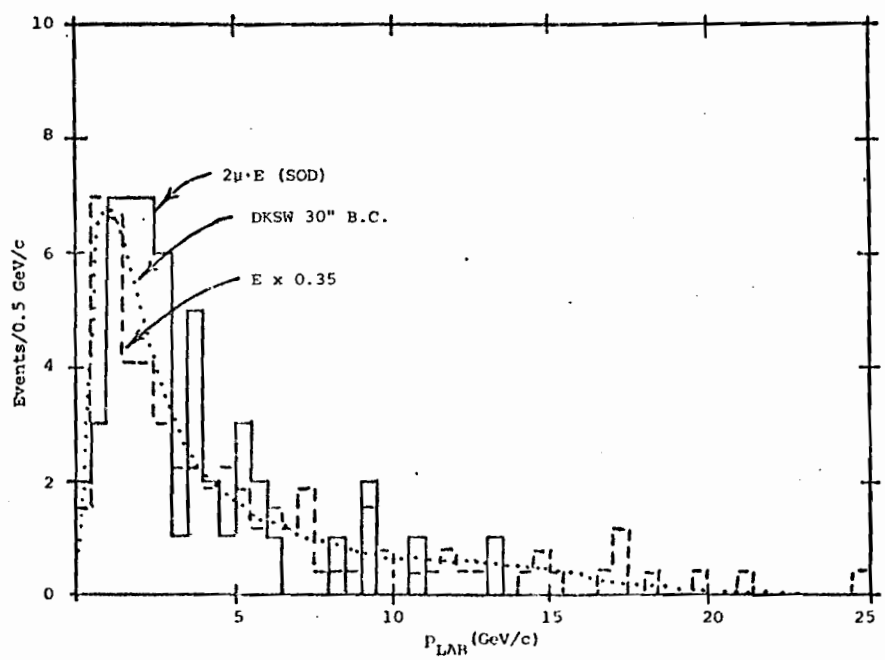

FIGURE 8-4b

NEUTRAL STRANGE PARTICLE LABORATORY MOMENTUM V° VERTEX POSITION CUTS

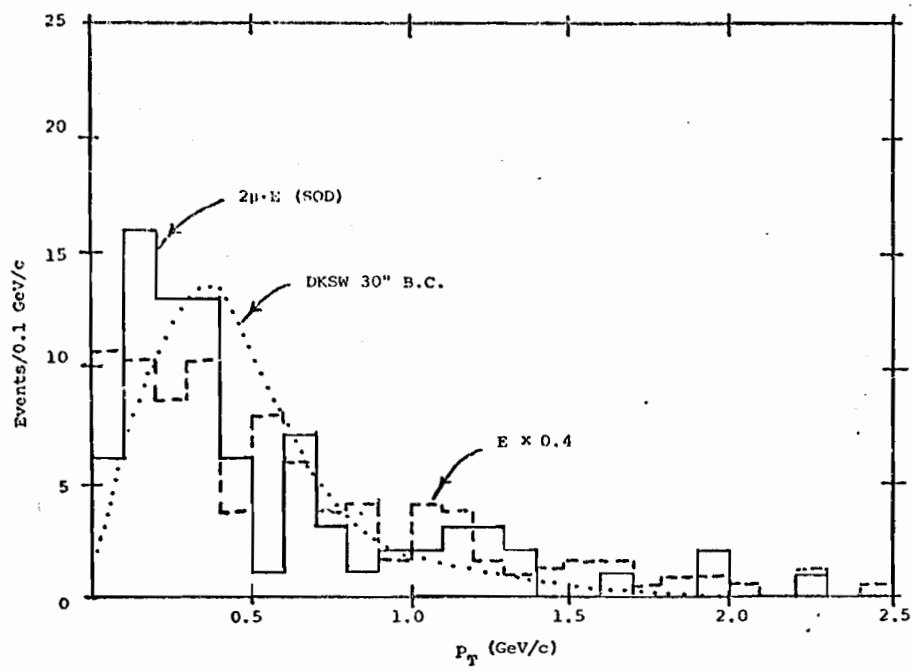

FIGURE 8-5a

NEUTRAL STRANGE PARTICLE TRANSVERSE MOMENTUM, NO DATA CUTS

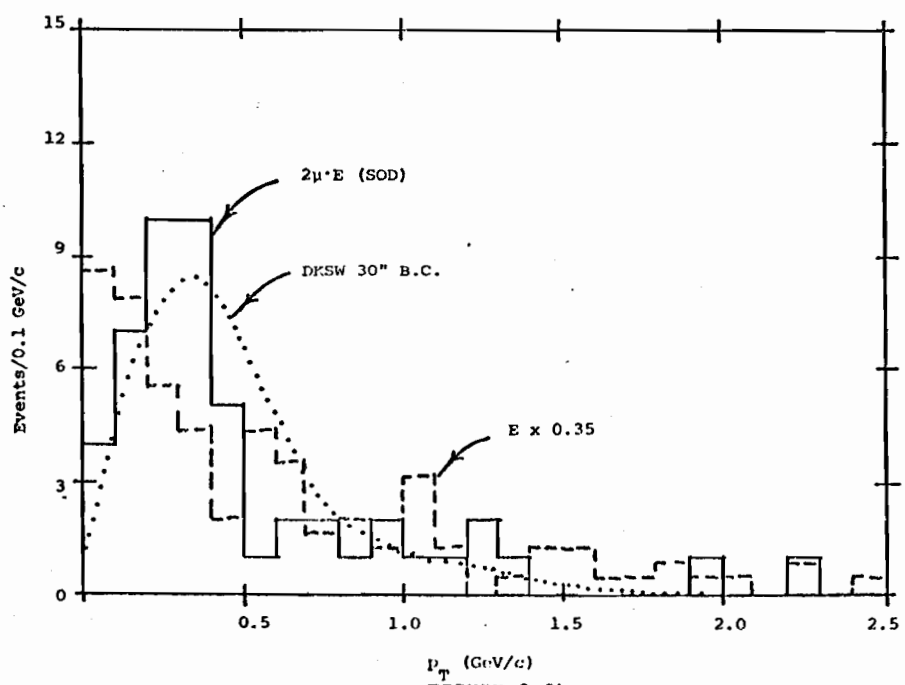

FIGURE 8-5b

NEUTRAL STRANGE PARTICLE TRANSVERSE MOMENTUM, WITH V° VERTEX POSITION CUTS

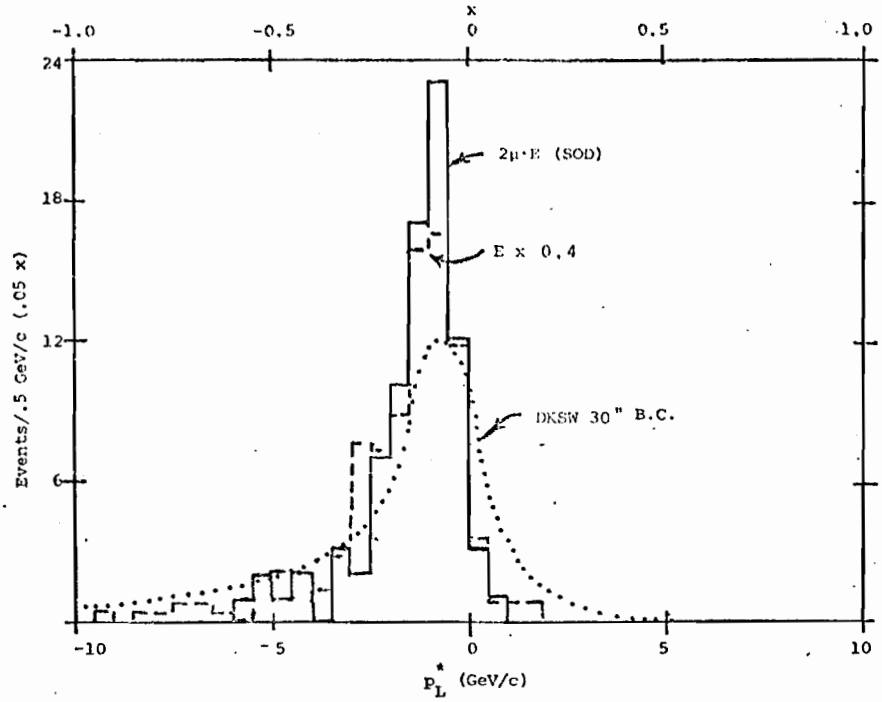

FIGURE 8-6a

LONGITUDINAL CENTER OF MASS MOMENTUM (p_L^*) AND $x = 2p_L^*/\sqrt{s}$, NO DATA CUTS

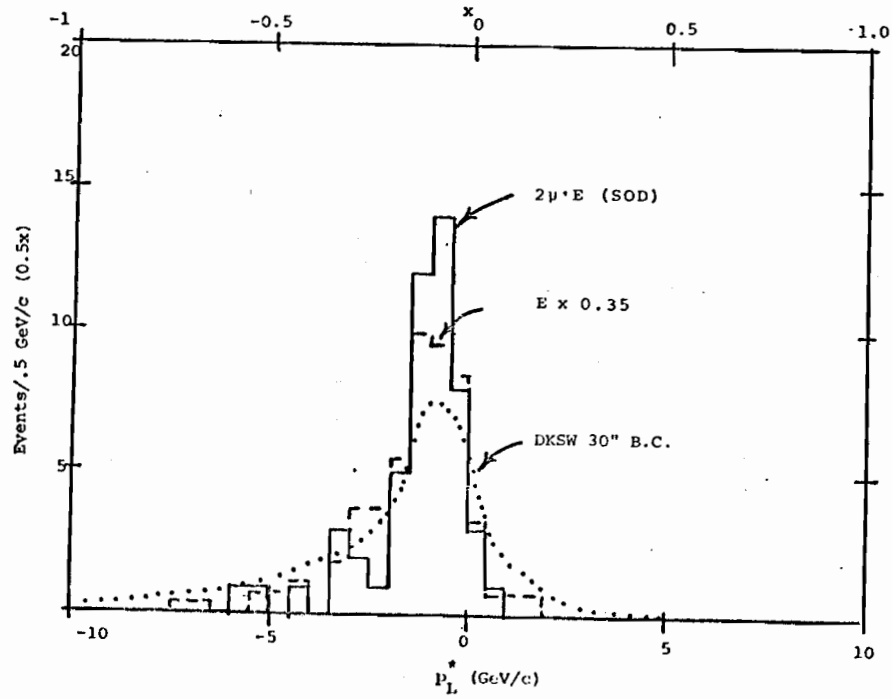

FIGURE 8-6b

LONGITUDINAL CENTER OF MASS MOMENTUM (p_L^*) AND $x = 2p_L^*/\sqrt{s}$, with V° VERTEX CUTS

streamer chamber samples.

There is one very important conclusion which can be drawn from these momentum plots - there is no enhancement of high momentum neutral strange particles. Such an enhancement would signal that perhaps charmed states were being produced which decay to muons and neutral strange particles but have such high momenta that they decay outside of the chamber. Such a result is not indicated by this data.

I noted earlier that our efficiency for detecting V°'s decreases for fast, forward neutrals. In Figure 8-7, I have plotted the probability that a K_s^o of a Λ^o would decay within the streamer chamber volume as a function of P_L^* and x, for a number of different p_T values. These curves have had the decay vertex cuts included; this produces the steep p_T dependence in the backward hemisphere. We see that there is a very high probability of a V° produced in the backward center of mass hemisphere decaying inside of the chamber, especially at high p_T, and that the acceptance falls rather quickly with momentum in the forward hemisphere. Thus, if the V°'s from the decay of a charm particle always had a large momentum forward in the center of mass, we would not see them. Such behavior is not expected, however, The charmed states should be fairly massive (a few GeV/c). The V°, therefore, should have a reasonably high momentum in the rest frame of the charmed state and should as often decay backward as forward in that frame. Thus, even if the charmed state were produced with a large momentum in the reaction center of mass, the V° should not always be highly forward in the reaction center of mass, and therefore fast in the lab. This question will be discussed in more detail in the next chapter.

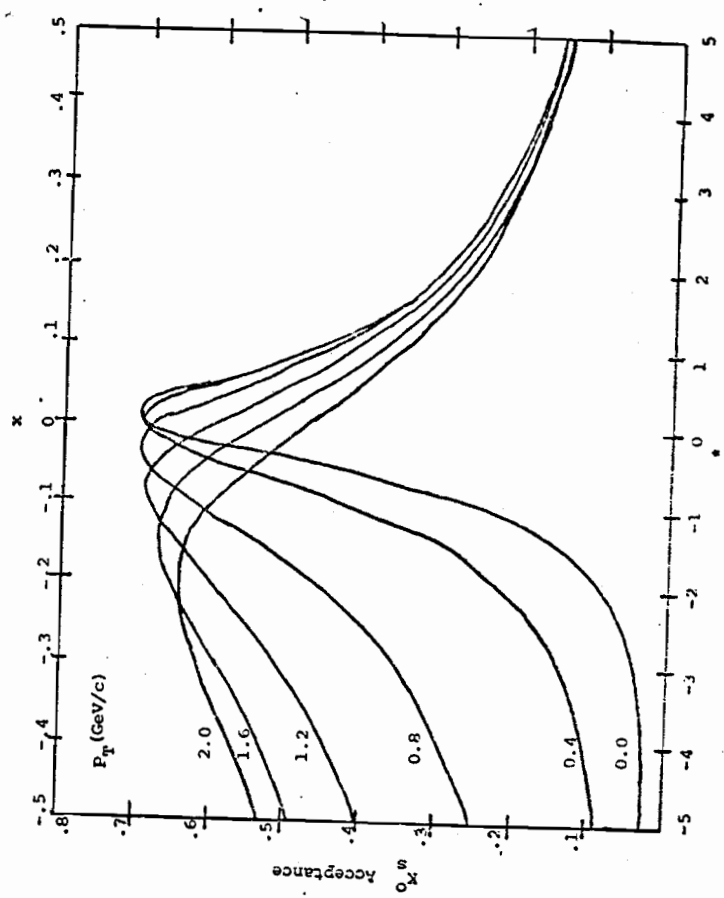

FIGURE 8-7a

$K_s^o + \pi^+ \pi^-$ ACCEPTANCE

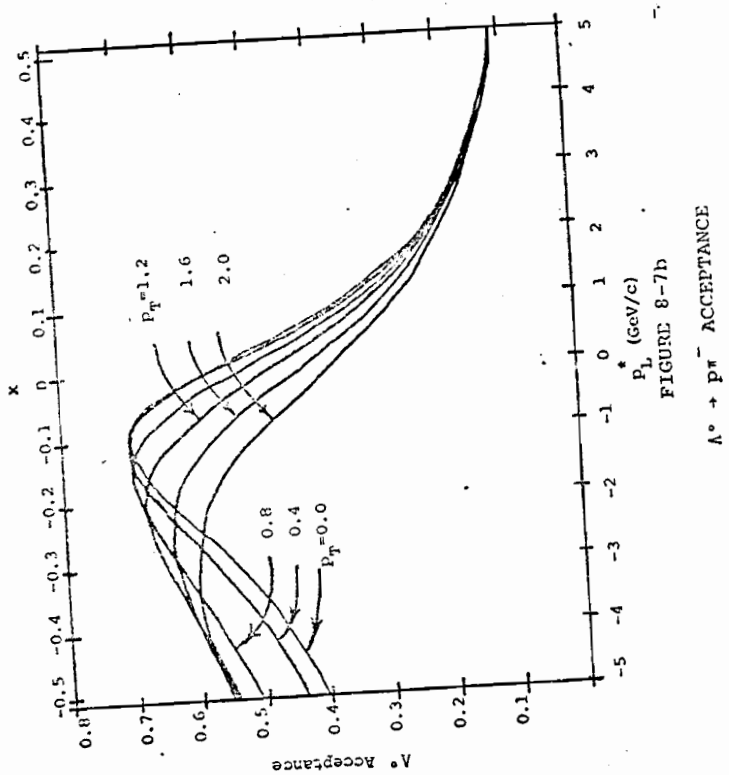

FIGURE 8-7b

$\Lambda^\circ + p\pi^-$ ACCEPTANCE

The data presented so far in this section indicates that the hadrons produced in association with muon pairs are surprisingly similar to those produced without the muon requirement. And thus that the upper limit we have calculated for the production of charmed states which decay to neutral strange particles and to muons is valid as stated.

We can now look to the muon data to see if there is any subsample of that data which shows anything peculiar and to get a feeling for the sensitivity of the experiment. I have not as yet discussed in precise terms the muon acceptance of the apparatus, since this has little bearing on the streamer chamber results presented thus far. However, it is now necessary to discuss to what portion of the muon's phase space we were sensitive. Figure 8-8a shows the probability that a single muon produced in the target would be accepted by the muon telescopes as a function of its longitudinal center of mass momentum (p_L^*) and the x variable for several values of transverse momentum (p_T), with the SOD magnet energized. Figure 8-8b shows the same thing for the non-SOD case. You will note that the acceptance is virtually all in the forward center of mass hemisphere at moderate to high p_T, although it does extend all the way to 90° in the center of mass. The fall at small $p_L^*(x)$ is due to energy loss in the absorber and the effect of the magnetic field in the SOD magnet. The fall at p_T less than 0.6 GeV/c is due primarily to the gap left in the muon telescope planes. You will also note that the overall muon acceptance is considerable. You can see this more clearly by assuming a p_T distribution and integrating the acceptance over p_T. Figure 8-9 shows the result of such a calculation for the SOD case where we have assumed an $e^{-p_T^2}$ dependence on p_T. Such a dependence is characteristic of ψ production.[43] We see that the single muon acceptance is more than 10% for $0.06 \leq x \leq 0.4$ for the SOD magnet data.

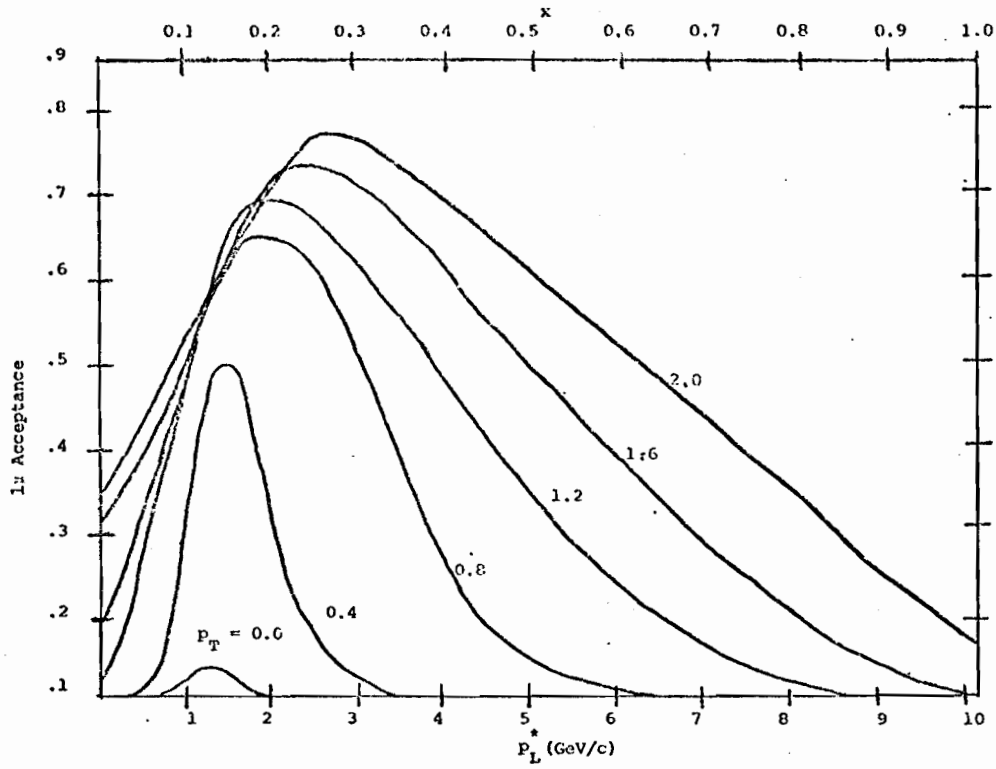

FIGURE 8-8a

SINGLE MUON ACCEPTANCE, WITH THE SOD MAGNET ENERGIZED (50 ± 6 kg-m)

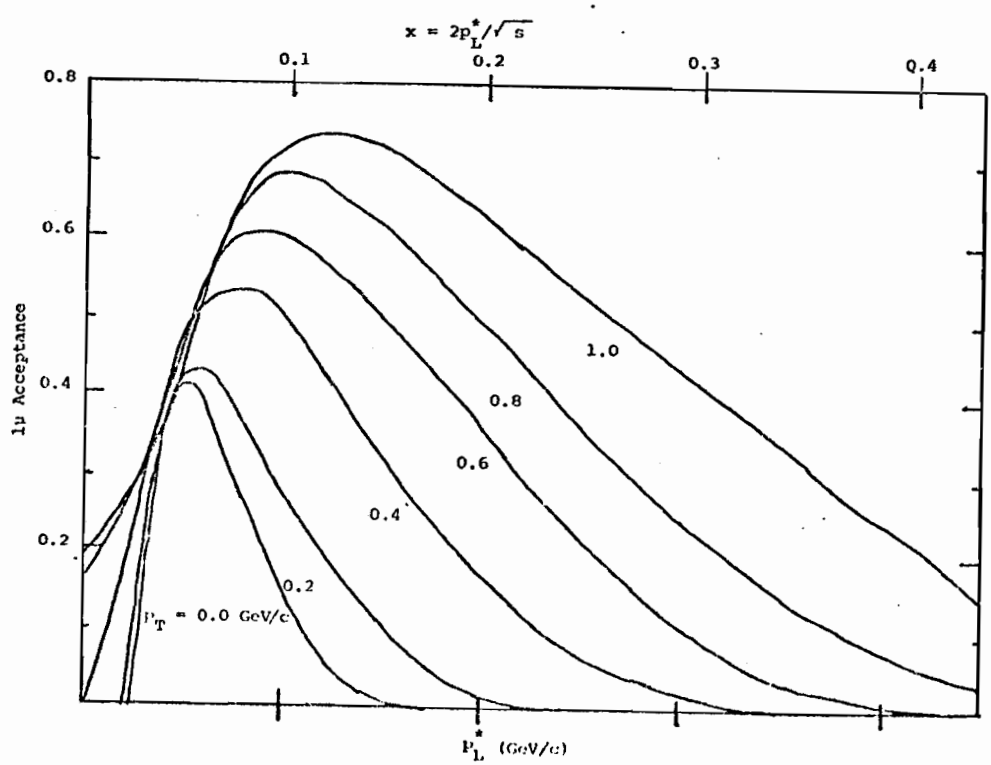

FIGURE 8-8b

SINGLE MUON ACCEPTANCE WITH NO FIELD IN THE SOD MAGNET

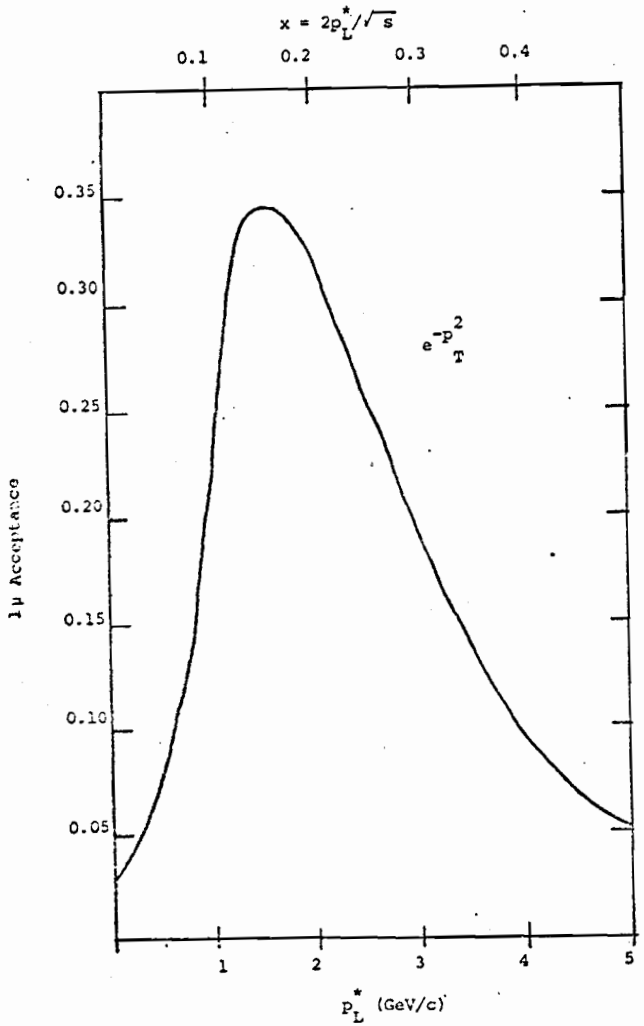

FIGURE 8-9

SINGLE MUON ACCEPTANCE VS. p_L^* (c.m.)
FOR $d\sigma/dp_T \sim e^{-p_T^2}$ SOD MAGNET ENERGIZED

This is a considerable portion of phase space.

The measured single muon momentum spectra have been plotted in Figures 8-10 and 8-11 in the lab frame and for completeness, I have included plots of the data as a function of p_L^* and x in Figure 8-12. We can, of course, only plot this data for the case where the SOD magnet was energized. These distributions are cut off by the acceptance at the low momentum end, but fall off much faster than the acceptance at high momentum, as expected. The shoulder in the p_T distribution is due to high-mass dimuon pairs. The shaded events are those (x 4) where two muons were reconstructed and have a mass greater than 2 GeV/c.

We can gain a feeling for the sensitivity of the experiment by plotting the reconstructed dimuon mass. Figure 8-13 shows the effective mass of the reconstructed dimuons. In making this plot, I have summed the 2μ·E and the 2μ·B data, but have shaded the 2μ·E events. These two samples have the primary interaction in the target and in the absorber, respectively. The smooth solid curve on this plot is a curve of the experimental acceptance as a function of mass for particle states produced with a flat x distribution ($0 \le x \le 1$) and with a p_T distribution which falls as $e^{-p_T^2}$ This p_T distribution is characteristic of the ψ.[43] We have also assumed that it decays unformly in its rest frame, for want of a better assumption.

We see a broad, low-mass enhancement with mass less than 2 GeV/c^2. We have calculated the number of vector mesons with mass lower than the ψ that we would expect to see in the low-mass peak. These are all small. For example, we would expect to see 11 ± 6 (5 ± 3%)ρ° mesons in this sample. This was calculated assuming that the rho is produced with an x distribution proportional to $(1-x)^{4.7}$ and a p_T distribution: $d\sigma/dp_T \approx p_T e^{-3.8P_T}$. [44] In addition, we have assumed that the average number of ρ°'s produced per

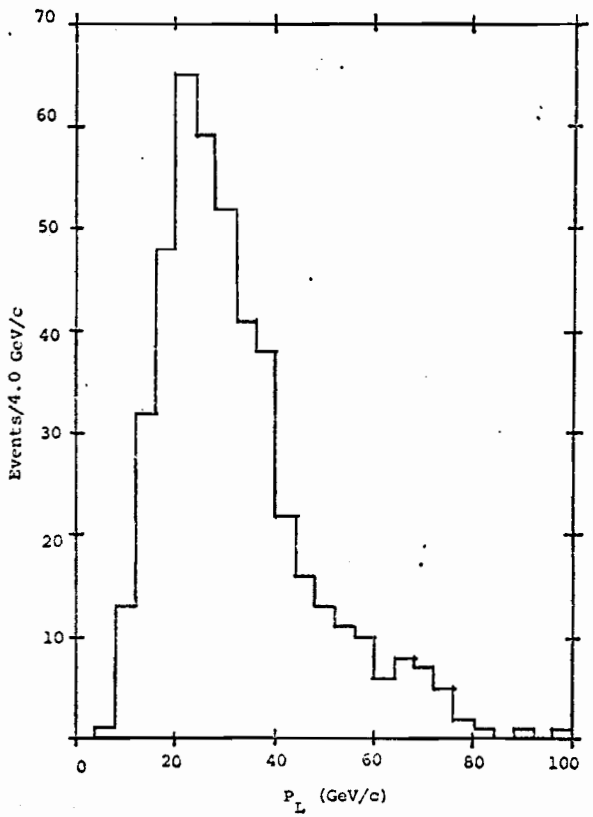

FIGURE 8-10

SINGLE MUON LONGITUDINAL LABORATORY MOMENTUM

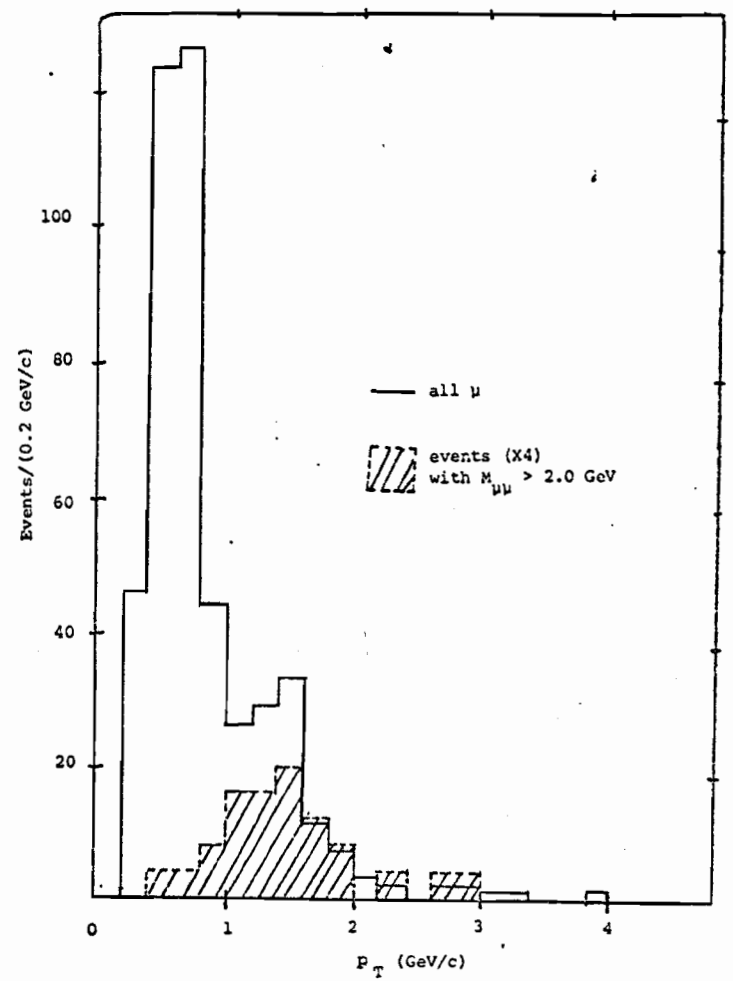

FIGURE 8-11

SINGLE MUON TRANSVERSE MOMENTUM

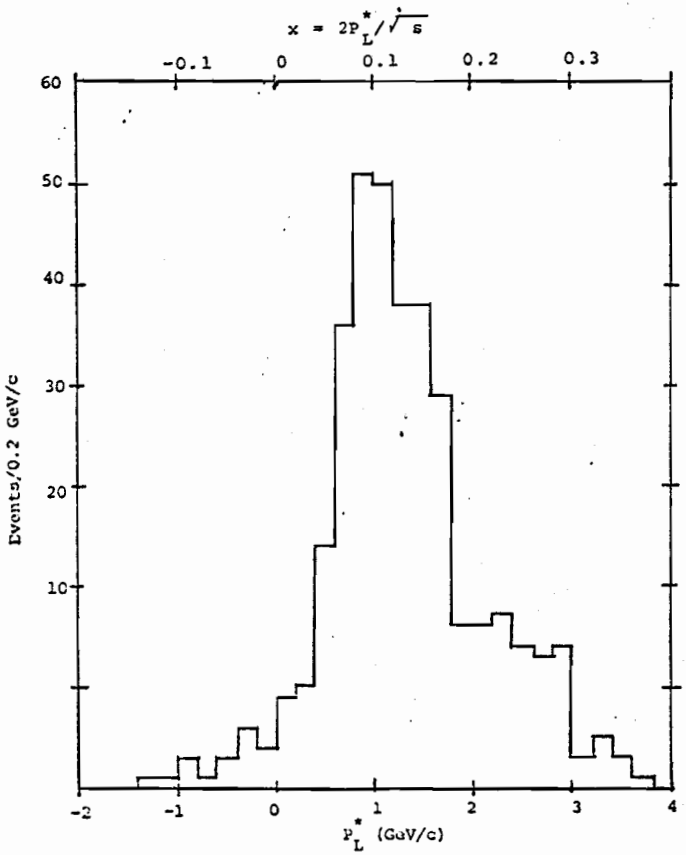

FIGURE 8-12

SINGLE MUON LONGITUDINAL CENTER OF MASS MOMENTUM (P_L^*)

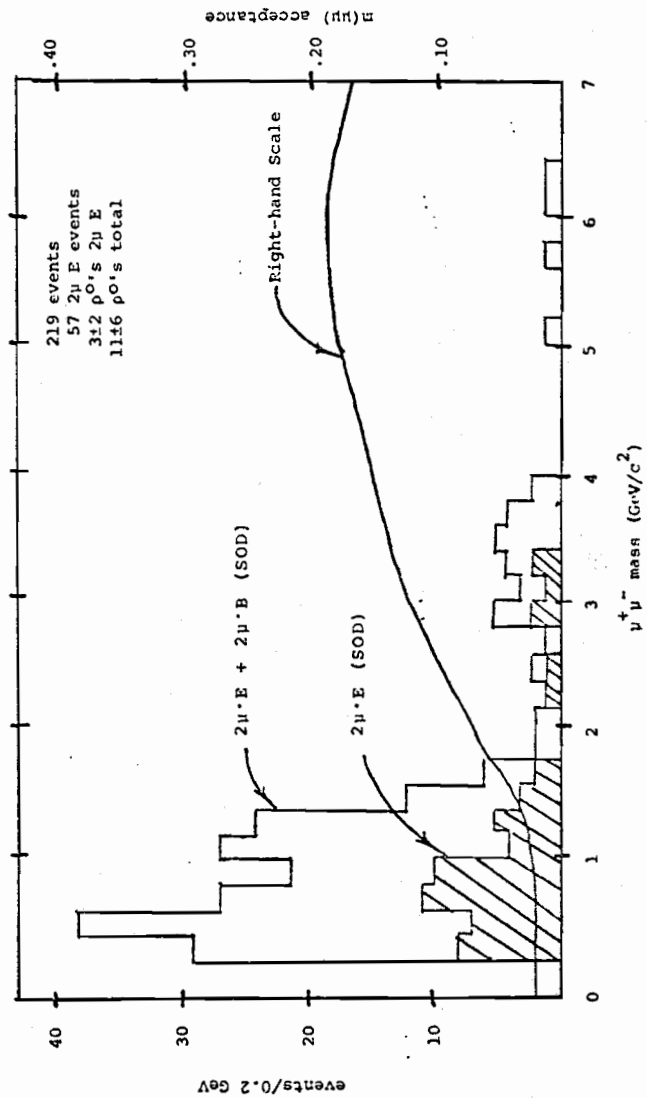

FIGURE 8-13

DIMUON MASS SPECTRUM

event is 0.35.[45] It would appear, therefore, that our trigger was not primarily due to the decay of the usual vector mesons. We do not have enough data to determine the production mechanism responsible for the low-mass events, nor was such an attempt contemplated for this experiment.

We see a ψ signal in the mass spectra which demonstrates the sensitivity of the experiment. Recall that only 1 in 10 dimuon events was fully reconstructed. The width of the ψ peak is consistent with our mass resolution. The resolution is dominated by multiple coulomb scattering of the muons in the 5 meters of absorber. This implies a mass resolution of approximately 20% for the dimuons.

We also see a few events at higher mass. We do not have enough data to say more about these events, other than that they are present. And, unfortunately, since these events come from $2\mu \cdot B$ triggers, none of them have interactions in the target.

We now separate those events where we have streamer chamber data and study correlations between the muons and the hadrons produced in association with them. One observes no enhancement of strange particles produced with the high mass dimuons. Only one of the "ψ" events contains a V°. One might expect an enhancement due to decays of charmed states produced in association with the ψ by the production process sketched in Figure 8-14. We see no evidence for this. However, with seven events we cannot say more.

There is one surprise in this data that is completely unexplained. When we plot the charged multiplicity of the fully-reconstructed dimuon events, we find a distribution which is consistent with that of the full dimuon sample. It has an average multiplicity of 13.3 ± 1.6 as compared to 12.7 ± .5 for the

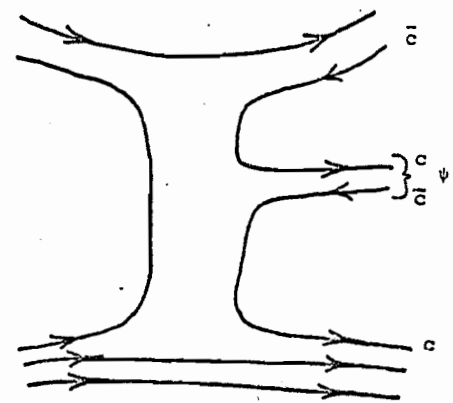

FIGURE 8-14

ψ - CHARM-ANTICHARM ASSOCIATED PRODUCTION MECHANISM

full 2μ·E (SOD) sample. However, when we look at the multiplicity of those events in the ψ region ($m_{\mu^+\mu^-} > 2$ GeV/c^2), we find that the lowest-multiplicity event contains 12 charged tracks with an average of 18.6 ± 7.0. This result is contrary to what one might naively expect. One would expect that producing a massive state like the ψ would extract a significant fraction of the energy which could go into producing other hadrons. Thus, one would expect that the number of hadrons produced in association with a ψ would be lower than the average, not higher. A plot of the average multiplicity is shown in Figure 8-15 as a function of the dimuon mass. This plot is very suggestive, but the statistics are too low for a good determination. However, it would be difficult to fit a falling curve to this plot.

The last distribution we can examine is the effective mass of the muon-strange particle pairs found in the experiment. This distribution is plotted in Figure 8-16. The smooth curve was calculated by combining a muon and a V° from different events and exhibits the lack of correlation in the μ-V° mass. The "peak" at 4 GeV/c^2 is probably not real. It is only one standard deviation above the background. The background curve could be renormalized to make this "peak" stronger, but it would still be marginal.

It is clear from the data presented here, that if charmed states are being produced in hadron-hadron collisions, we are unable to find evidence of it, even though our sensitivity was good, as exhibited by the presence of a ψ signal in the dimuon mass distribution. We have found no evidence for charm production in any of the available variables, and as stated earlier, we do not need to make any corrections to the calculated upper limits. We need only chose that upper limit from Table 8-6 which we feel is the most

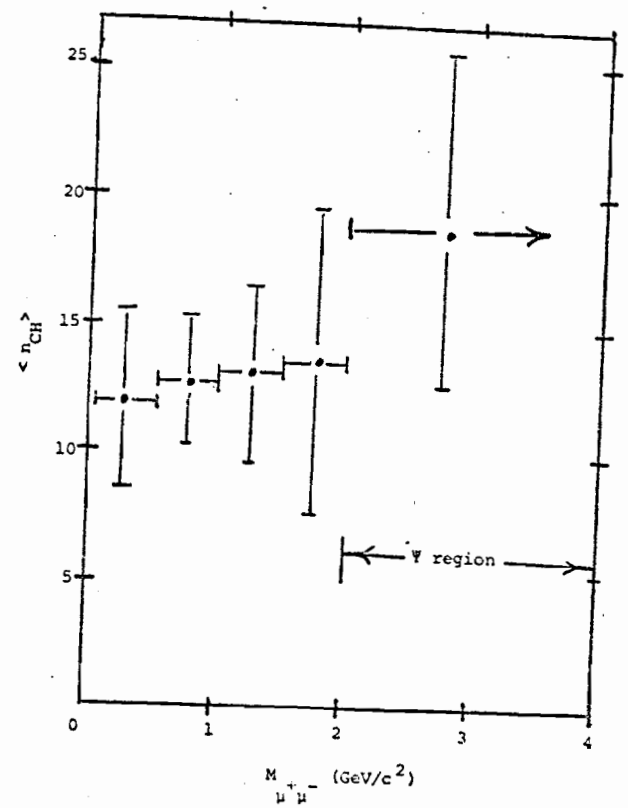

FIGURE 8-15

AVERAGE CHARGED MULTIPLICITY VERSUS DIMUON MASS

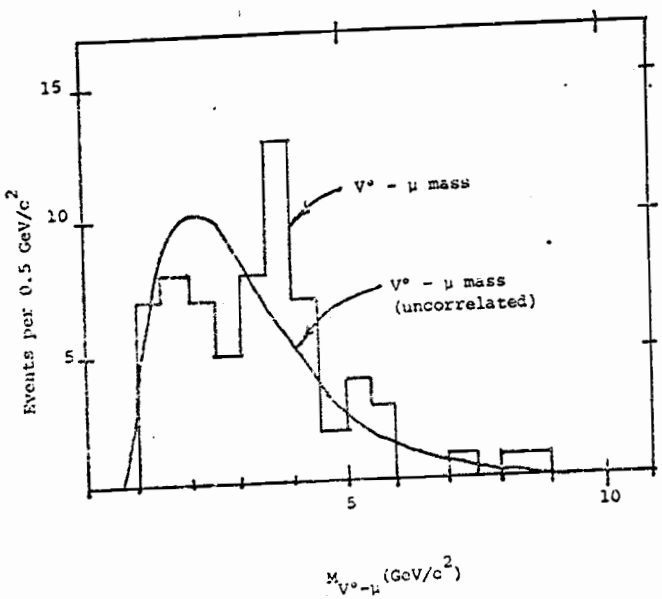

FIGURE 8-16
MUON-STRANGE PARTICLE EFFECTIVE MASS

valid. In making this choice, we note two points. The upper limits are stable with respect to the details of the data selection, but we do not wish to choose either of the extremes in the value calculated. And, as far as is possible, we feel that the gamma contamination should be removed. For the SOD data, we have, therefore, chosen to use the limit calculated after deleting those neutral decays which lie within 10 cm of the primary vertex, and within ± 1.5 cm of the central high-voltage wire plane. For the non-SOD data, we use the weighted average of the data scanned at Seattle, Orsay, and Davis. This data has no cuts made. Table 8-7 lists the values of these four upper limits using all three of the assumed atomic number dependences which lead to the cross sections listed in Table 8-2. I have kept both the SOD and non-SOD limits, and the limits calculated from α_c and from $\langle V° \rangle_c$ since these could in principle have very different acceptances in our apparatus. I will discuss this question of acceptances in the next chapter.

Three features of the data presented in this chapter are especially interesting. The first is that we do not observe a charm signal. Upper limits at the 90% confidence level of the charm signal which could be present in the data are given in Table 8-7. The second is that we see no difference between the spectra of the hadrons produced with dimuons when compared to an all inclusive reaction (the E trigger). This is surprising when one considers the difference in the trigger cross sections:

$$\sigma\ (\pi^- A \to \mu\mu + x)/\sigma\ (\pi^- A \to x) = 3.6 \times 10^{-6}.$$

One would naively expect at least some differences in the data samples. This result implies that in some fashion, the dimuon "piece" of the reaction factors from the rest of the interaction. The only exception to this last statement is that we see some evidence that the multiplicity of those

LIMIT TYPE	$n = 0.67^+$	$n = 0.75^+$	$n = 1^+$
Σ_α (SOD) (nb)	1.4	1.1	0.64
$\Sigma_{\langle V^* \rangle}$ (SOD) (nb)	1.2	1.0	0.57
Σ_α (NON-SOD) (nb)	11.4	9.5	5.4
$\Sigma_{\langle V^* \rangle}$ (NON-SOD) (nb)	6.3	5.3	3.0

$^+$ Nuclear Cross Sections Vary as A^n

TABLE 8-7

UPPER LIMITS AT 90% CONFIDENCE LEVEL OF THE CROSS SECTION OF THE CHARM SIGNAL PRESENT IN THE DATA

events which contain massive dimuon pairs, in the "ψ" mass region above 2 GeV/c^2, is higher than average. Unfortunately, our data are extremely limited in this region, so a definitive statement on this point must be left for a later experiment.

IX. MODEL CALCULATIONS

In the previous chapter, we presented the experimental results of the search for charm in the streamer chamber. We found very low upper limits on the charm signal present in the dimuon data samples, with and without the magnetized iron energized, and we found nothing in the particle distributions which would indicate charm was present in a subsample of the data. These limits are model independent. We found no differences between the dimuon samples and the control sample which would indicate a need to apply corrections to the results. However, the limits, as stated, are strong functions of our experimental acceptance. Removing this dependence cannot be done in a model independent way. Therefore, we have calculated model acceptances using several different models.[46] These span a range of possible types and indicate the types of production mechanisms to which we were sensitive.

As mentioned earlier, the upper limits we have calculated are upper limits on a quantity like: $\sigma_{c\bar{c}}\, B_\mu^2(V^\circ)\, g$, where $\sigma_{c\bar{c}}$ is the production cross section of a Charmed-anti-charmed pair, $B_\mu^2(V^\circ)$ is the square of the branching ratio to muons and V°'s, and g is the acceptance. The charmed pair could in principle be any charmed states which can decay directly or through a cascade of charmed states to a muon and a strange particle. This could include any of the charmed mesons or baryons. Any of these could produce an excess of V°'s (either K_S^0 or Λ°) in the dimuon sample. In addition, the mechanism pictured in Figure 8-14 could contribute. However, for simplicity in the calculations we have neglected all of the heavier pairs of charmed states and have concentrated on the lightest, presumably the 0^- D meson of Figure 2-4. The $D\bar{D}$ pair should have the largest production cross section simply because it should be the lightest. We have

also restricted ourselves to two and three-body decay modes. We wanted to keep the assumptions necessary for the calculations to a minimum. One should keep in mind that the acceptances we have calculated are, in a sense, lower bounds on our true acceptance. We were sensitive to many more production modes and decay modes than those considered here.

These restrictions limit our investigation to production of D^+D^- pairs with the subsequent decays: both semi-leptonically, $D \to K^0\mu\nu$; one semi-leptonically and one leptonically, $D \to \mu\nu$. The upper limits we have found then correspond to:

$$\Sigma \geq \sigma_{D^+D^-}(B_{SL}^2\, g_1 + B_{SL}B_L g_2) \qquad (9\text{-}1)$$

where B_{SL} and B_L are the semi-leptonic and leptonic branching ratios, respectively, g_1 and g_2 are the corresponding acceptances, and $\sigma_{D^+D^-}$ is the production cross section for the D^+D^- pair. Since the D^+ or D^- decays to $\bar{K}^\circ$ or K°, respectively, with a strength proportional to $\cos^2\theta_c$ as mentioned earlier, we have assumed that this portion of the branching ratio is unity. The branching ratios of the K° and $\bar{K}^\circ$ to K_S^0 and then to $\pi^+\pi^-$, which can be seen in the chamber have been absorbed into the acceptances.

Recall that we have calculated two different upper limits; one based on the number of events containing neutral strange decays observed (Σ_a) and one based on the average number of strange decays per event observed ($\Sigma_{\langle V^\circ \rangle}$). The acceptance for the leptonic-semi-leptonic decay mode (g_2) is the same for these cases, only one V° could be observed. The semi-leptonic-semi-leptonic acceptance (g_1) is slightly different for the two cases. In calculating the average number of decays seen, those events where two are seen are counted twice. However, we will see that in these models, the difference is so small that it can be neglected.

Three different D^+D^- production models have been investigated. The first was an independent production model (the Independent Model), where each D was independently produced like a ψ, that is with a flat x distribution, $0 \le x \le 0.6$ and $e^{-13.6x}$ for $x > 0.6$ and $e^{-p_T^2}$ transverse distribution.[47] The only correlation built into this model was that momentum must be conserved, $x_{D+} + x_{D-} \le 1$. In the second model (the Correlated Model), the D^+D^- system was given a momentum determined by the ψ distribution, and was then allowed to decay, with no relative momentum between the D^+ and the D^-. And in the third model (the Diffractive Model) the D^+D^- system was given 225 GeV/c longitudinal momentum and a transverse momentum according to an $e^{-10p_T^2}$ distribution. The D^+D^- system was then allowed to decay isotropically with a total kinetic energy of 400 MeV in the D^+D^- rest frame.

Each of the D's were then allowed to decay isotropically in the decay center of mass, either both semi-leptonically, or one semi-leptonically and the other leptonically. The muons were propagated through the streamer chamber magnet's magnetic field and the absorber, both with and without the magnetic field in the SOD magnet, taking multiple scattering and energy loss into account. It was then determined if the two muons would have been counted by two different muon telescopes. The probability that the X°'s would have decayed in the streamer chamber was also determined. The fraction of Monte Carlo generated events which satisfied the requirements that both muons and at least one of the V°'s were accepted was recorded. This entire process was repeated for three assumed D masses; two, three, and five GeV/c^2. The resulting values for g_1, g_2, and $g = g_1 + g_2$ for all of the various cases are tabulated in Tables 9-1. The value $g = g_1 + g_2$ is included because if we assume that $B_{SL} = B_L = B$, then our limit becomes

D mass (GeV/c^2)	g_1^{a} +	$g_1^{<V^\circ>}$ +	g_2 #	$g = g_1 + g_2$ g^{a}	$g^{<V^\circ>}$
INDEPENDENT MODEL					
2	.0078	.0085	.0148	.023	.023
3	.0136	.0150	.0178	.031	.033
5	.0161	.0175	.0038	.040	.041
CORRELATED MODEL					
2	.0059	.0065	.0098	.016	.016
3	.0106	.0118	.0142	.025	.026
5	.0141	.0154	.0196	.034	.035
DIFFRACTIVE MODEL					
2	.0112	.0119	.0158	.027	.028
3	.0184	.0198	.0270	.045	.047
5	.0202	.0219	.0252	.045	.047

+ Acceptance for Semi-leptonic - Semi-leptonic Mode
# Acceptance for Leptonic - Semi-leptonic Mode

TABLE 9-1a

D^+D^- ACCEPTANCE (SOD)

D mass (GeV/c^2)	g_1^{α} +	$g_1^{<V^\circ>}$ +	g_2 #	$g = g_1 + g_2$ g^{α}	$g^{<V^\circ>}$
INDEPENDENT MODEL					
2	.0172	.0187	.0222	.039	.041
3	.0244	.0267	.0318	.054	.059
5	.0234	.0252	.0300	.053	.055
CORRELATED MODEL					
2	.0153	.0169	.0230	.038	.040
3	.0192	.0212	.0252	.044	.046
5	.0202	.0204	.0286	.049	.049
DIFFRACTIVE MODEL					
2	.0178	.0189	.0214	.039	.040
3	.0256	.0273	.0300	.056	.057
5	.0287	.0308	.0364	.065	.067

+Acceptance for Semi-leptonic - Semi-leptonic Mode
#Acceptance for Leptonic - Semi-leptonic Mode

TABLE 9-1b

D^+D^- ACCEPTANCE (NON-SOD)

$\Sigma \geq B^2 g\, \sigma_{D^+D^-}$. In the table g_1 and g are listed twice. The first (g_1^{α} and g^{α}) corresponds to the upper limit using the number of events containing one of more V°'s (Σ_{α}). The second ($g_1^{<V^\circ>}$ and $g^{<V^\circ>}$) corresponds to using the average number of V°'s per event ($\Sigma_{<V^\circ>}$).

We see from the tables that the difference between the acceptance for Σ_{α} and $\Sigma_{<V^\circ>}$ is, indeed negligible. We also see that none of the acceptances are large but none are extremely small. The overall values of g are between 1.6% and 4.5% for the SOD case, and between 3.8% and 6.7% with the SOD magnet off. Notice that these acceptances are very similar. The higher momentum required for a muon to pass through the apparatus with the SOD magnet on, makes at most a factor of two difference in the acceptance.

We have purposely avoided models which would have given very high acceptances at the expense of being more artificial than are these. Such models would be those which peak strongly at small x. The decay of such a state could easily put the K° and the muon into opposite center of mass hemispheres, and thus into the part of phase space with the largest acceptance for each.

What can we now say about the cross sections for producing Charmed-anticharm states? Tables 9-2 lists $\sigma_{D^+D^-}B^2$ for the three models discussed above, and for three masses, using the upper limits $\Sigma_{<V^\circ>}$ (SOD) and $\Sigma_{<V^\circ>}$ (non-SOD) of Table 8-7, with the assumptions that:

i) $D\bar{D}$ production dominants charm production;

ii) Only $D \to \mu\nu$ and $D \to K\mu\nu$ are important;

iii) $B_{SL} = B_L = B$;

iv) Nuclear Cross Sections vary as A.

The first two assumptions are almost certainly wrong. However, restricting the calculation this way, overestimates the cross sections, so it is the

MODEL (SOD)*

D mass (GeV/c^2)	Independent	Correlated	Diffractive
2	24.8 nb	35.6 nb	20.4 nb
3	17.3 nb	21.9 nb	12.1 nb
5	13.9 nb	16.3 nb	12.1 nb

MODEL (NON-SOD)*

D mass (GeV/c^2)	Independent	Correlated	Diffractive
2	73.2 nb	75.0 nb	75.0 nb
3	50.8 nb	65.2 nb	52.6 nb
5	54.5 nb	61.2 nb	44.8 nb

---

* Cross Sections Assume:

i) $D\bar{D}$ dominates charm production;

ii) Only $D \to \mu\nu$ and $D \to K\mu\nu$ are important;

iii) $B_{Semi\text{-}leptonic} = B_{Leptonic}$;

iv) Nuclear Cross Section varies as A.

TABLE 9-2

UPPER LIMIT ON $\sigma_{D^+D^-}B^2$ FOR THREE MODELS OF $D\bar{D}$ PRODUCTION

safe thing to do. We can now go one step further. If we assume that B = 0.1, as was discussed in Chapter II, and take, as a representative number the cross section for a D of 2 GeV/c^2, produced diffractively, then:

$$\sigma_{D^+D^-} \leq 2.0\ \mu b.$$

The calculations discussed in this section are really only guesses. We would be very surprised if any of them turned out to be correct. However, they do show that this experiment did have considerable acceptance for charmed states. It is very likely that the D^+D^-, two and three-body decay modes considered here are only a small part of the total charm cross section to which we were sensitive. In fact, it is not at all unreasonable that one could replace $\sigma_{D^+D^-}$ by σ^{Total}_{Charm} everywhere in the tables.

X. CONCLUSION

In this dissertation, I have discussed a streamer chamber search for new states of matter performed in early and mid 1975 at the Fermi National Accelerator Laboratory by the Seattle-Orsay-Davis collaboration.

We triggered the streamer chamber on interactions of a 225 GeV/c π^- beam incident on a Lucite ($C_5H_8O_2$) target in the streamer chamber, both with and without a directly produced muon pair. We then looked in the streamer chamber for correlations between the triggering muons and the co-produced hadrons. In particular we searched for an enhancement in the number of neutral strange particle decays observed with the dimuon trigger. An enhancement, if found, would be strong evidence for the existence of the production of pairs of particles which carry the charm quantum number. No enhancement was found. We therefore set a rather low upper limit on the strength of charmed particle production in the experiment, of 0.6 nb to 1.2 nb with part of the iron hadron absorber magnetized and 3.0 nb to 6.4 nb without it magnetized. The range in the limits corresponds to assumptions of A and $A^{0.67}$ atomic number dependence of the nuclear cross section. The data and method by which these limits were calculated were presented in detail in Chapter VIII.

Inserting acceptances found by assuming the three different production mechanisms discussed in Chapter IX, and assuming an A cross section dependence, we find the very conservative upper limits on the charm cross section times branching ratio to muons squared listed in Table 9-2.

We have shown that the background signals present in the data are small, except that approximately 45% of the triggering dimuons were produced by secondary interactions in the hadron absorber. This background, however, does not effect the result, since it could not effect the number of strange particles observed in the streamer chamber. The possible background signals were discussed in detail in Chapter VII,

along with the details of the measurements made.

We have shown that we were sensitive enough to detect a ψ signal in 10% of the data where we were able to fully reconstruct the dimuon pair. We had an overall sensitivity of 22 events per nanobarn of dimuon cross section, assuming that the cross section depends on the target's atomic number as A. We have also shown that the probability of detecting a dimuon plus at least one neutral strange particle from D^+D^- decays was good, being near 2-4% for some reasonable models, as discussed in Chapter IX.

And lastly, although our search for new states of matter was negative, we did find two very surprising results. The first is that within the statistical significance of this experiment, there is no difference between the spectrum of hadrons produced with and without directly produced dimuons. This result is presented in Chapter VIII, Figures 8-1 through 8-6. The second, and even more surprising result is that the events in which a ψ is produced, seem to have an above average number of charged secondaries. This completely unexpected and unexplained result is presented graphically in Figure 8-15.

APPENDIX A

This appendix gives the details of the derivation of an upper limit on decay contributions to a dimuon trigger, assuming that the measured single muon rate is principally due to such decay. This is included in this dissertation because there has been much controversy among our collaborators on the subject and I believe that it is worth setting down in detail.

First, I must define a few quantities.

Let $a(p)$ = the probability that a secondary pion, or kaon of momentum p will reproduce a muon, which is in our experimental acceptance either by decay or by secondary interaction.

Let $a'(p)$ = the probability that a secondary pion, or kaon will produce a second muon which is counted. In general, $a'(p) = c \cdot a(p)$ where c is a constant to be determined.

Let P_1^N = the probability of counting one or more muons from an event with N charged tracks

Let P_2^N = the probability of counting two or more muons from an event with N charged tracks

Then:
$$P_1^N = \sum_i^N \frac{1}{\sigma_N} \int dp_i\, a(p_i) \frac{d\sigma_N}{dp_i} = \frac{N}{\sigma_N} \int dp\; a(p) \frac{d\sigma_N}{dp} \tag{1}$$

and:
$$P_2^N = \sum_i^N \sum_{j>i}^N \frac{1}{\sigma_N} \int dp_i dp_j\; a(p_i) a'(p_j) \frac{d^2\sigma_N}{dp_i dp_j} \tag{2}$$

where $\frac{d\sigma_N}{dp_i}$ and $\frac{d^2\sigma_N}{dp_i dp_j}$ are the inclusive and semi-inclusive differential cross sections for charged particles in N prong events,

and:
$$\sigma_N = \int dp_i \frac{d\sigma_N}{dp_i} = \int dp_i\, dp_j \frac{d^2\sigma_N}{dp_i dp_j}.$$

Replacing $a'(p)$ by $c \cdot a(p)$ and $\frac{d^2\sigma_N}{dp_i dp_j}$ by $\frac{1}{\sigma_N}\frac{d\sigma_N}{dp_i}\frac{d\sigma_N}{dp_j}$, that is neglecting correlations we have:

$$P_2^N \approx \frac{c}{\sigma_N^2} \sum_i^N \sum_{j>i}^N \int dp_i dp_j\; a(p_i)\, a(p_j) \frac{d\sigma_N}{dp_i} \frac{d\sigma_N}{dp_j}$$

Let $I_i^N = \frac{1}{\sigma_N} \int dp_i\, a(p_i) \frac{d\sigma_N}{dp_i}$ and $I^N = \frac{1}{\sigma_N} \int dp\; a(p) \frac{d\sigma_N}{dp}$

then:
$$P_2^N \approx c \sum_i^N I_i^N \sum_{j>i}^N I_j^N = \frac{c}{2} \sum_i^N I_i^N \sum_j^N I_j^N (1-\delta_{ij}).$$

Summing over i and j we have:

$$P_2^N \approx \frac{c}{2} N\,(N-1)\,(P_1^N)^2 \tag{3}$$

And Equation (1) can be written:

$$P_1^N = N p^N \tag{4}$$

Summing over charged prongs and weighting by the probability of producing N charged prongs:

$$P_1 = \sum_N \left(\sigma_N/\sigma_T\right) P_1^N = \sum_N \left(\sigma_N/\sigma_T\right) N p^N \tag{5}$$

and

$$P_2 = \sum_N \left(\sigma_N/\sigma_T\right) P_2^N \approx \sum_N \left(\sigma_N/\sigma_T\right) (c/2)\, N(N-1)\, (p^N)^2 \tag{6}$$

If we assume that our one muon trigger is dominated by decays, then:

$P_1 = 1\mu \cdot E/E$ and we can write:

$p^N = \frac{1}{N}\left(\frac{n_N}{n_T}\right)_{1\mu} \frac{\sigma_T}{\sigma_N} P_1$ where $\left(\frac{n_N}{n_T}\right)_{1\mu}$ is the fraction of one muon events measured to have had N charged prongs. Likewise

$\frac{\sigma_N}{\sigma_T} = \left(\frac{n_N}{n_T}\right)_E$ where these are measured using the E or total cross section trigger.

Then:

$$P_2 \approx \frac{c}{2} \sum_N \left(\frac{n_N}{n_T}\right)_E N(N-1) \left[\frac{1}{N} \left(\frac{n_N}{n_T}\right)_{1\mu} \left(\frac{n_T}{n_N}\right)_E P_1\right]^2$$

$$P_2 \approx \frac{c}{2} P_1^2 \left[\sum_N \frac{n_{(N-1)}}{N^2} \left(\frac{n_N}{n_T}\right)^2_{1\mu} \left(\frac{n_T}{n_N}\right)_E\right] \tag{7}$$

But the one muon and E multiplicity distributions are not very different.

$$\langle n_{CH} \rangle_E = 12.3; \quad \langle n_{CH} \rangle_{1\mu} = 13.0 \qquad \text{So:}$$

$$P_2 \approx \frac{c}{2} P_1^2 \left[\sum_N \frac{N(N-1)}{N^2} \left(\frac{n_N}{n_T}\right)_{1\mu}\right] \tag{8}$$

Dropping the 1 compared to N and making this an upper limit we have:

$$P_2 \lesssim \frac{c}{2} P_1^2 \quad \text{or} \quad \frac{2\mu \cdot E}{E}\Big|_{\text{Decay}} \lesssim \frac{c}{2} \left(\frac{1\mu \cdot E}{E}\right)^2 \tag{9}$$

This is the result required except for determining the constant c. We once more turn to the data, in this case, the spark chamber and muon telescope data. With the SOD magnet off nearly all of the muons were counted by the central four counters. Thus c ≈ 3/4, if one muon had already been counted, the second had only 3 out of 4 telescopes to traverse. With the SOD magnet on, we know from the spark chambers that most negative muons passed through the bottom two telescopes and most positive muons through the top two telescopes. Thus, the probability of counting a second muon of a given sign which traversed one of the four telescopes depends on its sign, and the sign of the first muon counted: $a^{++} = a^{--} = 1/2$;

$a^{+-} = a^{-+} = 1$ with obvious notation. Assuming that the sign of the muons is uncorrelated, i.e., $p^+ = p^- = 1/2$ where the p's are the probability of producing a muon of a given sign, then:

$c = p^+p^-a^{+-} + p^+p^+a^{++} + p^-p^-a^{--} + p^-p^+a^{-+} = 3/4$. Therefore c = 3/4 for both field conditions and

$$(2\mu \cdot E/E)_{\text{decay}} \lesssim 3/8\ (1\mu \cdot E/E)^2 \tag{10}$$

APPENDIX B

This appendix details an estimate of an upper limit on the increase in observed neutral strange particle production due to associated production of a charged kaon which then decays to a muon.

First, we must define some functions.

Let: $\langle n_i \rangle g_i(\vec{p})\, d^3p$ be the probability of a particle of type i being produced in the momentum volume d^3p, where $\langle n_i \rangle$ is the average number of particles of type i produced per interaction. Then $\int g_i(p)\, d^3p = 1$.

The probability that such a particle will decay in a distance ℓ is just: $1-\exp(-\ell/c\tau_i\gamma_i) \approx \ell/c\tau_i\gamma_i \approx \ell m_i/c\tau_i p$. Of the particles which decay, a fraction $\langle \mu_i \rangle$ will decay to a muon. The muons have a probability $P_i(\vec{p}_\mu,\vec{p})\, d^3p_\mu$ of having momentum $\vec{p}_\mu$ and a probability $A(\vec{p}_\mu)$ of being accepted by the apparatus. The rate for counting muons from decays of a given species is then:

$$R_i = \iint d^3p\, d^3p_\mu \left(\langle n_i \rangle g_i(\vec{p})\right)\left(\ell m_i/c\tau_i p\right)\langle \mu_i \rangle P_i(\vec{p}_\mu,\vec{p})A(\vec{p}_\mu).$$

At this stage the only assumption is that ℓ is the independent of species. This assumption is not crucial to the argument.

The quantity of interest is:

$$R_K^\mu/R_\pi^\mu = \left(\frac{\langle n_K \rangle}{\langle n_\pi \rangle}\right)\left(\frac{m_K}{c\tau_K}\ \frac{c\tau_\pi}{m_\pi}\right)\frac{\langle \mu_K \rangle}{\langle \mu_\pi \rangle}\ \frac{\iint d^3p\, d^3p_\mu\, g_K\, \ell\, P_K\, A/P}{\iint d^3p\, d^3p_\mu\, g_\pi\, \ell\, P_\pi\, A/P}\ .$$

From 205 GeV/c π^-d bubble chamber data: $\langle n_K \rangle \approx 0.4 \langle n_\pi \rangle = 8$.[48]

The constants in front of the integrals may be evaluated to give $R_K^\mu/R_\pi^\mu = 0.24\ I_K/I_\pi$, where the I's are the integrals.

Evaluating the integrals requires a detailed Monte Carlo study. However, a simple argument is sufficient to establish that the ratio of the integrals is less than unity. One need only note that the kinematics of the decays, at

a given particle momentum will produce muons which are slower from kaons than from pions. Thus, a low momentum cutoff on the P_μ's imposed by the absorber and reflected in $A(\vec{p}_\mu)$ will have a larger effect on kaons than on pions. This is especially important at the lower particle momenta. At the higher momenta, the pion distribution g_π is larger than g_K since, for a pion beam, leading particle effects are present in g_π but not in g_K. Thus, we may write: $R_K^\mu/R_\pi^\mu \lesssim 0.24 \cong 1/4$.

Now the total rate of decay is the sum of these two rates: $R^{1\mu} = R_\pi^\mu + R_K^\mu$, and as was derived in Appendix A, the decay contribution is proportional to the single decay rate squared: $R^{2\mu} \sim (R_\pi^\mu + R_K^\mu)^2 = (R_\pi^\mu)^2 + 2R_\pi^\mu \cdot R_K^\mu + (R_K^\mu)^2$. Thus less than 32% of the dimuon decay triggers will involve one pion and one kaon, the two kaon mode is only 4%.

Now when a charged kaon is produced, we can produce another charged kaon, a neutral kaon, or a strange baryon. The charged and neutral kaons will be produced in approximately equal numbers, but only one-half of the K^o's will be K_S^o which we can see, K_L^o's almost never decay in the streamer chamber. Thus, only 25% of the time will we have a chance of seeing a neutral K^o decay, with the decaying charged K, and only 69% of these will decay: $K_S^o \to \pi^+\pi^-$, which can be visible in the chamber. From the 205 GeV/c π^- data[48] we know that the ration of K_S^o to $\Lambda^o(\Sigma^o)$ is approximately 2 to 1. But of the Λ^o only 64% will decay to the visible: $\Lambda^o \to p\pi^-$. Then assuming that the 2 to 1 ratio holds with the decaying charged kaon, we have at most 14% (.69 x .5 x 2/3 + .64 x 1/3) x .32 of the decay dimuon triggers can preferentially have a detectable K_S^o or Λ^o in the interaction. This is assuming 100% detection efficiency for these strange particles. But only some 30% of such neutral strange particles are, in fact, detected.

Thus, this limit is dropped to 4%. This is the desired result. I should note that this is probably very much overestimated.

REFERENCES

Chapter I

1. J. E. Augustin, Phys. Rev. Lett., 33, 1406 (1974).
2. J. J. Aubert, Phys. Rev. Lett., 33, 1404 (1974).

Chapter II

3. An elementary review of the properties of the Ψ and the Ψ' and their related states is given in the October and November 1975 issues of the SLAC Beam Line. More extensive reviews on the early theoretical speculations concerning the Ψ and Ψ' can be found in informal notes from SLAC:

   H. Harari, SLAC Informal Note, Ψ CHOLOGY (Nov. 1974).

   I. Bars, et. al., SLAC-PUB-1522 (Jan. 1975).

   A later review by J. Rosner, in the Proceedings of the 1975 APS/DPF Conference (Seattle) surveys various models and their status as of August 1975. In addition, the Proceedings of the 1975 Symposium on Lepton and Photon Interactions at High Energies, J. Ballam, Chairman, at SLAC contains a large number of papers on every aspect of the data and theory, as of August 1975.
4. B. J. Bjorken and S. L. Glashow, Phys. Lett. 11, 255 (1964).
5. S. L. Glashow, J. Iliopoulos and L. Maiani, Phys. Rev. D2, 1285 (1970).
6. M. Einhorn, Fermilab Preprint, Fermilab-Lecture-75/1-Thy/Exp (Feb. 1975).
7. M. K. Gaillard, B. W. Lee, J. L. Rosner, Rev. Mod. Phys. (April 1975).
8. W. Braunschweig, et al, Phys. Lett. 57B, 407 (1975).

   W. Tanenbaun, et al, Phys. Rev. Lett. 35, 1323 (1975).

   G. Feldman, et al, Phys. Rev. Lett. 35, 821 (1975).

   W. Tanenbaun in the Proceedings of the American Physical Society, Division of Particle and Fields Conference, Seattle (August 1975).

9. This rule has become known as "Zweig's Rule" partly as a result of oral tradition. It was first stated explicitly by S. Okubo, Phys. Lett. 5, 165 (1963).

10. G. Snow, Nucl. Phys. and Electromagnetic and Weak Interactions (8th Rencontre de Morcond), 379 (CNRS) (1973).

11. R. D. Field and C. Quigg, Fermilab-75/15-Thy (1975).

12. J. Ellis, M. K. Gaillard, D. V. Nanopoulos, CERN Preprint, TH2030 (August 1975).

13. G. K. O'Neill, Bull. Am. Phys. Soc. 20, 96 (1975).

Chapter III

14. G. Goldhaber, et al., "Observation in e^+e^- Annihilation of a Narrow State at 1865 MeV/c^2 Decaying to $K\pi$ and $K\pi\pi\pi$", SLAC Preprint (May 1976).

15. M. L. Perl, et al., Phys. Rev. Lett. 35, 1489 (1975).

16. A. Benvenuti, et al., Phys. Rev. Lett. 35, 1203 (1975).

17. V. Hagopian, et al., Phys. Rev. Lett. 36, 296 (1976).

18. C. Baltay, et al., Phys. Rev. Lett. 34, 1118 (1975).
E. J. Blesser, et al., Phys. Rev. Lett. 35, 76 (1975).

19. J. Klems, et al., "A Search for Charmed Particle Production in π^-d Interactions at 200 GeV/c", Acta Phys. Pol. (to be published).

20. D. Bintinger, et al., Phys. Rev. Lett. 35, 72 (1975).

21. E. J. Blesser, et al., Phys. Rev. Lett. 35, 76 (1975).
J. J. Aubert, et al., Phys. Rev. Lett. 35, 416 (1975).

22. M. A. Abolins, et al., "Search for Narrow High Mass States at Fermilab", Mich. State U. Preprint (1976) (unpublished).

23. J. P. Boymond, et al., Phys. Rev. Lett. 33, 112 (1974).
J. A. Appel, et al., Phys. Rev. Lett. 33, 722 (1974).
F. W. Busser, et al., Phys. Lett. 53B, 212 (1974).
L. B. Leipuner, et al., Phys. Rev. Lett. 34, 103 (1974); also see ref. 19.

Chapter IV

24. Track reconstruction of streamer chambers compared to bubble chambers was discussed by F. Villa in the Proceedings of the 1973 International Conference on Instrumentation for High Energy Physics, edited by S. Stipcich, page 115. He used the formulae for contributions to measuring errors from multiple coulomb scattering and setting errors taken from C. N. Fisher, "Optimization of Bubble Chamber Design Parameters: Measuring Accuracies for Charged Particles", CERN 67-26 Vol I (1967) P. 25, simplified for the flat track case. I repeat Villa's formulae here for convenience.

$$\frac{(\Delta p)^2}{p} = \frac{A}{H^2\ell} + \frac{1.4 \times 10^{-4} p^2 \varepsilon^2}{H^2 \ell^5}$$

$$(\Delta\theta)^2 = \frac{B\ell}{p} + \frac{3.8 \times 10^{-6} \varepsilon^2}{\ell^2}$$

H in kG, magnetic field
p in MeV/c, particle momentum
ε in μm, setting error
ℓ in cm, track length

The first terms in these formulae are the multiple scattering terms, the second are due to setting errors. For bubble chambers: A = 2.7, B = 4×10^{-2} and ε is typically 50-100 μm. For streamer chambers: A = 0.09, B = 0.13×10^{-2} for a Ne-He gas mix and ε is typically 200-300 μm. The setting error for both instruments is a strong, linear function of the demagnification used in the optics systems. The setting errors quoted here are for a nominal demagnification of 40. Villa also shows that the mass resolution in a streamer chamber can actually be better than in a bubble chamber of comparable size.

25. R. W. Morrison, Proceedings of the First International Conference on Streamer Chamber Technology, edited by J. M. Watson, ANL-8055-Instruments, 167 (1972).

26. W. S. Risk, Proceedings of the First International Conference on Streamer Chamber Technology, edited by J. M. Watson, ANL-8055-Instruments, 188 (1972).

27. C. GreyMorgan, et al., "Tests on a Small Hydrogen Streamer Chamber", TC-L. Inst. 70-10 CERN (1970).

28. F. Rohrbach, et al., Proceedings of the First International Conference on Streamer Chamber Technology, edited by J. M. Watson, ANL-8055-Instruments, 81 (1972).

29. V. Cook, et al., Proceedings of the First International Conference on Streamer Chamber Technology, edited by J. M. Watson, ANL-8055-Instruments, 29 (1972).

V. Cook, et al., Proceedings of the First International Conference on Streamer Chamber Technology, edited by J. M. Watson, ANL-8055-Instruments, 69 (1972).

Chapter V

30. J. R. Orr and A. L. Read, "Meson Laboratory Preliminary Design Report", FNAL (1971) (unpublished).

31. Beam Tune Calculations by P. Koehler, Fermilab, and O. Fackler, Rockefeller Univ., New York, N. Y.

32. W. F. Baker, et al., Phys. Lett., 51B, 303 (1974).

33. J. Klems, UC-Davis, Private Communication.

Chapter VII

34. D. Fournier, Laboratoire de l'Accélérateur Linéair, Orsay, France, Private Communication.

35. Data furnished by F. R. Huson, Fermilab, from 200 GeV/c $\pi^- p$ interactions in the 30" bubble chamber, taken by the Fermilab-Berkeley Collaboration.

36. This work was primarily performed by D. Fournier, Orsay and B. Robinson, Seattle; a detailed discussion is given in: B. Robinson, "Muon Reconstruction and Results", U of W - VTL HEP-42 (1976) (unpublished internal note).

37. Chisquare method due to D. Fournier, Orsay.

38. The A dependence was predicted by: J. Pumplin, E. Yen, Phys. Rev. 110, 1812 (1975), and has been observed for dimuon mass, $m_{\mu^+\mu^-} > 1$ GeV/c^2; M. Binkley, et al., "Dimuon Production on Nuclear Targets", Fermilab-PUB-76/41-EXP, 7300.358 (May 1976) (Submitted to Phys. Rev Lett.).

39. W. Busza, et al., Phys. Rev. Lett. 34, 836 (1975).

40. D. S. Ayres, et al., Phys. Rev. Lett. 35, 1195 (1975).

41. A. S. Carroll, et al., Phys. Rev. Lett. 33, 932 (1974).

42. Bubble Chamber Data is from the 205 GeV/c $\pi^- d$ exposure in the 30" chamber at Fermilab of the Davis-Krakow-Seattle-Warsaw Collaboration, Fermilab experiment E-218.

43. Distributions are crude fits to the data of: K. J. Anderson, et. al., Phys. Rev. Lett. 36, 237 (1976).

44. K. J. Anderson, et. al., "Inclusive Vector Meson Production in Dimuon Final States at FNAL", Bulletin of the APS 21, 567 (1976).

45. P. D. Higgins, et. al., "Inclusive $\rho^0(750)$ and $\Delta^{++}(1236)$ Production in 200 GeV/c $\pi^- p$ Reactions", Bulletin of the APS 21, 544 (1976).

Chapter IX

46. Most of the Monte Carlo calculations were run by D. Holmgren, University of Washington.

47. Distributions are crude fits to the data of: K. J. Anderson, et. al., Phys. Rev. Lett. 36, 237 (1976).

Appendix B

48. S. Csorna, Private Communication, data from 205 GeV/c $\pi^- d$ bubble chamber data of the Davis-Krakow-Seattle-Warsaw collaboration.

VITA

Alan Mathew Jonckheere was born on the 12th of February, 1947 in Howell, Michigan to Elizabeth and August Jonckheere. He graduated from Howell High School, Howell, Michigan in 1965 and then entered Michigan State University. At MSU he was a member of the Honors College, and Phi Kappa Phi Honorary Fraternity, and he was a National Science Foundation Undergraduate Research Assistant working with Dr. C. Gruhn at the MSU Cyclotron Laboratory. He graduated with Honors in 1969, after which he entered Graduate School at the University of Washington. He became associated with the Visual Techniques Laboratory in the U of W Physics Department in the spring of 1970 and began his research career. He received his M.S. in 1970 just prior to taking time off from graduate study to fulfill his military obligation. Upon his return he continued his work on the streamer chamber experiment.